THE MOTION OF MACROMOLECULES AND IMMISCIBLE DROPS IN CREEPING FLOW

Thesis by

William Lee Olbricht

In Partial Fulfillment of the Requirements

for the Degree of

Doctor of Philosophy

California Institute of Technology

Pasadena, California

1981

(Submitted August 21, 1980)

Acknowledgements

The guidance provided by Professor L. Gary Leal is gratefully acknowledged. Furthermore, every member of Professor Leal's research group at CalTech supplied constructive comments and instructive lessons at various stages of this project.

The equipment was built by George Griffith, Chic Nakawatase, and Ray Reed, and many of their ideas were successfully incorporated in the design of the apparatus.

I also appreciate the help of several friends, including Russell Bone, Michael Duncan, and Barry Bentley, who "came to the rescue" whenever asked. Ms. Kathy Lewis typed the manuscript.

Finally, my parents have given me years of enthusiastic encouragement which has made this work possible.

Abstract

Experimental studies were conducted on the creeping motion of immiscible drops of a Newtonian liquid through a circular tube. The mobility of the drop, the additional pressure gradient owing to the presence of the suspended drop, and the deformation and breakup of the drop were determined as a function of the drop size, flow rate and viscosity ratio, for both Newtonian and viscoelastic suspending fluids. Two tube geometries were employed to generate kinematically distinct flows. First, the effects of density differences between the fluids were studied in a tube of constant diameter for comparison with available results for neutrally buoyant drops. Surprisingly small density differences produced highly eccentric drop positions, and the data, including the steady shape of the drop, were correlated with the gap width between the drop and the tube wall using simple lubrication approximations. The results suggest the presence of both viscometric and time-dependent non-Newtonian effects for the viscoelastic suspending fluid. Experiments were then conducted for the case where the diameter of the tube varies periodically with axial position. The conformation of the drop depends strongly on the value of the inverse capillary number. For small values of this parameter, the shape of the drop, and hence, the measured quantities were periodic and in-phase with the drop's passage through the oscillatory tube. When the inverse capillary number was large, a drop suspended in a Newtonian fluid became highly elongated

and eventually broke into several fragments. Under the same conditions, a drop suspended in a viscoelastic fluid did not elongate, but instead, developed tails which issued satellite drops. The effect of increasing the polymer concentration in the suspending fluid was to stabilize the tails. The different conformations of the drop produced qualitatively different behavior for the additional pressure gradient and drop mobility. The observed dispersion processes appeared as onset phenomena at critical values of the material parameters.

The dynamics of fluid systems which are comprised of a suspended material in a Newtonian continuous phase were investigated theoretically. Important dynamical phenomena for such fluids are often a consequence of significant flow-induced deformation and/or orientation of the suspended elements. Hence, conditions under which large-scale distortion of the microstructure occurs were predicted via criteria for the flow strength, which is a measure of the form and magnitude of the velocity gradient tensor. The form of the criteria depends on the model chosen to describe the microstructure, but the properties which describe the specific fluid system enter only as parameters. Thus, the theoretical framework encompasses a wide class of fluids including macromolecular solutions and particulate suspension. Two examples illustrate the approach: the macromolecular stretching induced by a turbulent flow and the breakup of immiscible liquid drops in a shear field.

Table of Contents

Chapter 1

"The Creeping Motion of Liquid Drops through a Circular Tube of Comparable Diameter: The Effect of Density Differences between the Fluids"

W. L. Olbricht* and L. G. Leal

Department of Chemical Engineering
California Institute of Technology
Pasadena, California 91125

*Present address: School of Chemical Engineering, Cornell University, Ithaca, New York 14853

Abstract

Results of experiments on the low Reynolds number flow of non-neutrally buoyant drops through a straight circular tube are reported. The undeformed radii of the drops are comparable to the size of the tube, and the drops adopt an eccentric lateral position owing to a density difference between the drop and the suspending fluid. Measured values for the extra pressure drop caused by the presence of the drop, the relative velocity of the drop, and the shape of the drop are correlated with the minimum gap width between the eccentrically located drop and the tube wall using simple lubrication approximations. The viscosity ratio, density difference, volumetric flow rate, and drop size are varied in the experiment. Comparisons with previous results for concentric, neutrally-buoyant drops show that the effects of eccentric position can be substantial for surprisingly small values of the density difference. Both Newtonian and viscoelastic suspending fluids are considered, and the results suggest that both viscometric and time-dependent non-Newtonian effects are present. For the Newtonian case, the data are compared with the predictions of available theories which account explicitly for the eccentric drop position.

1. Introduction

The creeping motion of drops suspended in a tube flow is important as a prototype problem in many industrial and biological processes. Immiscible additives, in the form of small particles or drops, are often used in polymer melt processing to alter the bulk properties of the final product; it is crucial that the kinematics and dynamics of the resulting two-phase flow be understood if the desired structure is to be achieved. The well known analogy between the motion of large droplets through tubes and the creeping motion of erythrocytes through capillaries has also served as a motivation for many earlier studies of this problem. Although there are recent studies, e.g. Tozeren and Skalak (1978), that present experimental and theoretical models for capillary blood flow which are far more realistic than the simple system considered here, the sensitivity of the results to density differences between the two phases has not been examined; and for this reason, the present study may still be of qualitative interest in the blood flow problem. Our own motivation for the general study, of which this present work is a part, is the development of a realistic laboratory model for investigation of the microdynamics of two-phase flows in porous media (i.e., the dynamics at the scale of the pores). This problem is of interest in tertiary oil recovery methods including polymeric and surfactant flooding. Here, oil droplets are displaced and carried by a so-called "pusher" fluid through the porous matrix toward a collection well. Much of the effort in making this process feasible has concerned an understanding of the macroscale dynamics at the scale of the whole reservoir. The present investigations

are aimed at an understanding of the detailed dynamics at the scale of the individual flow channel. Specifically, we aim ultimately to achieve a more fundamental grasp of the relationships between "dependent" parameters such as the flow resistance, drop mobility, or stable drop size (i.e. drop breakup), and "independent" parameters of the system such as fluid properties, channel geometry and interfacial tension.

A large number of previous experimental and theoretical studies have been concerned with the flow of single-phase Newtonian and viscoelastic fluids through tubes with axially varying cross-sectional area employed as a model for the porous matrix. Neira and Payatakes (1979), Fedkiw and Newman (1977), Payatakes and Neira (1977), and Deiber and Schowalter (1979) have all calculated the flow fields for Newtonian liquids in periodically constricted tubes. In addition, Deiber and Schowalter report experimental data for the pressure drop as a function of flow rate for a Newtonian fluid and a particular choice of tube geometry. Although the periodically constricted tube is a gross oversimplification of the flow channel geometry in a porous medium, it does allow some of the effects associated with a rapidly varying cross-sectional area to be investigated. For a single phase flow, however, a crucial missing element is the lack of any necessity for the flow to constantly split apart and merge as the fluid passes along the "flow channel". Thus, unlike the motion in a porous matrix, or a packed bed, the fluid can pass straight through the central portion of the channel, effectively "ignoring" the streamwise variations in cross-sectional area. Although this critical "defect" may also be present in a two-phase flow, the presence of a suspended drop of comparable size to the tube will force the fluid to follow the wall geometry to a

greater extent and the model consequently appears to us to be more realistic for this case. In this case, the effect of the flow field on the conformation of the suspended elements must be considered and the published results for single-phase flow give little information of direct relevance. This is the problem investigated in the present studies.

In an earlier paper, Ho and Leal (1975) [hereafter referred to as (I)] considered the case of neutrally buoyant drops in a straight-wall tube for both Newtonian and viscoelastic suspending fluids. The straight-wall tube problem is of some intrinsic interest in its own right, and is a necessary preliminary to the investigation of the wavy-wall tube flow. Here, we consider the effect of differences in density between the drops and the suspending fluid, again for creeping motion through a straight, circular, horizontal tube. In an accompanying paper (Olbricht and Leal, 1980), the effects of flow channel geometry will be investigated.

In the present experiments, we measure: the incremental pressure drop, ΔP^+, which is required to maintain a specified flow rate relative to the pressure drop which would be required without any drops; the velocity of the drops U relative to the average velocity of the two-phase flow V; the shapes of the drops; and the minimum gap width, h, between the lower surface of the drops and the tube wall. In the context of two-phase flow through porous media, ΔP^+ is related to the accessibility of individual channels to flow compared to channels which contain no drops (i.e., the microscale "sweep efficiency"), U is a measure of the drop mobility, and the shape is important as a precursor to dispersion (breakup) processes. The major focus of the present experiments is the effect of the

lateral position of the drop in the horizontal tube as a consequence of the density difference between the two fluids. A neutrally buoyant particle travels along the tube centerline. This problem has been studied extensively in (I) for both Newtonian and viscoelastic suspending fluids. The results obtained here for non-neutrally buoyant drops do, in some cases, provide additional insight which helps to understand physical behavior observed for neutrally buoyant drops, but not fully explained in (I). In addition, and more central to the present study, we attempt to understand how the lateral position of the drops influences the relationship between measured features of the flow (listed above) and the independent parameters of the system. These parameters include the volume of the drops, the viscosity of the drops, the velocity of the bulk flow, and the suspending fluid rheology. The lateral position of the drops in these experiments is varied through changes in the specific gravity of the drop relative to that of the suspending fluid. An important additional qualitative objective of our work is thus a determination of the sensitivity of the results to small density differences between the two phases, and a delineation of the domain where non-neutral buoyancy is a significant factor.

The relevant independent dimensionless parameters for the problem include: λ, the undeformed drop radius relative to the radius of the tube R_o; σ, the ratio of the drop fluid viscosity μ_i to that of the suspending fluid μ_o; a deformation parameter which is the inverse of the so-called capillary number, $\Gamma = \mu_o V/\gamma$, where γ is the interfacial tension between the drop and suspending fluid; and $\Delta\rho/\rho_o$, where $\Delta\rho$ is the difference between the specific gravity of the drop fluid ρ_i and that of the suspending fluid ρ_o. In the case of a viscoelastic suspending fluid, the

results will also depend on the dimensionless parameters which characterize the rheological properties of the fluid. Foremost among these is the Deborah number, $De = \theta/t$, where θ is the intrinsic relaxation time for the fluid ($\theta = 0$ in a Newtonian fluid) and t is a convective timescale of the flow. In the experimental data which are presented in section 3, the additional pressure drop ΔP^+ is scaled by the characteristic viscous pressure $\mu_o V/R_o$.

Existing theories for the motion of particles through tubes are largely concerned with Newtonian suspending fluids. Two investigations are of special relevance to the present study because they consider the effect of an eccentric position of the drop. Hetsroni et al. (1970) used the method of reflections to solve for the velocity fields associated with the motion of a small, spherical (undeformed) drop which is not too near a wall in a Poiseuille flow. The lateral position of the drop is specified, in dimensionless terms, by $\beta = b/R_o$ where b is the distance between the centerline of the tube and the center of the undeformed drop. The relative velocity of the drop for this case is predicted to be

$$\frac{U}{V} = 2(1 - \beta^2) - \frac{4\sigma}{3\sigma + 2}\lambda^2 + O(\lambda^3) \quad . \tag{1}$$

Brenner (1973) used the reciprocal theorem for creeping flow to obtain the additional pressure drop for this flow:

$$\frac{\Delta P^+ R_o}{\mu_o V} = \frac{16[(9\sigma + 2)^2 - 40]}{27(\sigma + 1)(3\sigma + 2)}\lambda^5 + \frac{32(5\sigma + 2)}{3(\sigma + 1)}\beta^2\lambda^3 + O(\lambda^6) \quad . \tag{2}$$

Later, Bungay and Brenner (1973a) also obtained results for a small rigid sphere near the tube wall. It will be noted that equations (1) and (2) contain the lateral position of the drop, explicity through β. Unfortunately,

though β depends mainly on the density difference, $\Delta\rho/\rho_0$ in the present experiments, its value has not been predicted in any of the existing theoretical developments. Thus, quantitative comparisons between the data for U and ΔP^+ and the predictions from (1) and (2), respectively, can be made only by estimating the value of β directly from photographs of the drops in the flow.

Some theoretical work has also been done for particles which are of a size similar to that of the tube, but only for neutrally buoyant, concentrically located particles. Hyman and Skalak (1972a,b) calculated ΔP^+ and U for deformable and nondeformable liquid drops, while Bungay and Brenner (1973b) considered the case of close-fitting rigid spheres. Lighthill (1968) and Fitz-Gerald (1969) also studied the motion of a large, elastic particle, but evaluation of ΔP^+ is difficult from their results and the calculation was subsequently improved, for the axisymmetric case, by Tozeren and Skalak (1978). As noted above, no theoretical work has so far been done which considers large eccentrically positioned particles.

Finally, we briefly mention earlier experimental investigations which are related to the present work. These include Hochmuth et al. (1970), Sutera et al. (1970), Seshardi et al. (1970), and Hochmuth and Sutera (1970) and involve the motions of erythrocytes, model cells, and spherical caps in Newtonian fluids through capillary tubes. Prothero and Burton (1961,1962) studied qualitatively the motion of gas bubbles in a Newtonian liquid, once again as a model for blood flow. Goldsmith and Mason (1963) reported U and h for very large drops ($\lambda >> 1$) in creeping flow. However, none of these experimental studies includes the effects of

non-neutral buoyancy.

The case of a viscoelastic suspending fluid has received scant attention in the literature, apart from the paper (I) cited earlier. Indeed, the only other work which is at all relevant to the present paper is due to Sigli and Coutanceau (1977), who measured the drag on rigid spheres falling through a cylindrical tube, when the particle and tube are of comparable diameter. The data show significant qualitative effects of fluid viscoelasticity when the interaction between the particle and the tube wall is important, even though the nominal Deborah number is small.

2. Experimental Apparatus and Materials

The apparatus used in this experiment is similar to the one used in (I) and is illustrated in Figure 1. The flow was driven by one of two available pumps capable of maintaining a constant flow rate with less than 0.1% variation over the course of a single experimental run. For the Newtonian suspending fluid, a Harvard Apparatus infusion/withdrawal syringe pump was used, while a Zenith Products Series BPB gear pump was employed with the more "viscous" viscoelastic suspending fluid.

The suspending fluid was held in an overhead reservoir before entering the pump. The fluid was then pumped into a large storage section which was immersed in a constant temperature bath maintained at 25 ± 0.1°C. The transit time through this storage section was always sufficiently long to ensure that the temperature of the suspending fluid had equilibrated with the bath before entering the test section. The test section consisted of a horizontal precision-bore glass tube with a diameter of 1 cm and a length of 120 cm. Pressure ports were positioned 50 cm apart, the first port being 50 cm downstream of the entrance to the test section. After

passing through the test section, the fluid exited the controlled temperature region and was held in a storage container.

The drops were manually injected upstream of the test section using a Hamilton precision micrometer syringe capable of producing drops of known volume to within 0.001 ml. The micrometer syringe was connected to a flexible tube fitted at its end with a 15 gauge hypodermic needle. The needle was inserted directly into the flow through a fitting containing a rubber septum. The drops were injected with the pump operating at a low speed so that they would detach from the needle shortly after injection. Once all the drops for a particular run had been injected, the pump was adjusted to the full desired flow rate. It was found that the drops attained an equilibrium position in the tube well before entering the region between the pressure ports. The equilibrium position was found to depend on all the material and flow parameters, but most strongly on the density difference between the drop and suspending fluid. Furthermore, the equilibrium position was completely independent of the initial lateral position of injection.

The pressure ports were connected to a differential manometer/transducer system capable of detecting changes in the pressure drop down to approximately 10^{-3} inches of water. This level of sensitivity is important because the extra pressure drop due to the presence of a drop in the flow can sometimes be exceedingly small. The manometer/transducer system is shown schematically in Figure 2. Since the total pressure drop between the pressure ports was much larger than the fullscale sensitivity of the transducer (a Validyne Engineering Co. Model DP45 with a fullscale range of only 0.5 inches of water), the manometer was used to balance the

(major) portion of the pressure drop due to the flow of the suspending fluid alone. The transducer then detected only the relatively small changes in the pressure drop due to the presence of the drop (or drops) in the test section. This can be accomplished, in principle, by first allowing the manometer to equilibrate with the pressure drop for flow of the suspending fluid alone. Then the two legs of the manometer can be physically separated by closing the valve between them (indicated by the letter "D" in Figure 2). The differential transducer is connected across the valve. Thus, provided the flow rate remains constant and no drops enter the test region, the pressure at the bottom of the two manometer legs will be identical, and the pressure "drop" across the transducer will be zero. When a drop (or drops) enter the test region, however, any changes in the pressure drop (i.e., ΔP^+) will be recorded directly by the transducer. In practice, our procedure for measuring ΔP^+ differed slightly from this due to the fact that the transducer response was found to be highly nonlinear for small deflections of the membrane. Consequently, the manometer was never allowed to completely equilibrate before the valve (D) was closed. Furthermore, in order to enhance the pressure signal, a train of six to ten drops was generally used in the test section. Although the drops were equally spaced, it was found, as in (I), that the pressure drop per drop was independent of the spacing if the drops were separated by at least one tube diameter.

The velocity of a drop, which was also independent of spacing if the drop were separated by at least one tube diameter, was measured by determining visually the time for transit between known points in the tube. The volumetric flow rate Q was measured by collecting a measured volume of fluid from the outlet of the test section over a measured time interval. Photographs were taken while the drops were in the test section between the pressure taps using a 35 mm Pentax camera fitted with a closeup lens. The refractive index of the fluid in the constant temperature circulating bath was matched with the refractive index of the suspending fluid in the manner outlined in (I), and this minimized distortion in the photographs due to the curved surface of the tube. The gap width, h was determined from the photographs.

The Newtonian suspending fluid was 95.75 wt. % glycerin in water. The density of the solution, measured with a hydrometer, was found to be 1.251 ± 0.001 g/cm^3 during the course of the experiment. The viscosity was also monitored during the runs, but was always found to be 4.17 ± 0.02 P. The slight variation is due primarily to the 0.1°C variations in temperature which existed in the circulating water bath.

The viscoelastic suspending fluid was a 0.5 wt. % aqueous solution of Dow Separan AP30, a polydisperse polyacrylamide with rheological properties that have been extensively studied (Leal, Skoog, and Acrivos, 1971; Huppler et al., 1967a,b). One difficulty in comparing experimental results for the Newtonian and viscoelastic suspending fluids is to determine an appropriate viscosity for the Separan solutions since these show a strong shear-thinning effect. However, we follow the precedent of (I) and simply evaluate the viscosity at the wall shear rate for the undisturbed flow

using a power-law model ($n = 0.45$) to estimate the shear-thinning behavior of the fluid. The resulting values of the suspending fluid viscosity at the flow rates for the present experiment can be determined from Table 1. Unfortunately, the viscoelastic fluid viscosity was found to vary significantly from batch to batch of the Separan solution. Although care was taken to prepare each batch of suspending fluid in an identical manner, variations in the fluid viscosity up to 10% appeared to be unavoidable.

In addition to a shear-thinning viscosity and normal stress differences in simple shear flow, dilute polymer solutions exhibit a finite response time in unsteady (Lagrangian or Eulerian) flow. This characteristic time is associated with the fluid's adjustment at the macromolecular level to a change in the bulk deformation gradient. When the fluid timescale is comparable to the characteristic timescale of a flow, the response of the system may be governed, at least in part, by the relative magnitude of these timescales. The ratio of the fluid response time, θ, to the timescale of the flow, τ (i.e. the timescale for variation in the deformation rate as seen by a fluid element), is the Deborah number, defined as $De = \theta/\tau$.

As far as the present experiment is concerned, if the suspended drop were sufficiently small, it would move with the local fluid velocity, and hence the flow would be steady everywhere. Furthermore, the flow field at any point would be nearly simple shear flow, and consequently the non-Newtonian properties could be described completely by variations in the viscosity and the normal stresses in a viscometric flow. However, when the drop is not asymptotically small, as is the case in the present experiments (cf. (1)), the drop travels at a velocity which differs from the local suspending fluid velocity. As a result, fluid elements

experience a local acceleration as they move around the drop. This unsteadiness is a possible source of time-dependent non-Newtonian effects. The importance of such effects can be measured by De. The appropriate timescale for the flow is approximately $2D\lambda R_o/(U - V)$, where the difference in velocity between the drop and the surrounding suspending fluid is estimated to be $(U - V)$, and $2D\lambda R_o$ is the "length" of the deformed drop (see section 3). The characteristic time for the fluid can be estimated from steady shear flow data, employing a constitutive model to relate θ to normal stress measurements. We have used the contravariant form of the convected Maxwell model for this purpose, and θ has been evaluated at the wall shear rate. Our estimates show that the maximum value of De under the conditions of the present experiment is approximately 0.20. Most previous experimental evidence suggests that time-dependent non-Newtonian effects are only significant when De $\geq$ 1 or 2. Thus, we expect to be able to interpret the experimental results reported here largely in terms of the fluid behavior in a steady simple shear flow.

The drops consisted of solutions of Dow Corning silicone oil mixed with carbon tetrachloride. The viscosity of the drops μ_i was determined primarily by the amount of carbon tetrachloride added. The values of $\sigma = \mu_i/\mu_o$ and $\Gamma = \mu_o V/\gamma$ for the systems used are listed in Table 1. The density differences employed in this study were small, never exceeding 0.04 g/cm^3. Nevertheless, the changes induced over this range of $\Delta\rho$ will soon be seen to be both qualitatively and quantitatively significant. Indeed, this magnitude is apparently sufficient to expose the asymptotic behavior for "large" values of $\Delta\rho$ in such quantities as $\Delta P^+ R_o/\mu_o V$ or U/V. These are important findings since density differences of this magnitude

are likely to be common in many systems of interest, in spite of the fact that no account has been taken of them in the majority of existing theoretical studies. The analysis of Hyman and Skalak (1972b), mentioned in section 1, provides a good example. Calculations were made for ΔP^+ and U for liquid drops taken as a model of erythrocytes in capillaries. It was assumed that the drops were neutrally buoyant and concentrically located, even though the authors point out that the density of erythrocytes differs from that of the suspending plasma by 0.07 g/cm^3. The neglect of even relatively small density differences may turn out to be a significant shortcoming of this and similar calculations.

The dimensionless parameter, Γ, characterizes the relative magnitude of viscous stresses as compared to interfacial tension forces at the drop surface, and is the inverse of what is often called the capillary number. This parameter was varied in the present experiments through variations in the flow rate V. The interfacial tension, γ, was measured using a Dunuoy ring tensiometer. The measured values are 22 dynes/cm and 26 dynes/cm for silicone oil drops with the Newtonian and viscoelastic suspending fluids, respectively.

The flow parameters, namely the size of the drops and the flow rates used in this experiment, are listed in Table 2.

3. Experimental Results

Measurements of ΔP^+, U, shape, and distance from the wall, h, have been made for the thirteen systems listed in Table 1. The material properties of each system, namely the drop viscosity and density, were chosen

so that comparisons between them would reveal the effects of the individual variables on the dependent quantities, such as ΔP^+ or U. Furthermore, comparisons between selected Newtonian and viscoelastic suspending fluid systems reveal the qualitative effects of viscoelasticity on the measured quantities. Finally, comparison between the data for the non-neutrally buoyant (eccentric) drops studied here, and the corresponding results for neutrally buoyant drops described in (I), provides a further indication of the effects of density differences between the two fluids. Measurements were made for each system for three flow rates ($0.3 \leq V \leq 0.8$ cm/s) and for six drop sizes ($0.5 \leq \lambda \leq 0.8$). Thus, two material properties, σ and $\Delta\rho$, and two "flow parameters", V and λ, have been independently varied. The main results are presented in four parts, organized according to the specific property which is being varied, rather than the quantity being measured. This scheme of presentation facilitates discussion of the results, since the variation of a single experimental parameter often affects more than one measured quantity simultaneously. Mechanistic explanations for the results are proposed whenever possible, and the ranges of their validity over the parameter space are estimated. In addition, the data are compared in section 5 to the small-λ theories of Brenner (1973) for ΔP^+ and Hetsroni et al. (1970) for U, which account explicitly for the eccentricity of the drop's position in the tube.

The data for $\Delta P^+ R_o/\mu_o V$ and U/V for each size drop and each flow rate are tabulated in Table 3. In an attempt to characterize the degree of drop deformation, a parameter D was defined as the maximum linear dimension of the drop (as measured from photographs) rendered dimensionless by the undeformed drop diameter $2\lambda R_o$. Clearly, the parameter D is insufficient

to describe the detailed shapes assumed by the drops during flow. We may note in this regard that the equilibrium drop shapes are actually non-axisymmetric due to the eccentric lateral positions of the drops for $\Delta p \neq 0$. Nevertheless, measurements of D will be useful for the purpose of comparison between various systems. Representative data for D and h will be presented later in this section. A complete accounting of numerical values for D and h is given by Olbricht (1980). The drop typically undergoes a larger deformation in the viscoelastic suspending fluid than it does in the Newtonian fluid under comparable flow conditions. Furthermore, the gap width, h, appears to be larger for the viscoelastic fluid, a result which we shall discuss in more detail in section 4.

Let us now turn to a more detailed examination of the data. In this section, we focus simply on the dependence of such variables as ΔP^+, U/V and D on the independent parameters Γ, σ, λ and $\Delta\rho/\rho_o$. These results are then discussed in section 4 with the objective of obtaining a qualitative understanding of the underlying physical mechanisms which are responsible for the observed trends.

3.1 Average Velocity

Let us now consider effects of the bulk flow rate or equivalently, the average velocity, V, for fixed values of λ, σ, and $\Delta\rho/\rho_o$. Measurements were made for three values of the average velocity, V = 0.32, 0.56, 0.80 cm/s, for each of the systems listed in Table 1 (including six drop sizes). In each case, the Reynolds number, $Re = \rho_o R_o V/\mu_o$ was very much less than unity, and a dimensional analysis of the problem thus suggests

that the primary effects of the bulk velocity in the case of a Newtonian suspending fluid should be manifested through variations in the parameter $\Gamma = \mu_o V/\gamma$. As noted earlier, this parameter gives the relative magnitudes of viscous and surface tension forces, and thus controls the degree of drop deformation. In the case of a viscoelastic suspending fluid, the rheological properties also depend upon the magnitude (and form) of the velocity gradient tensor and this provides the potential for additional dependence on V. The effects of V on $\Delta P^+ R_o/\mu_o V$ and on U/V for both Newtonian and viscoelastic fluid systems are illustrated in Figure 3, where $\Delta P^+ R_o/\mu_o V$ and U/V are plotted as a function of Γ for several systems which have approximately the same values of σ, λ, and $\Delta\rho/\rho_o$. Also shown are results for $\Delta P^+ R_o/\mu_o V$ and U/V as a function of Γ for the neutrally buoyant case studied in (I). The differences between the two non-neutrally buoyant Newtonian systems are primarily a consequence of the difference in drop size ($\lambda = 0.62$ and $\lambda = 0.72$, respectively), and this is also true of the two viscoelastic fluid cases from this study. The differences between the present results for $\lambda = 0.72$ and those obtained in (I) are a consequence of the difference in $\Delta\rho/\rho_o$ (0.037 and 0, respectively). We shall indicate the dependence of $\Delta P^+ R_o/\mu_o V$ and U/V on λ and $\Delta\rho/\rho_o$ in subsequent sections of this paper. Here, let us concentrate on the effect of variations in Γ.

Newtonian Suspending Fluid

One consequence of an increase in the flow rate (i.e., an increase in Γ), is a lower value for the dimensionless additional pressure drop $\frac{\Delta P^+ R_o}{\mu_o V}$,

for every Newtonian fluid system studied. Indeed, for system 4, if the size of the drop is fixed and the flow rate increased, the decrease is sufficient to cause $\Delta P^{+}R_o/\mu_o V$ to become negative at the highest flow rate. In general, it appears that $\Delta P^{+}R_o/\mu_o V$ approaches a constant asymptotic value for the highest flow rates. This result is noteworthy because it indicates that it is not possible to indefinitely lower the resistance to flow associated with a drop by simply increasing the flow rate. The velocity of the drop was always found to exceed the average velocity of the fluid. Furthermore, an increase in the average velocity V resulted in an increase in the relative velocity of the drop, U/V, in every case. It may also be noted that the shape of the drop, as measured by D, shows a greater deformation for increased flow rates. In addition, non-neutrally buoyant drops attain an equilibrium position which is farther from the wall as the average velocity increases, while the increased deformation causes the gap between the drop surface and the wall to increase even for neutrally buoyant drops. All of these effects of increased average velocity are slightly more dramatic for larger drops. Furthermore, the identical qualitative trends are observed for both neutrally buoyant and non-neutrally buoyant drops, indicating that drop eccentricity is not an important factor with regard to flow rate variations.

Viscoelastic Suspending Fluid

The most significant result for the case of a viscoelastic suspending fluid is that the effects of variations in the average velocity (or Γ), are qualitatively identical to those discussed above for a Newtonian

suspending fluid. In particular, it is evident from Figure 3 that $\Delta P^+ R_o/\mu_o V$ decreases and U/V increases in response to an increase in the flow rate at a rate which is very close to that for the Newtonian case.

3.2 Drop Size

The effects of drop size were studied for each system by taking measurements for six different sizes, $0.51 \leq \lambda \leq 0.87$. The larger sizes are directly comparable to those chosen in (I) for neutrally buoyant drops. Although the dimensionless radius, λ, varies by only about one-half, the drop volume varies by over a factor of four in these experiments. Although it is impossible to illustrate all of the data, Figure 4 provides an indication of the dependence of ΔP^+ on λ. The degree of deformation as a function of λ is shown for systems with $\Delta\rho/\rho_o \simeq 0.04$ in Figure 5. Let us now consider these results in detail, beginning with the Newtonian suspending fluid systems.

Newtonian Suspending Fluid

The dependence of the additional pressure drop, ΔP^+, on the size of the drop is not qualitatively changed by variations in $\Delta\rho/\rho_o$. Thus, although the majority of systems studied here show a monotonic increase in $\Delta P^+ R_o/\mu_o V$ with drop size, the previous work on neutrally buoyant drops shows clearly that this behavior must depend upon the value of σ. In particular, for σ small enough and λ large enough, the extra pressure drop will decrease with increased drop size, for the simple reason that fluid of higher viscosity is being replaced by fluid of lower viscosity. The fact that $\Delta P^+ R_o/\mu_o V$ increases with drop size in all cases shown in Figure 4 is almost

certainly a consequence of the fact that the minimum value of σ was only 0.3, and the maximum in λ was 0.87. Indeed, the system 4 (see Table 3) illustrates a partial transition to the small σ, large λ behavior noted in (I). This system has the lowest viscosity ratio ($\sigma = 0.30$) of those studied here, and the additional pressure drop first increases with ΔP^+ in this particular system, achieves a maximum around $\lambda \sim 0.6$ (for $V = 0.80$ cm/s), and then decreases as the size of the drop is made larger.

In contrast to the effect on ΔP^+, the qualitative dependence of the relative velocity of the drop on drop size does depend on the eccentricity of the drop. It was shown in (I) that the velocity ratio U/V for a neutrally buoyant drop decreases monotonically with increasing λ until a constant limiting value is attained around $\lambda \sim 0.9$. The least non-neutrally buoyant drops studied here, system 4 ($\Delta\rho/\rho_0 = 0.011$), also show a monotonic decrease in U/V up to $\lambda = 0.87$, which was the largest value covered in this study. However, for the other non-neutrally buoyant systems ($\Delta\rho/\rho_0 = 0.02, 0.04$), U/V first increases with λ, attains a maximum around $\lambda \approx 0.6 - 0.7$, and then decreases monotonically with further increase in λ. The maximum appears to be more pronounced for the lowest flow rate in each case.

Finally, let us consider the effect of drop size on the degree of droplet deformation. Representative data for the Newtonian suspending fluid are shown in Figure 5, where the deformation parameter D is plotted as a function of the viscosity ratio for three different size drops. Here, D is the ratio of the maximum linear dimension of the drop to its

undeformed diameter. It can be seen from Figure 5, that the drop undergoes larger shape deformations as its size (i.e., λ) is increased. In contrast to this, the relative degree of deformation in an unbounded creeping flow would be independent of the drop size. However, in the present case, the drop is deformed, in part, due to the presence of the walls, and it is this effect which is presumably responsible for the observed increase in deformation with larger λ.

Viscoelastic Suspending Fluid

The value of ΔP^+ remains positive for all systems in the present study with a viscoelastic suspending fluid. Not only is a monotonic increase in $\Delta P^+ R_o/\mu_o V$ observed as the drop is made larger, but both the rate of increase and the actual nondimensionalized values of $\Delta P^+ R_o/\mu_o V$ are apparently independent of all the material parameters, including σ (cf. Figure 4). No maximum or asymptotic limit is observed for $\Delta P^+ R_o/\mu_o V$ over the size range covered.

The value U/V as a function of λ (Table 3) shows no maximum for the viscoelastic suspending fluid systems. Instead, U/V only decreases monotonically with increasing drop size at a rate which again seems to be independent of other material parameters, including σ.

The quantitative influence of viscoelasticity on drop mobility depends on drop size. A comparison between various Newtonian and viscoelastic systems shows that U/V is often larger (especially at the lowest value of V) in the viscoelastic systems for small drops, but always smaller for large drops in the size range covered here. Typical curves for the difference between U/V for the Newtonian systems and U/V for a

corresponding viscoelastic system (same $\Delta\rho/\rho_o$, σ) are shown in Figure 6 as a function of λ.

3.3 Drop Viscosity

The effect of drop viscosity relative to the viscosity of the suspending fluid was studied by taking measurements for various grades of drop fluid at each value of $\Delta\rho$ ($\sim 0.1 < \sigma < \sim 5$). The results are shown in Figures 4, 5 and 7, as well as Table 3.

Newtonian Suspending Fluid

It can be seen from Figure 4 that the magnitude of $\Delta P^+ R_o/\mu_o V$ in Newtonian fluid systems is critically dependent on the value of σ. If σ is sufficiently large, the additional pressure drop is always positive, but if σ is small (not merely less than unity), the sign of ΔP^+ can be negative, depending on other material parameters and λ.

Equation (1) predicts that the drop velocity should decrease with σ for undeformed drops in a Newtonian fluid. This trend is also shown by the data in Figure 7, even though the drops deform. However, results from Table 3 show that the effect of σ is larger for more eccentric drops, a feature that cannot be predicted by the small-λ theory.

Finally, drop deformation, as measured by D, shows only a slight increase with σ, as shown in Figure 5. Furthermore, the drop viscosity does not affect the gap width between the drop and the tube wall over the entire range of experimental conditions.

Viscoelastic Fluid Systems

Let us now turn to the effects of drop viscosity when the suspending fluid is viscoelastic. Figure 7 shows clearly that for eccentric drops, the additional pressure drop is independent of the value of σ over the range of σ studied, in marked contrast to the Newtonian result. Indeed, no systematic changes in the value of ΔP^+ can be discerned (for a given value of $\Delta\rho/\rho_o$) even though σ varies by more than a factor of fifty. The additional pressure drop is positive for all cases studied, even for viscosity ratios as low as $\sigma = 0.09$. Furthermore, $\Delta P^+ R_o/\mu_o V$ is larger for viscous drops in a Newtonian suspending fluid than for the same drops in a viscoelastic system, if all other parameters remain unchanged. The opposite is found for inviscid drops.

No major effect of σ was found on either the drop velocity or the gap width for a viscoelastic suspending fluid.

3.4 Density Difference

Finally, let us consider the effects of the eccentric position of non-neutrally buoyant drops. The eccentricity of the drop is determined by the difference between the specific gravity of the drop fluid and the specific gravity of the suspending fluid if the other variables are fixed. Specifically, the equilibrium position of the drop is determined by the balance between buoyancy forces and hydrodynamic lift generated in the gap between the drop and the tube wall. The value of $\Delta\rho/\rho_o$ ranges from zero in (I) to 0.04 in the present study.

Newtonian Suspending Fluid

The value of the additional pressure drop increases for a Newtonian suspending fluid as a drop of fixed size is made more eccentric by increasing the drop density. Also, the velocity of the drop decreases, and the drop suffers a larger deformation as the eccentricity increases.

These trends for $\Delta P^{+}R_o/\mu_o V$ and U/V are illustrated in Figure 8. It can be seen that the sensitivity of $\Delta P^{+}R_o/\mu_o V$ to variations in $\Delta\rho/\rho_o$ diminishes above $\Delta\rho/\rho_o = 0.02$ for the drops with $\lambda = 0.83$. In contrast, the smaller drops show an appreciable increase in $\Delta P^{+}R_o/\mu_o V$ up to $\Delta\rho/\rho_o = 0.04$. Small drops also show a much stronger dependence of U/V on $\Delta\rho/\rho_o$ than the corresponding large drops.

Viscoelastic Suspending Fluid

The same qualitative trends noted above for Newtonian systems were also observed for viscoelastic suspending fluids, though the effects are less pronounced.

A key difference between the two cases is in the gap width, h. For a given value of $\Delta\rho/\rho_o$, drops suspended in a viscoelastic fluid are farther from the wall than those in a Newtonian fluid. For example, the values of h for two corresponding viscoelastic and Newtonian systems, with $\Delta\rho/\rho_o = 0.019$, are 0.32 (System 6V) and 0.12 (System 2) for $\lambda = 0.62$, and 0.18 (System 6V) and 0.12 (System 2) for $\lambda = 0.83$.

Comparison between the results obtained here and those in (I) for neutrally buoyant drops shows that the effects of a given magnitude of $\Delta\rho/\rho_o$ on the drop eccentricity decreases as the size of the drop is made larger. Consequently, a given value for $\Delta\rho/\rho_o$ induces a relatively smaller change in the measured quantities as the drop is made larger.

4. Discussion

It has already been pointed out that the eccentric lateral positions of the drops in the horizontal tube in this experiment are a consequence of the density differences between the drop fluid and the fluid in which the drop is suspended. The initial lateral point of injection in no way affects the equilibrium position of the drop during the course of the experiment. Rather, this position depends on a balance between buoyancy and hydrodynamic lift forces which keep the drop from contacting the wall. Photographs of the drops in flow suggest the possibility that the fluid-filled gap between the drop's lower surface and the tube wall is actually a lubrication layer capable of producing an upward thrust on the drop which balances buoyancy. It is essential, then, that the drop is able to deform in the flow, since a spherical drop can generate no hydrodynamic lift. The lateral position of an undeformed neutrally buoyant drop would be determined exclusively by its initial lateral position in the tube, provided the Reynolds number and Deborah number are sufficiently small that "lateral migration effects" are negligible (cf. Chan and Leal, 1979).

For non-neutrally buoyant deformable drops, previous lubrication analyses of related flows may be useful. The most relevant study is by

Lighthill (1968), who considered the motion of an elastic particle taken as a model for the red blood cell moving through a capillary in a Newtonian suspending fluid. The particle in Lighthill's theory is assumed to be neutrally buoyant and close-fitting, but capable of deforming to "squeeze through" the tube. Lighthill applied classical lubrication theory to determine the flow field in the gap between the particle and the wall. The results predict that both the thickness of the lubrication layer and the additional pressure drop should vary with $U^{\frac{1}{2}}$.

The qualitative relevance of Lighthill's analysis for non-neutrally buoyant viscous drops can be tested by plotting measured values of h^2 as a function of $U/\Delta\rho$. The results for both Newtonian and viscoelastic suspending fluids are shown in Figure 9. Each point for the Newtonian systems actually represents an average value for h^2 over all drop sizes for each choice of drop fluid and V, since it was previously found for Newtonian systems that there is no measurable variation of h with λ for sufficiently large values of $\Delta\rho/\rho_o$ where the lubrication approximation is likely to be most valid. In the viscoelastic systems, h varies with λ and in these cases only the values of h for the largest drops were used in Figure 9. The linear relationship between h^2 and $U/\Delta\rho$ suggests that indeed, the velocity of the particle and gap width are determined by forces generated in a lubrication layer, albeit one which acts on only one "side" of the drop, since the particles in the present study are neither concentric nor close-fitting. The analysis of Lighthill applies to solid elastic particles, and the data for the Newtonian cases shown in Figure 9 exhibit a slight dependence on the drop viscosity, especially near the origin.

Although no direct dependence of the drop velocity and gap width on the value of σ could be established, Figure 9 suggests the coefficient of proportionality for the lubrication correlation between h^2 and U is larger for smaller values of σ for the Newtonian suspending fluid. Indeed, when the lubrication analysis is modified to account for the fact that the particle is a liquid drop, the gap thickness h remains dependent on $U^{\frac{1}{2}}$, even as $\sigma \to 0$, but the constant of proportionality increases by a factor of two as σ decreases fron infinity to zero. Also, the lubrication estimation of the dependence of the additional pressure drop on $U^{\frac{1}{2}}$ is strongly affected by σ, as will be seen shortly.

The pressure generated in the lubrication layer which balances the non-neutral buoyancy of the drop is proportional to $\mu_o U/h^2$ for any value of σ. Thus, we expect that the effect of an increase in the viscosity of the suspending fluid will be a greater gap thickness for a fixed value of $\Delta\rho/\rho_o$ and, strictly, for fixed σ. However, since the variation of the coefficient of proportionality with σ is relatively small for Newtonian cases over the range of σ covered here, and since no variation can be discerned for the viscoelastic cases, we approximate each set of data by a single curve. The values of h^2 and hence the slopes of the two lines which approximate the Newtonian and viscoelastic data shown in Figure 9 should therefore be related to the viscosities of the suspending fluids. The viscosity of the Newtonian solution, 95.75% aqueous glycerin, was determined to be 4.17 P. The viscosity of the shear-thinning 0.5% Separan solution depends strongly, of course, on the flow rate. However, for sufficiently small values of V (and U), the viscosity is just the zero-shear rate viscosity which we have estimated from viscometric data to be $\sim$14.5 P. Thus, the ratio of slopes in Figure 9 for small values of U (i.e., near the origin) is expected to be 14.5/4.17 = 3.5. This agrees well with the actual ratio of 3.1.

It is surprising, however, that the linear relationship between U and h^2 holds for the viscoelastic case over a wide range of flow rates.

The effective viscosity of the suspending fluid, which can be deduced from Table 1, decreases by as much as 70% based on the wall shear rate as the flow rate increases over the range covered in Figure 9. We would expect, on the basis of the dependence of h^2 on μ_o alone, that h^2 should decrease by as much as 50% from its "zero-shear rate" value due to shear-thinning. Instead, there appears to be no effect of the variations in the suspending fluid viscosity. We believe that the explanation for this fact involves the normal stresses which are present in the viscoelastic suspending fluid. The primary normal stress difference gives rise to a hoop stress by creating a tension in the curved streamlines around the drop. This tension in the streamlines is greatest at the location of greatest shear rate, which is clearly in the gap between the particle and the tube wall. The net effect of normal stress induced hoop stresses is thus to "push" the particle away from the tube wall, toward the center-line. Now the magnitude of the primary normal stress difference for 0.5% Separan AP-30 increases approximately as the square of the shear rate in the range of interest (Leal, Skoog and Acrivos, 1971), but the viscosity of 0.5% Separan AP-30 decreases as the square of the shear rate. Thus, as U is made larger, the "increase" in h^2 from the increased hoop thrust and the decrease in h^2 which is caused by the decrease in suspending fluid viscosity tend to balance one another. An apparent consequence of this off-setting effect is that the qualitative variation of h^2 with U is not changed in a viscoelastic fluid from the Newtonian lubrication result.

The lubrication analysis for a solid particle predicts also that the additional pressure drop ΔP^+ should vary with $U^{\frac{1}{2}}$. This result depends crucially on the axial force on the lubrication surface which, in turn,

depends on the shear stress at the particle surface. If the particle is fluid, the appropriate boundary condition at the particle surface is continuity of stress and velocity rather than the no-slip condition which is appropriate for a solid particle. Most notably, the shear stress approaches zero on the drop surface as the viscosity of the drop tends toward zero. Hence, the axial force evaluated from lubrication considerations alone must also approach zero in the same limit and the lubrication estimate for the axial force clearly becomes inadequate as the viscosity of the drop is made smaller. In this case, the drag on the particle, and therefore the additional pressure drop, must be determined by other mechanisms. We expect, then, that ΔP^+ will scale with $U^{\frac{1}{2}}$ only for "highly viscous" drops. Data from Table 3 show that this is the case. For the more viscous drops, System 2 and System 6 (σ = 2.63 and 2.68, respectively), the measured values for ΔP^+ scale (to within 20%) with $U^{\frac{1}{2}}$. Furthermore, when the lubrication approximation is written for a shear-thinning fluid using a power-law model, it can be shown that ΔP^+ should vary with $U^{n/n+1}$ where n is the power-law index. Thus, for fluids with $n < 1$, ΔP^+ should be less sensitive to U than for a Newtonian fluid ($n = 1$). Indeed, the data for ΔP^+ from Table 3 for viscous drops suspended in 0.5% Separan (Systems 2V and 5V) scale with $U^{0.31}$ (to within 20%), the exponent computed using $n = 0.45$ (see section 2).

The lubrication model also provides a useful qualitative explanation of the fact, noted in section 3, that ΔP^+ becomes relatively independent of $\Delta\rho/\rho$ for large drops, once $\Delta\rho/\rho$ exceeds ~ 0.02. From the point of view of lubrication theory, as the gap becomes smaller it takes smaller decreases in the gap width to yield a given incremental increase in the hydrodynamic lift.

This reflects the fact that pressures in the lubrication layer scale with $1/h^2$. Thus, as $\Delta\rho/\rho$ is made larger, the variation in h which is required to balance drop buoyancy becomes smaller, and quantities such as ΔP^+, which depend on h itself, should become relatively insensitive to further increases in $\Delta\rho/\rho$. [This reasoning assumes that ΔP^+ shows a dependence on h which is weaker than $1/h^2$. In fact, lubrication analysis predicts that ΔP^+ varies as only 1/h.] Indeed, it would take an infinite value of $\Delta\rho$, from the strict viewpoint of lubrication theory, to reduce the gap width, h, to zero. Thus, $\partial h/\partial(\Delta\rho)$ must obviously decrease as $\Delta\rho$ increases. For example, if we consider the case of large drops ($\lambda < 0.83$) in a highly viscous fluid ($\sigma > 1$), with reference to Figure 8, the values for h are approximately 0.30, 0.12 and 0.10 corresponding to $\Delta\rho/\rho_0$ ranging from 0.0, 0.020 to 0.037, respectively. Further, since h will be smaller for a larger drop (other factors such as $\Delta\rho$ being equal), larger drops should be expected to display asymptotic behavior for lower values of $\Delta\rho/\rho$. The small drops, too, will become less sensitive to $\Delta\rho$, but only at larger values of $\Delta\rho/\rho_0$, apparently outside the range of this study.

We have already noted that drop deformation is essential to the generation of hydrodynamic lift. This would seem to suggest that the results for ΔP^+ and U/V should show a dependence on the degree of deformation induced by the flow. Indeed, it was noted in the preceding section, for both the Newtonian and viscoelastic suspending fluids, that the effects of an increase in the value of the deformation parameter Γ were an increased mobility and a decreased additional pressure drop. The theoretical

analyses of Hyman and Skalak (1972b) and Fitz-Gerald (1969) suggest that any factor which causes increased drop deformation will result in a simultaneous increase in the drop's relative velocity and a decrease in the additional pressure drop. Together these factors indicate a decreased resistance to flow as the flow rate increases, a behavior which is at least superficially similar to a "shear-thinning" rheological response. The data for both the Newtonian viscoelastic systems studied here tend to confirm these implications of the available theories.

Although drop deformation is sensitive to the value of the flow rate (through Γ), especially for the Newtonian suspending fluid cases, it is relatively insensitive to the drop viscosity. This is not altogether surprising. Taylor (1932) showed that the degree of drop deformation in a simple shear flow with negligible wall interaction is proportional to $(19\sigma + 16)/(16\sigma + 16)$. This coefficient varies only from 1.00 to 1.19 as σ varies from zero to infinity. Although the flow field in the present study is not simple shear and wall effects cannot be neglected, D shows a variation with σ which is comparable in magnitude to Taylor's result. The present data and Taylor's theory both indicate that a more viscous drop deforms to a greater degree than a less viscous one in a Newtonian fluid, but the measured effect is so small that it does not lower the additional pressure drop appreciably.

The value of the drop viscosity makes a more substantial "direct" contribution to the additional pressure drop for the Newtonian case through the simple replacement of suspending fluid by drop fluid of a different viscosity. The contribution to ΔP^+ from this mechanism is

clearly negative for $\sigma < 1$ and positive for $\sigma > 1$. However, the fact that the profile of data for ΔP^+ as a function of λ for System 4 exhibits a maximum at an intermediate value of λ in a Newtonian suspending fluid for viscosity ratios near unity suggests that there are other competing mechanisms involved in the determination of ΔP^+. We have noted already one such mechanism, namely, drop deformation which increases with λ and tends to cause a decrease in the additional pressure drop. This effect is relatively insensitive to σ and other material parameters as noted above. Other mechanisms which contribute to the additional pressure drop have been shown by the experimental results of (I) and the calculation of Brenner (1973) for Newtonian suspending fluids to include alteration of the flow field external to the drop and interaction between the drop and the tube wall. Both of these effects increase in magnitude with an increase of λ and contribute an increment to ΔP^+ which is positive for all choices of the material parameters. For $\sigma > 1$, these latter mechanisms and fluid replacement all contribute to an increase in ΔP^+ with λ. For $\sigma < 1$, on the other hand, the effects of flow field alteration by the drop and the walls compete with fluid replacement and the effect of variations in ΔP^+ with λ depends upon which is dominant. Apparently, for small λ drops in the Newtonian suspending fluid, flow field alterations are more important and ΔP^+ increases with λ, even for $\sigma < 1$. Eventually, however, the fluid replacement effect must become dominant, and the value of ΔP^+ then decreases as the drop size is increased further. Thus, for system 4, which has a relatively low viscosity ratio, $\sigma = 0.35$, the positive contributions of flow field alteration and wall interaction are eventually cancelled, as λ is made larger, by the negative contribution from simple fluid replacement. The important inference here

is that simple fluid replacement must eventually establish the large λ behavior for ΔP^+ regardless of the additional mechanisms that are significant for smaller drop sizes, and the magnitude of ΔP^+ will then depend mainly on the value of σ. It is, of course, not clear how large λ must be for the fluid replacement mechanism to become dominant, and it must be expected that this will depend significantly upon all the material parameters. Support for this view is provided by our Newtonian suspending fluid data for the largest values of λ which show that ΔP^+ increases with σ at a rate which appears to be independent of the drop eccentricity, as would in fact be expected when the dominant mechanism is simple fluid replacement.

Equation (2) indicates that the other mechanisms, such as flow field alteration, will also act to increase ΔP^+ as σ is made larger, but in a manner which depends on the degree of eccentricity. All of the Newtonian suspending fluid data do, in fact, display larger values of ΔP^+ with increased values of σ.

A very different result was noted in Section 3 for the viscoelastic suspending fluid. In this case, the effect of drop viscosity on the extra pressure drop was found to be negligible. This result is apparently a consequence of the limited range of values for λ covered by the experiments. It was shown in (I) that ΔP^+ for sufficiently large neutrally buoyant drops in a viscoelastic suspending fluid is dominated by the simple fluid replacement mechanism, and the sign of ΔP^+, which is positive for small λ, will depend, as in the Newtonian case, upon whether σ is greater or less than unity. That is, for $\sigma < 1$, ΔP^+ eventually becomes negative as λ is made larger. In partial explanation of the independence of ΔP^+

on σ in the present experiment, even at the largest values of λ, we can suggest only that the values of λ at which ΔP^+ is dominated by simple fluid replacement [say, for example, the value at which ΔP^+ changes sign from positive to negative (for $\sigma < 1$)], is larger for the viscoelastic case than for the Newtonian suspending fluid. Apparently, the values of λ studied here were simply not large enough for the effect of fluid replacement to dominate contributions from the remaining mechanisms for non-neutrally buoyant drops. For example, if the ΔP^+ versus λ curves from (I) for Newtonian System 3c ($\sigma = 0.58$) and viscoelastic System 7c ($\sigma = 0.44$) are compared, it can be seen that ΔP^+ changes sign from positive to negative at a value of $\lambda = 0.95$ for the Newtonian case (3c), but not until $\lambda = 1.12$ for the viscoelastic case (7c). From these observations, it may be suggested that if λ were made sufficiently large, ΔP^+ for non-neutrally buoyant drops would also begin to display a strong dependence on σ owing to fluid replacement.

This does not, of course, address the question as to why $\Delta P^+ R_o/\mu_o V$ should be independent of σ for smaller values of λ for drops suspended in the viscoelastic fluid. One possibility is that the behavior of smaller drops is dominated by elastic properties of the suspending fluid rather than shear-thinning which is used to correlate the data for large drops. The Deborah number from Section 2 is written as

$$De = \frac{(U - V)\theta}{2D\lambda R_o}$$

where $2D\lambda R_o$ is the "length" of the deformed drop, $(U - V)$ is the difference between the drop velocity and the suspending fluid average velocity, and θ is the fluid relaxation time. Values for De in the present experiment

are actually larger for the smaller values of λ. The data for the viscoelastic suspending fluid show that as λ is made larger, D increases and U tends toward V (i.e. U/V decreases monotonically). Both of the effects of larger λ, in the range of λ covered here, act to decrease the value of De. This indicates that elastic effects should be more significant for the smaller values of λ studies here. This reasoning cannot hold, of course, as $\lambda \to 0$ since in this limit, the particle velocity tends toward the local velocity of the suspending fluid with λ^2 dependence, and hence, $De \to 0$. Thus, if elastic effects are significant for any cases in this experiment, we expect them to be observed for smaller but nonzero values of λ. It is possible that as λ is increased from zero, De becomes sufficiently large for the onset of elastic behavior in the suspending fluid which renders σ unimportant. However, as the drop size is made larger, the gap width between the drop and the wall decreases and so does De. The large λ behavior is then governed by the lubrication considerations and eventually the simple fluid replacement mechanism described previously. It should be noted, however, that the largest value of De estimated for the conditions of the present experiments is only 0.20, and it is usually held that strong elastic effects are not observed until De is increased to a value of one or two. In point of fact, the "onset" value of De at which elasticity is important for a given experiment can be verified only by a systematic variation of the fluid response time which was not done in the present study. The idea that dominant fluid elasticity may be responsible for the observed insensitivity to σ for smaller values of λ must be regarded as speculative. We may, however, mention that results from related experiments by Sigli and Coutanceau (1977) on a rigid sphere ($0.25 \leq \lambda \leq 0.75$) sedimenting in a vertical cylindrical tube are at least

qualitatively consistent with the suggestion of dominant elasticity for relatively small values of De. In that case, fluid elasticity was found to have a strong effect on the drag on the sphere for values of the Weissenberg number, $We = \theta V_o/R_o$ where V_o is the terminal velocity of the sphere, as low as 0.05. It was observed that elasticity of the suspending fluid was enhanced by the presence of the tube wall.

The data for the relative velocity of the drop shows a maximum at intermediate λ for some drops in a Newtonian suspending fluid. This suggests that drop mobility, too, is determined by competitive effects. Existing theoretical calculations for small λ suggest that there are two primary factors which determine the velocity of eccentric drops in a Newtonian fluid. First, there is the hydrodynamically induced slip velocity, which causes the drop to move at a velocity less than the undisturbed velocity of the surrounding fluid. Second, the drops move at a velocity that reflects the undisturbed fluid velocity at the radial position occupied by their centerpoint, and the undisturbed velocity varies relative to the mean, as a function of radial position (it may be noted, for example, that the ratio of the local undisturbed fluid velocity to the mean velocity, V, varies from zero at the tube wall to two at the centerline in a simple Poiseuille flow). The drops in the present study are not "small", but still, the velocities of the undisturbed pathlines "occupied" by the drop apparently remain significant to the determination of the drop velocity at intermediate values of λ, and it is this fact which we believe accounts for the qualitative changes in U/V as a function of λ as the density difference, $\Delta\rho/\rho_o$, is increased. Let us consider these ideas in more detail.

When $\Delta\rho/\rho_o$ is small, the gap between the drop and the tube wall decreases as the drop is made larger and though the center of the drop remains near the center of the tube, it gradually moves outward toward the wall, thus occupying undisturbed streamlines with velocities lower, on average, than those closer to the centerline. For example, Newtonian System 4 exhibits a monotonic decrease in h from 0.40 for λ = 0.51 to 0.16 for λ = 0.87 for V = 0.56 cm/s (see Table 1), and U/V is expected, as a consequence, to also decrease monotonically as it is, in fact, observed to do. On the other hand, higher density drops show comparatively little effect of λ on h. For Newtonian System 6, for example, h varies only between 0.12 and 0.14 over the entire range of drop sizes. Since the data show that gap width does not change with size, the center of the smallest drop must be situated closer to the tube wall then the center of a larger drop in this case. Thus, as the size of the drop increases in a Newtonian suspending fluid, the center of the drop "moves" toward the tube centerline, and the drop occupies more of the region of greater undisturbed velocities. As a result, the drop at first moves with a greater relative velocity in the Newtonian suspending fluid as λ is increased.

However, the drop exhibits a maximum velocity around $\lambda \simeq 0.7$ for all Newtonian systems except System 4. For large drops with values of $\lambda > 0.7$, the drop nearly fills the tube and wall interactions, which tend to retard the motion of the drop, apparently become more significant, as in the neutrally buoyant case. Thus, U/V decreases with further increase in λ until $\lambda \to 1$. Then, U/V remains constant with increasing λ since further increases in volume lead to increases in drop length rather than changes in its cross-section [cf. (I)].

In contrast to the Newtonian case, U/V is a monotonically decreasing function of λ for all of the viscoelastic suspending fluid systems which we studied. Once

again, this result appears to be correlated with the relationship between λ and the gap width, h. We have already noted that h is significantly larger for the viscoelastic suspending fluids than for the Newtonian fluids. This difference is greater for smaller drops and lower flow rates. In addition, the viscoelastic systems show a monotonic decrease in the gap width as the size of the drop increases for all flow rates. Thus, the behavior for the viscoelastic systems is qualitatively similar to the Newtonian System 4, the least non-neutrally buoyant case in the present study.

The suggestion that drop mobility depends, at least in part, on the undisturbed pathlines sampled by the drop also helps to explain the results of Figure 6 which show that U/V is often larger for small drops in the viscoelastic systems compared to the Newtonian cases, but never larger for large drops. The cross-over in magnitude of U/V with λ which occurs in comparing results for Newtonian and viscoelastic suspending fluids appear to be a consequence of differences in the undisturbed velocity profiles for Newtonian and viscoelastic fluids. We have already noted that a Newtonian fluid flowing through a straight tube will exhibit a parabolic velocity profile with a maximum local velocity at the tube centerline which is twice the average veloctiy, 2V. On the other hand, if a power-law model with index $n = 0.45$ (see Section 2) is used to describe the suspending fluid, the undisturbed velocity profile is considerably blunted near the center of the tube. The maximum velocity on the centerline is less than the Newtonian case, only 1.6 V. For a fixed volume flow rate, the Newtonian fluid exhibits larger velocities than the viscoelastic fluid for dimensionless distances from the tube centerline,

β, up to $\beta = 0.6$. From $\beta = 0.6$ to $\beta = 1.0$ (the tube wall), on the other hand, the power-law fluid exhibits the greater velocities. Since the relative velocity of the drop depends in part on the velocity of the undisturbed streamlines occupied by the drop, it follows that small, highly eccentric drops which occupy the region adjacent to the wall should move more rapidly in a power-law fluid than in a Newtonian fluid (because the shear-thinning fluid itself is moving faster). Thus, it is clear that the mobility of small non-neutrally buoyant drops is favored for a shear-thinning fluid, at least insofar as the undisturbed profiles are concerned. The data from the present experiments show that increased values of $\Delta\rho/\rho_o$ and decreased values of V (for $\Delta\rho/\rho_o \neq 0$), alone or together, cause the drop to assume a more eccentric position in the tube. Figure 6 shows that U/V (Newt.) - U/V (Visco.) is more negative for smaller values of V and for larger values of $\Delta\rho/\rho_o$. This is in accord with the simple mechanism proposed above. As a small drop is made larger, however, more of the center of the tube is occupied by the drop, i.e., β decreases, and the drop becomes less eccentric. The undisturbed velocity in this region is not only greater than that near the tube wall, but is also relatively greater for the Newtonian suspending fluid than for the viscoelastic fluid. Thus, as λ is made larger, it may be expected that the mobility of drops will ultimately be favored for the Newtonian suspending fluid.

We now turn to the relative magnitude of ΔP^+ for the two suspending fluids. It is noteworthy that $\Delta P^+ R_o/\mu_o V$ (and ΔP^+ itself) in the viscoelastic suspending fluid falls well below the Newtonian values, for approximately equal values of σ, λ, and $\Delta\rho/\rho_o$. However, the complete quantitative significance of this observation is difficult to assess,

because the dimensionless values plotted in Figure 3 for the viscoelastic fluids use the viscosity evaluated at the wall shear-rate. Since this is the highest shear rate in the flow, the value of μ_o used in Figure 3 is the minimum possible value for the particular undisturbed flow conditions and thus $\Delta P^+ R_o/\mu_o V$ (as plotted) is the maximum value which could have been assigned to the viscoelastic data for a given ΔP^+, R_o, and V. Any other choice for μ_o in scaling ΔP^+ will tend to drive the Newtonian and viscoelastic data further apart. Although $\Delta P^+ R_o/\mu_o V$ is obviously lower for the viscoelastic suspending fluid, values for the dimensionless extra pressure drop in Figure 3 show similar dependence on Γ for both suspending fluids. It appears as if the data correlate without need for explicit consideration of the Deborah number, or any other viscoelastic parameter which depends, in principle, on V. This seems to contradict our previous speculation that ΔP^+ may be independent of σ for smaller drops owing to elastic effects in the suspending fluid. However, the data of Sigli and Coutanceau (1977) suggest another possible explanation consistent with our results. Their results show that the drag on a rigid sphere moving through a viscoelastic fluid in a circular tube ($0.25 \leq \lambda \leq 0.75$) is considerably smaller than the drag on the same sphere in a Newtonian fluid, even when shear-thinning is taken into account. The decrease in the relative drag takes place as We ($= \mu_o V_o/R_o$) is increased from zero (Newtonian) to approximately 0.5 for $\lambda = 0.5$. For values of We > 0.5, the relative drag is nearly independent of We, and in this regime of We, the drag shows the same qualitative dependence on V_o in both Newtonian and viscoelastic suspending fluids, even though the magnitude of the drag is smaller in the viscoelastic fluid. The implications of these results are that elastic effects

are observed at values of We considerably smaller than usually expected, and that these effects may become asymptotic in We at relatively small values of We.

5. Comparison with Theory

Our discussion of the experimental results has focused until now on a description of the qualitative effects of the various independent variables on the measured quantities. Now, a comparison between the data for Newtonian fluid systems and the available theoretical calculations for ΔP^+ and U in a Newtonian fluid will hopefully provide additional insight into the various physical phenomena involved and test the range of applicability of the analyses. It should be remembered, in making such a comparison, that the analytical theories leading to equations (1) and (2) are restricted to small drops, $\lambda << 1$, which have spherical shapes and to a Newtonian suspending fluid. Furthermore, there is no consideration of wall effects, except insofar as the bounding wall gives rise to the undisturbed, Poiseuille flow.

Equation (1) for the relative drop velocity consists of two terms. The slip velocity, which arises due to the parabolic nature of the undisturbed velocity profile, is negative, indicating that the particle moves more slowly than the adjacent fluid, and is independent of the lateral position of the drop in the tube. The second term is more important here and accounts for the eccentric position of the drop due to its non-neutral buoyancy. The small λ expansion indicates, at leading order, that a drop moves more with the velocity of a fluid element at the same radial position, and it is the variation in this fluid velocity with radial position which is responsible for the variation in drop velocity with β.

No theory presently exists for predicting the position of the drop relative to the wall, i.e., β which appears in equations (1) and (2). Although this position is presumably a consequence of a balance between buoyancy forces and hydrodynamic lift forces, calculation of the latter would require an accurate calculation of the deformed drop shape — an exceedingly difficult problem. Consequently, (1) is not capable of *à priori* predictions for some of the qualitative trends displayed by the data — the variation of U/V with V, for example. However, β can be measured from photographs and then used in (1) to evaluate U/V for quantitative comparison with the data.

Figure 11 shows U/V as a function of λ for two systems selected to illustrate the effect of σ. Equation (1), using the appropriate measured value for β for each case, is compared to the data. Qualitative agreement between the two is good, inasmuch as a maximum value for U/V at intermediate λ is predicted only for the systems which actually show one. Otherwise, (1) predicts a monotonic decrease in U/V as λ is made larger. It may be noted that the maximum in U/V actually results from a minimum in the experimentally observed values of β as a function of λ.

Quantitative comparison between the data and (1) shows that the effect of σ on U/V is not as significant as indicated by the slip velocity term. The data exceed the predicted values for U/V for the high viscosity drop systems, 2 and 6. However, the reverse is true for the low viscosity drop systems, 3, 4, and 5. The coefficient in (1), $4\sigma/(3\sigma + 2)$, varies from 0.41 (σ = 0.30, System 5) to 1.07 (σ = 2.68, System 2), while the term involving β is independent of σ. The predicted variation in U/V with σ for the

range of values of σ used in this experiment is then $(1.07 - 0.41)\ \lambda^2$. However, the data display a much weaker dependence on σ especially for large values of λ (see Figure 11).

The only means by which (1) predicts any variation in U/V with V is through the measured value of β. Figure 11 shows that the variation in U/V with V is not adequately predicted by (1). An effect not taken into account in the derivation of (1) is the deformed shape of the drop. It has already been suggested that deformation is partly responsible for the observed increase in U/V with V, but the theory which leads to (1) predicts that the deformation of the drop should be unimportant if

$$\frac{\mu_o V \lambda \beta}{\gamma} << 1$$

The value of the left side of the inequality never exceeds 0.06 for the range of material parameters used in the present study indicating that drop deformation should be insignificant. Nevertheless, the photographs show that the drop undergoes appreciable deformation, and the data show a dependence on the degree of deformation, as already outlined in Section 3. A mechanism that could induce increased deformation which is not included in the theoretical analysis is the hydrodynamic interaction between the drop and the wall.

Equation (2) for the additional pressure drop also contains one term for the concentric contribution and another for the effect of non-neutral buoyancy. The neutrally buoyant term depends on λ^5 while the non-neutrally buoyant one contains $\beta^2\lambda^3$. Table 4 shows the magnitude of these terms, relative to each other, at the values of σ used in the present experiment.

The predicted contribution due to drop eccentricity is always positive and only weakly dependent on the viscosity of the drop. The concentric term, which includes the contribution due to the replacment of fluid, can be positive or negative, depending on the viscosity ratio but is always considerably smaller in magnitude than the eccentric term. The effect of drop eccentricity is always to increase ΔP^+ over the neutrally buoyant case. The value of σ where $\Delta P^+ = 0$ is predicted to depend on β^2/λ^2, decreasing from $\sigma = 0.48$ for $\beta^2/\lambda^2 = 0$ to $\sigma = 0$ for $\beta^2/\lambda^2 = 0.5$.

Once again, β must be evaluated from photographs of the drops for quantitative comparison of the theoretical equation (2) with the data, The dependence of ΔP^+ on λ for selected Newtonian systems is shown in Figure 10. For viscous drops, agreement between data and theory is good with the values for ΔP^+ from the data exceeding the value given by (2) by 50% at most. The deviation is smaller for small values of λ which is to be expected since the theory is strictly valid only in the small λ limit. Somewhat surprisingly, though, quantitative agreement is also better at large values of λ for viscous drops. As λ is made larger, the degree of drop eccentricity decreases as indicated by the measured value for β, $0.1 < \beta < 0.2$ for $\lambda > 0.7$. For such small values of the eccentricity parameter, the contribution to ΔP^+ due to non-neutral buoyancy in equation (2) is small compared to the remaining term. Thus, it appears that agreement is better when the neutrally buoyant term is the dominant component of ΔP^+. The small λ theory lacks the effect of the wall which apparently acts to increase the necessary additional pressure drop.

Agreement between data and theory is not as good for low viscosity drops because the eccentricity term, which unrealistically neglects the

effect of the wall, is relatively more important for low values of σ than for highly viscous drops, as indicated in Table 4. As a result, the value of ΔP^+ calculated from (2) even has the incorrect sign over the entire range of λ for System 4 ($\sigma = 0.30$). The deviation between theory and experiment increases with λ, a consequence (presumably) of an increase in the magnitude of the neglected wall interaction. On the other hand, in the small λ region, quantitative agreement is still satisfactory, even for low viscosity drops.

Dependence of $\Delta P^+ R_o/\mu_o V$ on V enters only through the effect of V on β, just as in equation (1) for U/V. A comparison shows the predicted variation of $\Delta P^+ R_o/\mu_o V$ with V is much less than indicated by the data, although (2) at least correctly predicts that the qualitative effect of an increase in V is a lower value for ΔP^+.

Bungay and Brenner (1973a) have shown that if wall effects are taken into account, a higher value of ΔP^+ is obtained for given values of λ and $\Delta\rho$, at least for rigid particles. They calculated ΔP^+ for a small, rigid sphere in the presence of the tube wall, using the method of reflections combined with the reciprocal theorem. The result for $\Delta P^+ R_o/\mu_o V$ shows the coefficient of the $\beta^2\lambda^3$ term to be 226. Now, as the authors point out, if (2) is used in the limits $\beta \to 1$, $\sigma \to \infty$, the coefficient of the eccentricity, $O(\lambda^3)$ term is only 160/3, less than one-fourth the value if wall interaction is included. The data for ΔP^+ for drops in the present experiment generally lie above the value from (2), but below the near-wall prediction for rigid particles. No theoretical result for wall effects on fluid drops is available at the present time.

6. Conclusions

Data from a study of the creeping motion of non-neutrally buoyant drops in a horizontal tube have been presented. The measured quantities were the additional pressure drop, the velocity of the drop, the shape, and the gap width between the drop and the wall. These were measured as a function of the material and flow parameters, including drop viscosity, drop density, the size of the drop, the flow rate, and the suspending fluid rheology.

A major purpose of the study was to identify the effects of variations in the lateral position of the drop and this was accomplished through variations in the density of the drop fluid. Even small density differences ($\Delta\rho/\rho_0 = 0.020$) produced qualitative differences in the dependence of the measured quantities on some variables. For example, eccentrically located particles showed a maximum mobility for an intermediate drop size which is not observed for concentric particles.

The effect of the eccentric position of the drop was to raise the pressure drop over the value for the concentric case. A simultaneous decrease in the relative velocity of the drop was also noted. The dependence of ΔP^+ and U/V on $\Delta\rho/\rho_0$ for large drops decreased as $\Delta\rho/\rho_0$ was made larger. Thus, it appears that although small density differences can make significant changes in the measured values for the quantities studied here, large density dfferences do not produce correspondingly large deviations from the neutrally buoyant results. Indeed, asymptotic behavior will be attained at lower values of $\Delta\rho/\rho_0$ as the size of the drop is made larger. The results of this study seem to indicate that small density differences

should definitely be considered in the motion of particles in porous media flow or other related problems, since most practical conditions will probable involve non-neutrally buoyant suspensions. However, above minimal values for $\Delta\rho/\rho_0$, further non-neutral buoyancy can be safely neglected.

The viscoelasticity of the suspending fluid was an important factor in the determination of the shape of the drops as well as the equilibrium lateral position assumed by the drops during flow. There were corresponding changes in ΔP^+ and U/V from the Newtonian case. Since the combination of increased viscosity and normal stress effects in the viscoelastic fluid provides a mechanism that tends to "move" particles further away from the wall, the effects of increased density differences were felt at larger values of $\Delta\rho/\rho_0$ than for the corresponding Newtonian case. Thus, the "asymptotic regime" mentioned above will apparently occur at larger values of $\Delta\rho/\rho_0$ for viscoelastic suspending fluids.

For the Newtonian systems, qualitative agreement was generally found between the data and available small λ theoretical expressions that take into account the eccentric position of the drop. For large values of λ, the effect of drop fluid viscosity is crucial to the value of ΔP^+, and, therefore, theoretical derivations for solid particles based on lubrication theory are of use in estimating the additional pressure drop only for viscous drops. However, the mobility of the drop is much less dependent on the drop viscosity and it was shown that lubrication theory can be used to correlate the mobility data. Furthermore, it was found that if a power-law model was used to account for the shear-thinning of the viscoelastic suspending fluid, data for ΔP^+ for large, viscous drops could be

correlated with results from lubrication theory.

Acknowledgment

This work was supported by a grant from the National Science Foundation. The authors wish to thank Chris Bockenstette for her assistance in carrying out some of the experiments.

References

Brenner, H. 1970 Pressure drop due to the motion of neutrally buoyant particles in duct flows. J. Fluid Mech. 43, 641.

Bungay, P. M. and Brenner, H. 1973a Pressure drop due to the motion of neutrally buoyant particles in duct flows. III. Non-neutrally buoyant spherical droplets and bubbles. ZAMM. 53, 187.

Bungay, P. M. and Brenner, H. 1973b The motion of a closely-fitting sphere in a fluid-filled tube. Int. J. Multiphase Flow 1, 25.

Chan, P. C.-H. and Leal, L. G. 1979 The motion of a deformable drop in a second-order fluid. J. Fluid Mech. 92, 131.

Deiber, J. A. and Schowalter, W. R. 1979 Flow through tubes with sinusoidal axial variations in diameter. A.I.Ch.E. J. 25, 638.

Fediw, P. and Newman, J. 1977 Mass transfer at high Peclet numbers for creeping flow in a packed-bed reactor. A.I.Ch.E. J. 23, 255.

Fitz-Gerald, J. M. 1969 Mechanics of red-cell motion through very narrow capillaries. Proc. Roy. Soc. London B174, 193.

Goldsmith, H. L. and Mason, S. G. 1963 The flow of suspensions through tubes. II. Single large bubbles. J. Colloid. Sci. 18, 237.

Hetsroni, G., Haber S. and Wacholder, E. 1970 The flow field in and around a droplet moving axially within a tube. J. Fluid Mech. 41, 689.

Ho, B. P. and Leal, L. G. 1975 The creeping motion of liquid drops through a circular tube of comparable diameter. J. Fluid Mech. 71, 361.

Hochmuth, R. M. and Sutera, S. P. 1970 Spherical caps in low Reynolds number tube flow. Chem. Engng. Sci. 25, 593.

Hochmuth, R. M., Marple, R. N. and Sutera, S. P. 1970 Capillary blood flow. I. Erythrocyte deformation in glass capillaries. Microvasc. Res. 2, 409.

Huppler, J. P., Ashare, E. and Holmes, L. A. 1967a Rheological properties of three solutions. I. Non-Newtonian viscosity, normal stresses, and complex viscosity. Trans. Soc. Rheol. 11, 159.

Huppler, J. P., MacDonald, I. F., Ashare, E., Spriggs, T. W., Bird, R. B. and Holmes, L. A. 1967b Rheological properties of three solutions. II. Relaxation and growth of shear and normal stresses. Trans. Soc. Rheol. 11, 181.

Hyman, W. A. and Skalak, R. 1972a Viscous flow of a suspension of liquid drops in a cylindrical tube. Appl. Sci. Res. 26, 27.

Hyman, W. A. and Skalak, R. 1972b Non-Newtonian behavior of a suspension of liquid drops in tube flow. A.I.Ch.E. J. 18, 149.

Leal, L. G., Skoog, J. and Acrivos, A. 1971 On the motion of gas bubbles in a viscoelastic fluid. Can. J. Chem. Engng. 49, 569.

Lighthill, M. J. 1968 Pressure-forcing of tightly-fitting pellets along fluid-filled elastic tubes. J. Fluid Mech. 34, 113.

Marshall, R. J. and Metzner, A. B. 1967 Flow of viscoelastic fluids through porous media. Ind. Engng. Chem. Fund. 6, 393.

Neira, M. A. and Payatakes, A. C. 1979 Collocation solution of creeping Newtonian flow through sinusoidal tubes. A.I.Ch.E. J. 25, 725.

Olbricht, W. L. and Leal, L. G. 1980 The creeping flow of immiscible drops through a converging/diverging tube, in press.

Olbricht, W. L. 1980 PhD Thesis, California Institute of Technology, Pasadena, CA.

Payatakes, A. C. and Neira, M. 1977 Model of the constricted unit cell type for isotropic granular porous media. A.I.Ch.E. J. 23, 922.

Prothero, J. and Burton, A. C. 1961 The physics of blood flow in capillaries. I. The nature of the motion. Biophys. J. 2, 199.

Prothero, J. and Burton, A. C. 1962 The physics of blood flow in capillaries. III. The pressure required to deform erythrocytes in acid-citrate-dextrose. Biophys. J. 2, 213.

Seshardi, V., Hochmuth, R. M., Croce, P. A. and Sutera, S. P. 1970 Capillary blood flow. III. Deformable model cells compared to erythrocytes in vitro. Microvasc. Res. 2, 434.

Sigli, D. and Coutanceau, M. 1977 Effect of finite boundaries on the slow laminar esothermal flow of a viscoelastic liquid around a spherical obstacle. J. Non-Newt. Fluid Mech. 2, 1.

Sutera, S. P., Seshardi, V., Croce, P. A. and Hochmuth, R. M. 1970 Capillary blood flow. II. Deformable model cells in tube flow. Microvasc. Res. 2, 420.

Taylor, G. I. 1932 The intrinsic viscosity of a fluid containing small drops of another fluid. Proc. Roy. Soc. A138, 41.

Tozeren, H. and Skalak, R. 1978 The steady flow of closely-fitting incompressible elastic spheres in a tube. J. Fluid Mech. 87, 1.

System	Suspending fluid	Drop Fluid Viscosity (P)	$\Delta\rho/\rho_o$	Viscosity ratio: Flow rate, V (cm/s) 0.32	0.56	0.80	$\Gamma = \mu_o V/\gamma$ Flow rate, V (cm/s) 0.32	0.56	0.80
2	glycerin/water	11.0	0.020	2.63	2.63	2.63	0.061	0.11	0.15
3	"	3.21	0.0.8	0.77	0.77	0.77	0.061	0.11	0.15
4	"	1.25	0.011	0.30	0.30	0.30	0.061	0.11	0.15
5	"	1.47	0.038	0.35	0.35	0.35	0.061	0.11	0.15
6	"	11.1	0.037	2.68	2.68	2.68	0.061	0.11	0.15
2V	0.5% Separan	20.0	0.039	3.1	4.3	5.1	0.08	0.10	0.12
3V	"	5.34	0.038	0.74	0.87	1.2	0.09	0.13	0.14
4V	"	2.06	0.037	0.32	0.44	0.52	0.08	0.10	0.12
5V	"	0.590	0.038	0.090	0.13	0.15	0.08	0.10	0.12
6V	"	19.5	0.019	2.9	3.8	4.6	0.08	0.10	0.12
7V	"	0.550	0.019	0.080	0.11	0.13	0.08	0.11	0.13
8V	"	1.82	0.018	0.23	0.31	0.39	0.09	0.12	0.13
9V	"	5.24	0.018	0.70	0.94	1.2	0.09	0.12	0.13

Table 1. Properties of the materials.

Drop volume (cm^3)	λ
0.070	0.512
0.100	0.577
0.150	0.660
0.200	0.726
0.250	0.782
0.300	0.831

Volumetric Flow Rate (cm^3/min)	V (cm/s)
15.0	0.32
26.4	0.56
37.7	0.80

Table 2. Flow parameters.

λ	SYSTEM:											
	2	3	4	5	6	2V	3V	4V	5V	6V	7V	8V	9V
	(V = 0.32 cm/s)												
0.512	1.99	1.48	0.06	1.01	1.99	0.70	0.79	0.47	0.90	0.34	0.28	0.20	0.17
	1.41	1.38	1.71	1.37	1.20	1.44	1.44	1.45	1.40	1.50	1.52	1.50	1.50
0.577	2.22	1.48	0.94	1.82	3.22	0.93	0.86	0.82	1.12	0.41	0.46	0.42	0.41
	1.49	1.49	1.66	1.41	1.29	1.39	1.43	1.41	1.38	1.46	1.48	1.46	1.47
0.660	2.89	1.68	1.12	1.62	3.54	1.23	1.23	1.23	1.35	0.93	0.91	0.78	0.78
	1.49	1.46	1.58	1.44	1.34	1.34	1.40	1.38	1.36	1.40	1.42	1.41	1.41
0.726	4.10	2.88	1.13	1.60	4.68	1.75	1.56	1.82	1.89	1.42	1.79	1.37	1.35
	1.43	1.40	1.52	1.43	1.36	1.32	1.36	1.34	1.34	1.36	1.37	1.36	1.35
0.782	4.68	3.12	1.25	2.26	5.20	2.10	1.93	2.45	2.50	2.51	2.39	1.98	2.12
	1.41	1.37	1.47	1.41	1.34	1.30	1.34	1.30	1.30	1.31	1.32	1.32	1.32
0.831	6.06	4.19	1.96	2.14	6.24	2.80	2.62	3.20	2.96	2.80	2.95	2.63	2.77
	1.37	1.32	1.42	1.38	1.33	1.28	1.31	1.27	1.28	1.27	1.29	1.28	1.27
	(V = 0.56 cm/s)												
0.512	1.49	0.97	0.00	0.71	1.56	0.44	0.40	0.30	0.43	0.19	0.22	0.19	0.15
	1.54	1.61	1.77	1.49	1.36	1.46	1.50	1.47	1.47	1.50	1.50	1.50	1.51
0.577	2.18	1.03	0.23	0.65	2.20	0.56	0.56	0.53	0.64	0.32	0.34	0.37	0.27
	1.57	1.62	1.73	1.53	1.40	1.43	1.46	1.45	1.44	1.47	1.47	1.47	1.47
0.660	2.38	1.46	0.25	0.68	2.49	1.00	0.89	0.87	1.02	0.71	0.71	0.68	0.65
	1.56	1.58	1.68	1.54	1.42	1.41	1.42	1.41	1.40	1.41	1.42	1.42	1.42
0.726	3.37	2.10	0.39	0.89	2.97	1.36	1.28	1.53	1.46	1.16	1.12	1.05	1.10
	1.55	1.51	1.60	1.50	1.40	1.37	1.38	1.38	1.36	1.37	1.38	1.38	1.37
0.782	4.19	2.72	0.32	0.89	3.79	1.95	1.78	1.97	2.00	1.81	1.79	1.62	1.67
	1.47	1.47	1.54	1.49	1.39	1.34	1.34	1.34	1.32	1.33	1.34	1.33	1.33
0.831	4.84	3.72	0.13	0.97	4.09	2.62	2.44	2.51	2.93	2.57	2.35	2.00	2.31
	1.44	1.44	1.50	1.46	1.36	1.32	1.32	1.30	1.30	1.30	1.30	1.31	1.30
	(V = 0.80 cm/s)												
0.512	1.15	0.67	0.07	0.45	0.89	0.34	0.31	0.31	0.33	0.17	0.18	0.18	0.19
	1.60	1.63	1.79	1.57	1.43	1.49	1.50	1.51	1.49	1.50	1.50	1.50	1.51
0.577	1.55	0.86	0.17	0.54	2.08	0.62	0.42	0.41	0.40	0.25	0.35	0.30	0.27
	1.59	1.66	1.75	1.57	1.47	1.46	1.47	1.47	1.46	1.47	1.47	1.47	1.47
0.660	2.09	0.93	0.11	0.52	2.43	1.05	0.74	0.66	0.74	0.59	0.66	0.58	0.65
	1.58	1.58	1.68	1.56	1.47	1.41	1.43	1.42	1.43	1.42	1.43	1.43	1.44
0.726	3.22	1.68	0.10	0.65	2.50	1.40	1.10	0.69	1.16	0.93	1.01	0.95	1.08
	1.53	1.54	1.65	1.55	1.47	1.37	1.41	1.38	1.38	1.37	1.40	1.38	1.39
0.782	3.92	1.45	0.22	0.69	3.72	2.26	1.56	1.15	1.70	1.49	1.55	1.32	1.54
	1.47	1.50	1.59	1.51	1.44	1.34	1.36	1.34	1.34	1.34	1.35	1.36	1.35
0.831	4.42	1.87	0.50	0.50	3.83	2.56	1.90	1.95	2.13	2.31	2.06	1.51	2.06
	1.44	1.48	1.56	1.49	1.42	1.29	1.35	1.32	1.31	1.31	1.32	1.35	1.32

Table 3. Data for ΔP^+ and U/V. For each system, drop size, and flow rate there is a pair of numbers. The upper is the measured value for $\Delta P^+ R_o/\mu_o V$ and the lower is the measured value for U/V.

	Coefficients of (2):	
Viscosity Ratio	Concentric (λ^5) Term	Eccentric ($\beta^2\lambda^3$) Term
0.30	-2.82	28.72
0.35	-1.94	29.63
0.77	3.09	35.25
2.63	10.22	44.52
2.68	10.30	44.64

Table 4. Coefficients of Equation 2.

Figure Captions

Figure 1. Schematic diagram of the apparatus (not to scale). (1) Constant-temperature bath. (2) Micrometer syringe. (3) Suspending fluid storage section. (4) Test section. (5) Pressure port. (6) Pressure port. (7) Camera. (8) Manometer by-pass valve. (9) Pressure transducer. (10) Transducer indicator. (11) Thermocouple. (12) Pump: syringe or gear type. (13) Waste storage. (14) Suspending fluid reservoir.

Figure 2. Schematic diagram of manometer-transducer system (not to scale). (A) Test section. (B) Upstream manometer leg. (C) Downstream manometer leg. (D) By-pass valve. (E) Pressure transducer. (F) Transducer indicator and recorder. (G) Suspending fluid. (H) Carbon tetrachloride. (I) Pressure difference due to suspending fluid alone.

Figure 3. Dimensionless extra pressure drop as a function of Γ ($= \mu_0 V/\gamma$):
○System 6 (Newtonian), $\sigma = 2.68$, $\Delta\rho/\rho_0 = 0.037$, $\lambda = 0.726$.
●System 6 (Newtonian), $\sigma = 2.68$, $\Delta\rho/\rho_0 = 0.037$, $\lambda = 0.576$.
□System 2v (Viscoelastic), $\sigma = 3.1\text{-}5.1$, $\Delta\rho/\rho_0 = 0.039$, $\lambda = 0.726$.
△System 2v (Viscoelastic), $\sigma = 3.1\text{-}5.1$, $\Delta\rho/\rho_0 = 0.039$, $\lambda = 0.576$.
×(Newtonian) $\sigma = 2.04$, $\Delta\rho/\rho_0 = 0$, $\lambda = 0.726$ [from (I)].
◇(Viscoelastic) $\sigma = 3.1\text{-}5.1$, $\Delta\rho/\rho_0 = 0$, $\lambda = 0.726$ [from (I)].

Figure 4. Dimensionless extra pressure drop as a function of λ. Shown are Newtonian systems 2, 3, 5, 6, and all viscoelastic systems for V = 0.32 cm/s.

Figure 5. D (= largest linear dimension/undeformed diameter) as a function of viscosity ratio for three dimensionless drop sizes. The points connected by solid lines represent viscoelastic Systems 2V-5V. The unconnected points correspond to Newtonian Systems 2 and 6.

Figure 6. h^2 vs. U/ . Each Newtonian point represents an average of all drop sizes for the particular system and flow rate. The viscoelastic points are taken for the largest drop sizes.

Figure 7. Difference between U/V for Newtonian and viscoelastic suspending fluids as a function of drop size. ●, U/V (System 2) - U/V (System 6V), V = 0.56 cm/s; □, U/V (System 2) - U/V (System 6V), V = 0.32 cm/s; △, U/V (System 6) - U/V (System 2V), V = 0.56 cm/s; ○, U/V (System 6) - U/V (System 2V), V = 0.32 cm/s.

Figure 8. Dimensionless extra pressure drop and relative velocity of drop as a function of viscosity ratio. Newtonian Systems 5 and 6: △, λ = 0.577; ○, λ = 0.726; Viscoelastic Systems 2V-5V: ▲, λ = 0.577; ●, λ = 0.726.

Figure 9. Dimensionless pressure drop and relative velocity as a function of $\Delta\rho/\rho_o$:

Newtonian systems: Systems 4 and 5: x, λ = 0.660 and ◇, λ = 0.831.

Systems 2 and 6: ●, λ = 0.660 and ○, = 0.831.

Viscoelastic systems: Systems 2V and 6V: ■, λ = 0.660 and □, λ = 0.831.

Systems 4V and 8V: ▲, λ = 0.660 and △, λ = 0.831.

All data for V = 0.32 cm/s. Also shown are results from (I) for $\Delta\rho/\rho_o$ = 0.

Figure 10. Data for dimensionless pressure drop as a function of drop size. (●) for Systems 2 and 5 (Newtonian). Also shown (○) are predicted values from (2). Note that predicted value does not vary with flow rate.

Figure 11. Data for relative drop velocity as a function of dimensionless drop size (●) for Systems 2 and 5 (Newtonian). Also shown (○) are predicted values from (I).

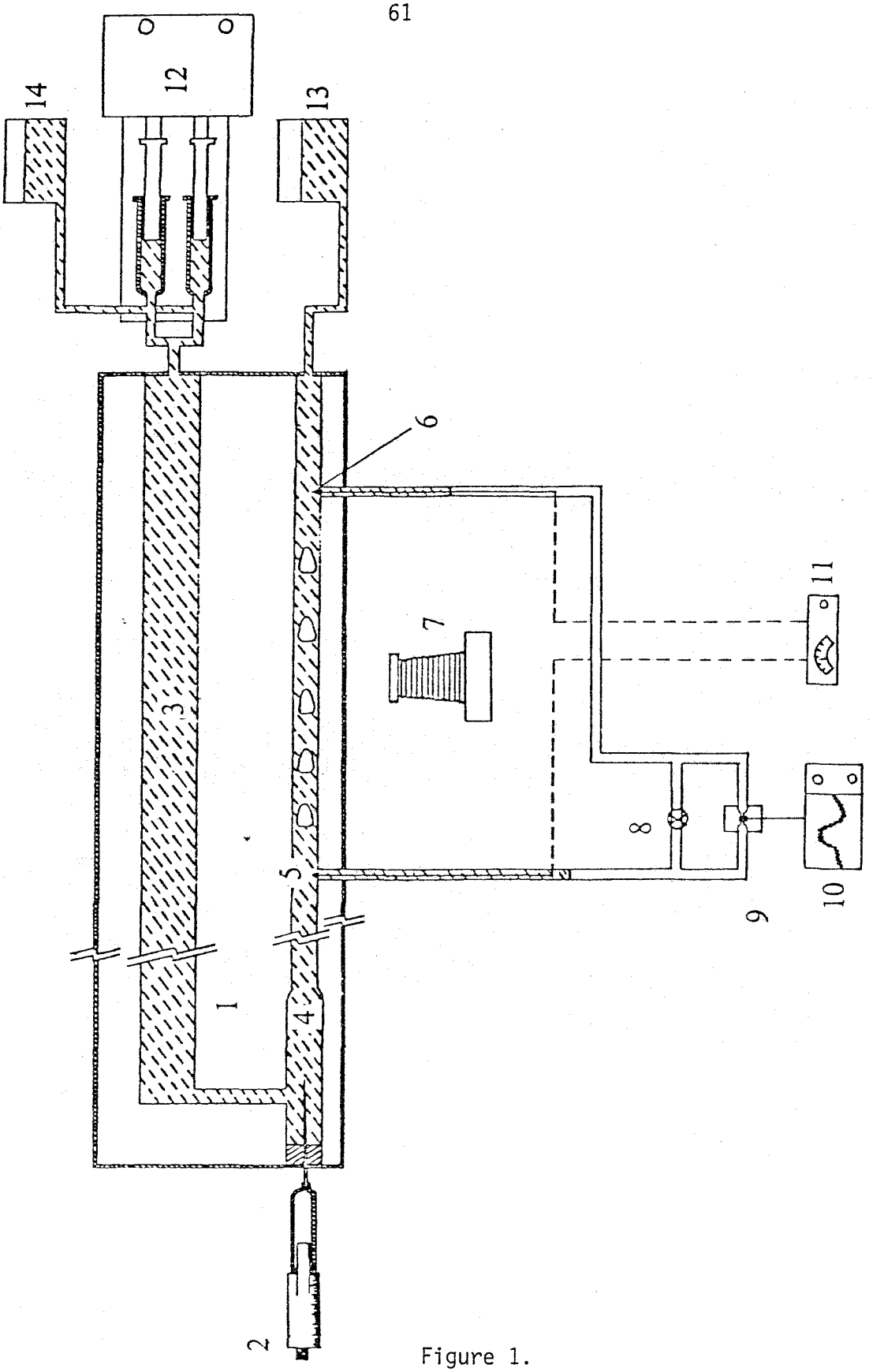

Figure 1.

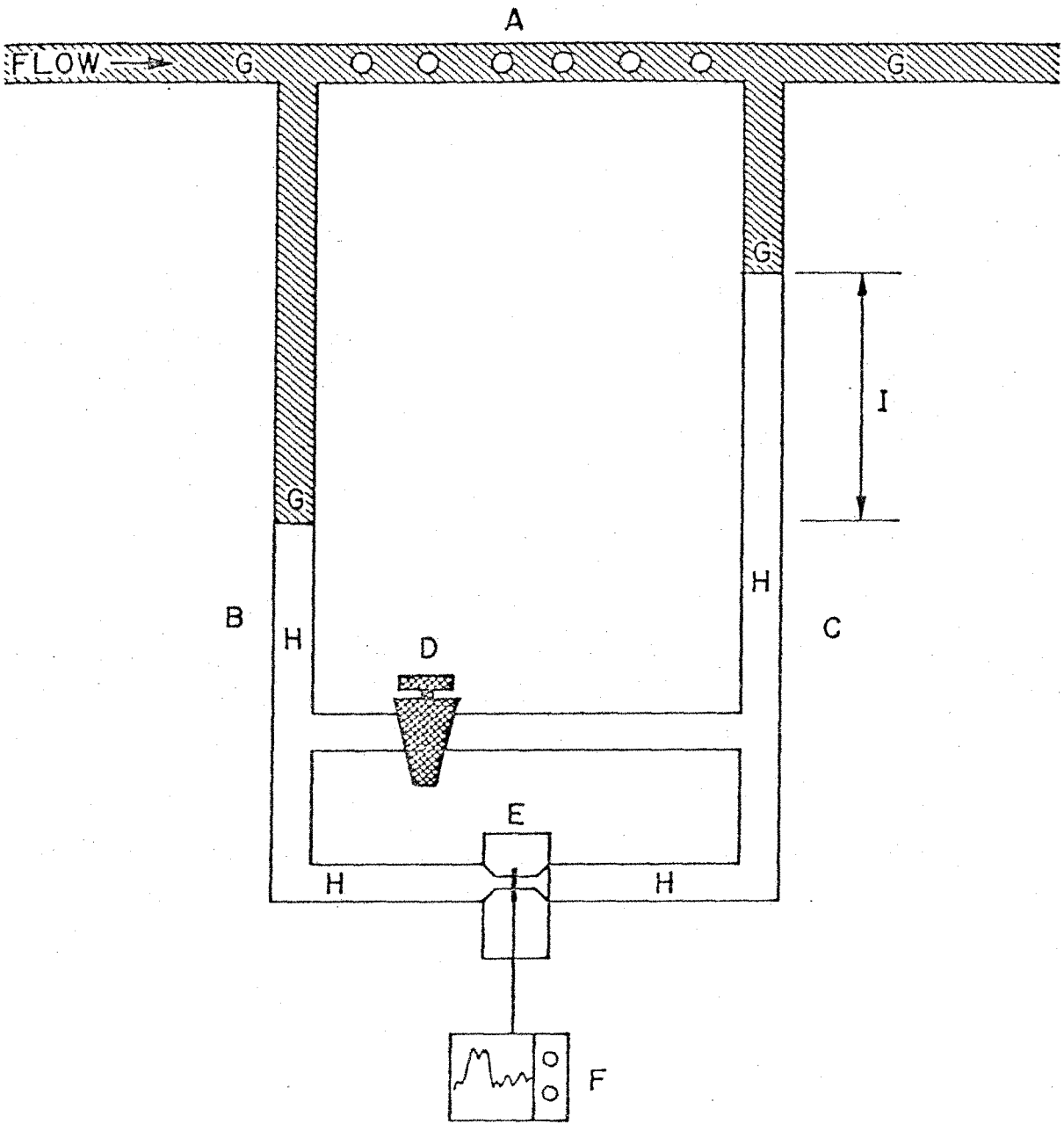

Figure 2.

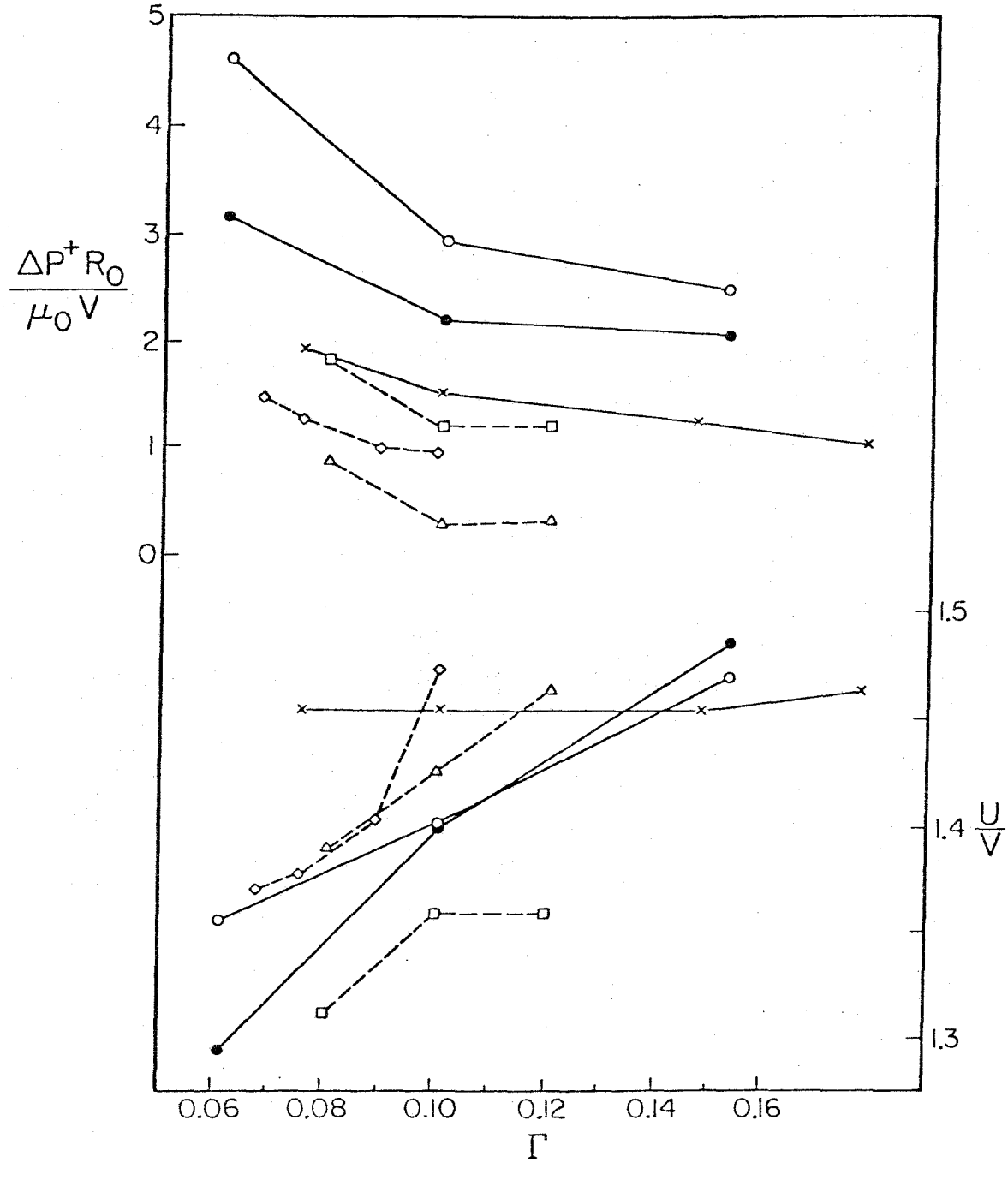
$\frac{\Delta P^+ R_0}{\mu_0 V}$
5
4
3
2
1
0
1.5
1.4
1.3
$\frac{U}{V}$
0.06
0.08
0.10
0.12
0.14
0.16
Γ

Figure 3.

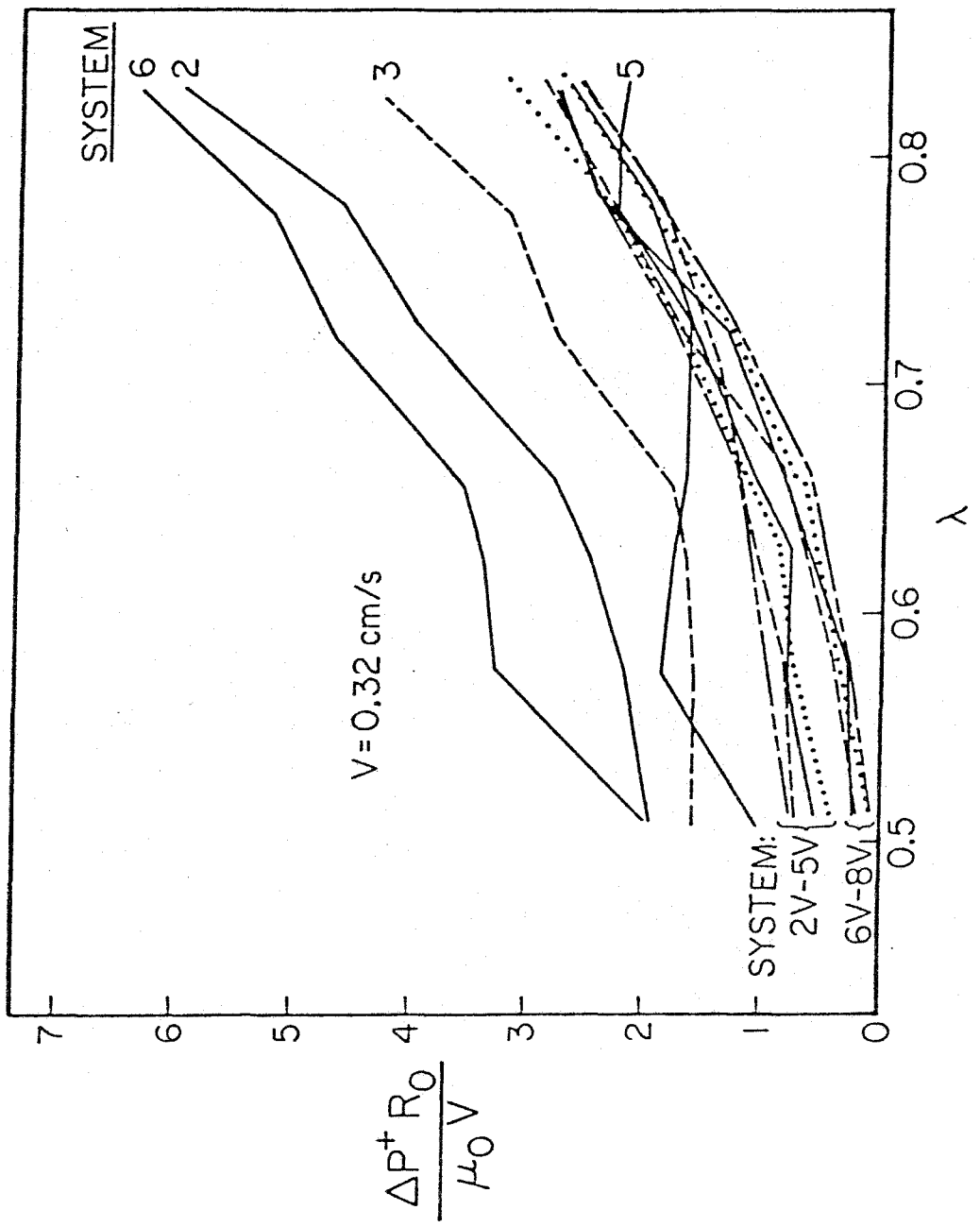
SYSTEM
6
2
3
5
V=0,32 cm/s
SYSTEM:
2V-5V
6V-8V
0.5
0.6
0.7
0.8
λ
0
1
2
3
4
5
6
7
$\frac{\Delta P^+ R_0}{\mu_0 V}$

Figure 4.

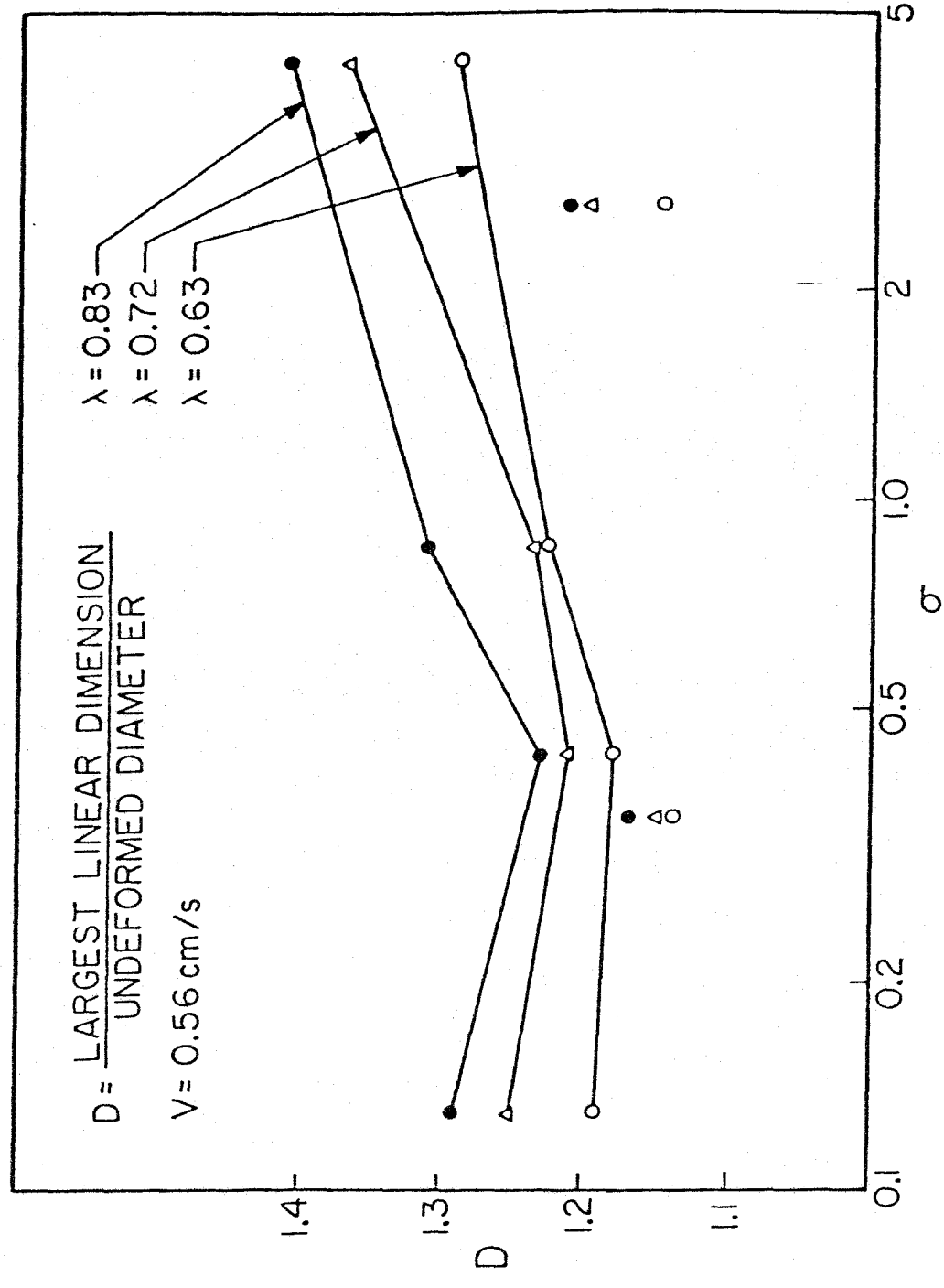
D = LARGEST LINEAR DIMENSION / UNDEFORMED DIAMETER
V = 0.56 cm/s
λ = 0.83
λ = 0.72
λ = 0.63
D
1.4
1.3
1.2
1.1
0.1
0.2
0.5
1.0
2
5
σ

Figure 5.

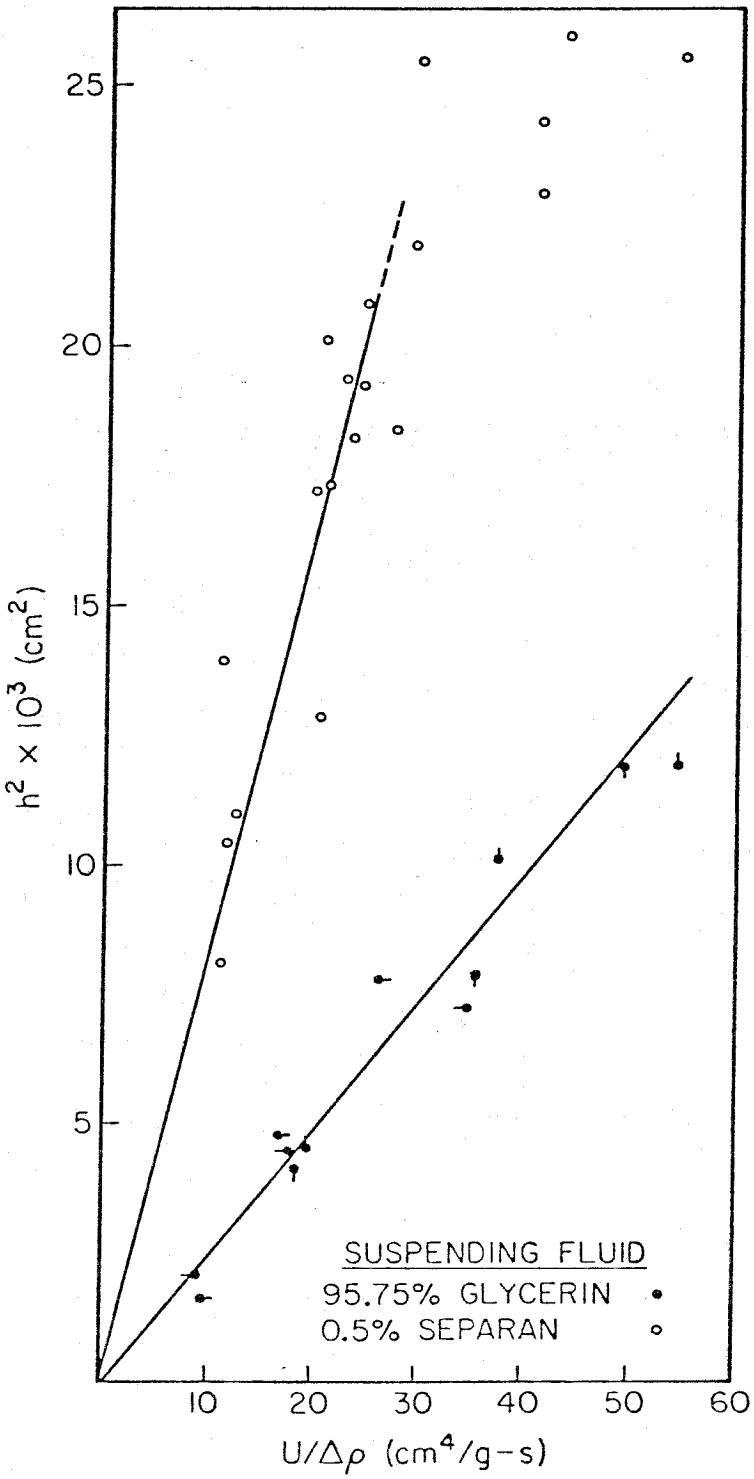
25
20
15
10
5
$h^2 \times 10^3$ (cm^2)
10
20
30
40
50
60
U/Δρ (cm^4/g-s)
SUSPENDING FLUID
95.75% GLYCERIN
0.5% SEPARAN

Figure 6.

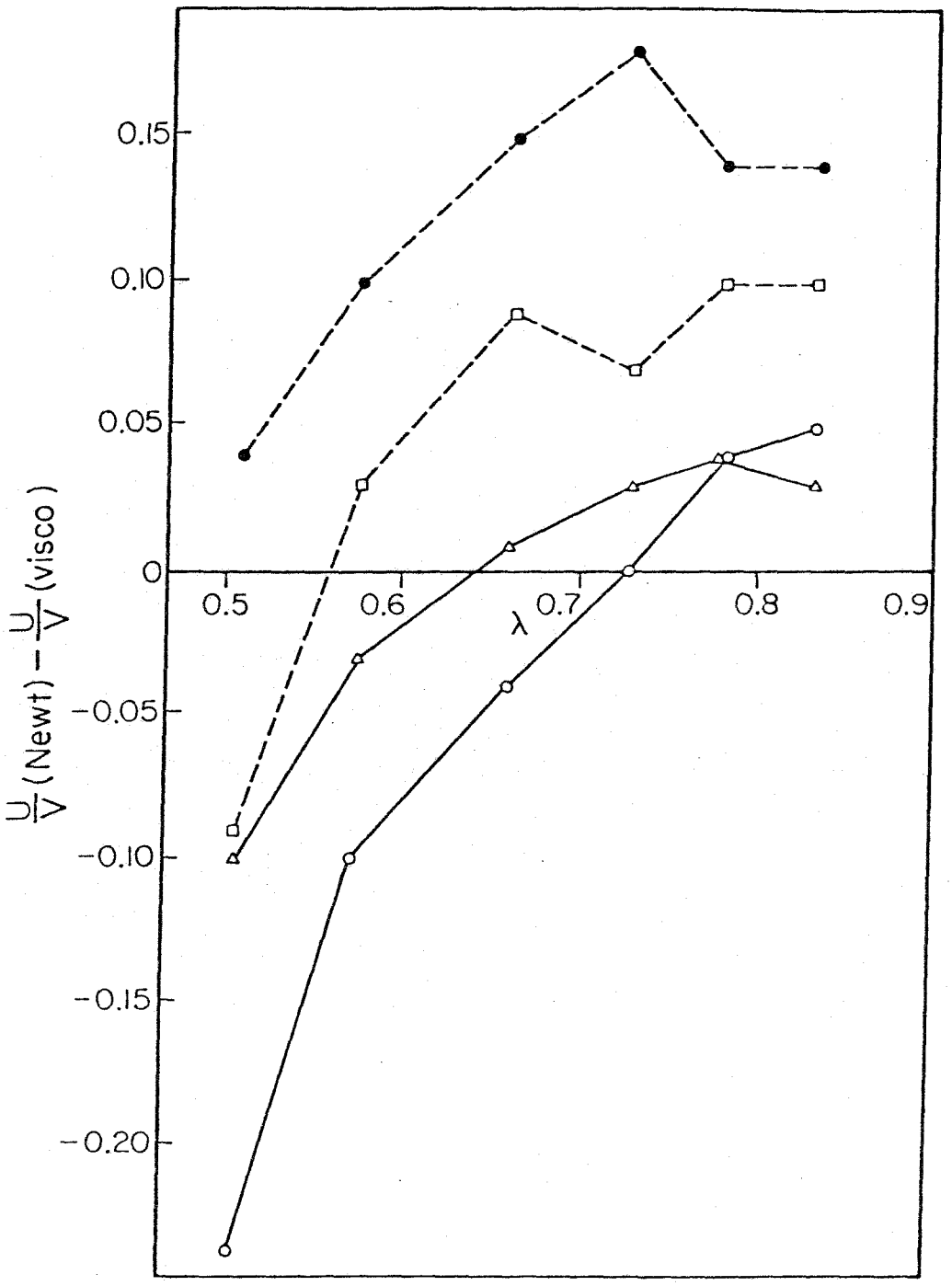

Figure 7.

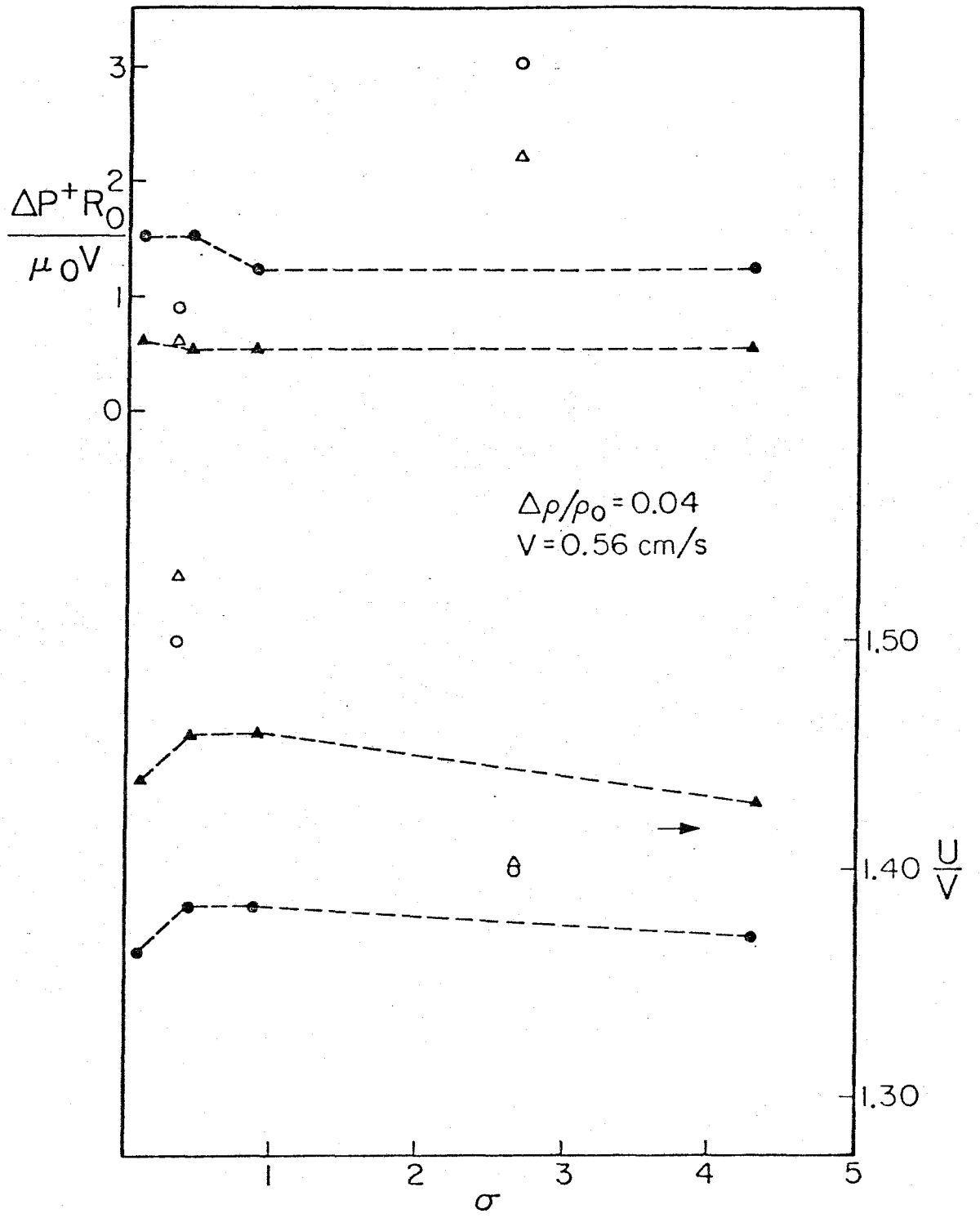
3
2
1
0
$\frac{\Delta P^+ R_0^2}{\mu_0 V}$
$\Delta\rho/\rho_0 = 0.04$
V = 0.56 cm/s
θ
1.50
1.40
1.30
$\frac{U}{V}$
1
2
3
4
5
σ

Figure 8.

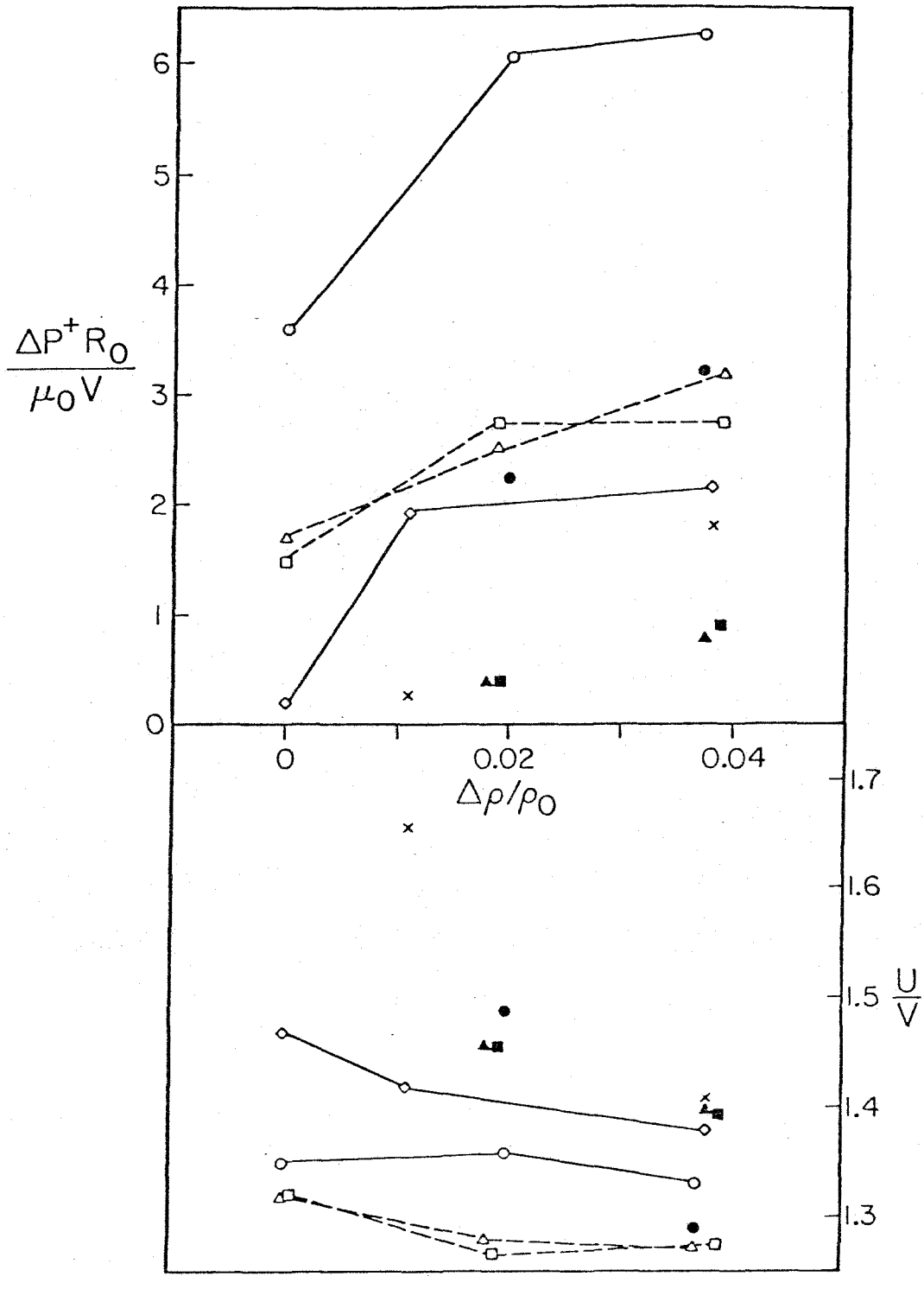
$\frac{\Delta P^+ R_0}{\mu_0 V}$
6
5
4
3
2
1
0
0
0.02
0.04
$\Delta\rho/\rho_0$
1.7
1.6
1.5
1.4
1.3
$\frac{U}{V}$

Figure 9.

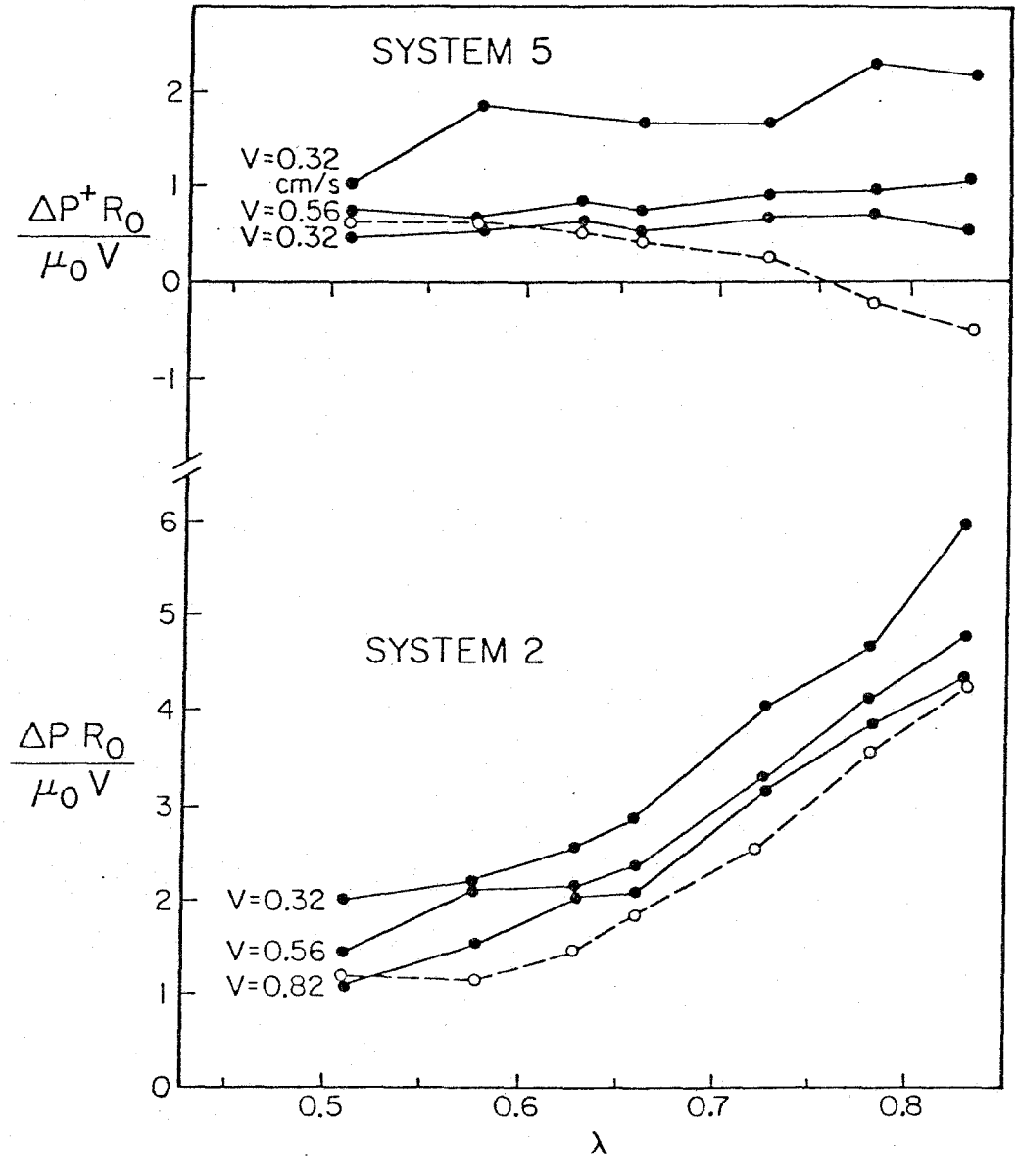
SYSTEM 5
$\frac{\Delta P^+ R_0}{\mu_0 V}$
V=0.32 cm/s
V=0.56
V=0.32
2
1
0
-1
SYSTEM 2
$\frac{\Delta P R_0}{\mu_0 V}$
V=0.32
V=0.56
V=0.82
6
5
4
3
2
1
0
0.5
0.6
0.7
0.8
λ

Figure 10.

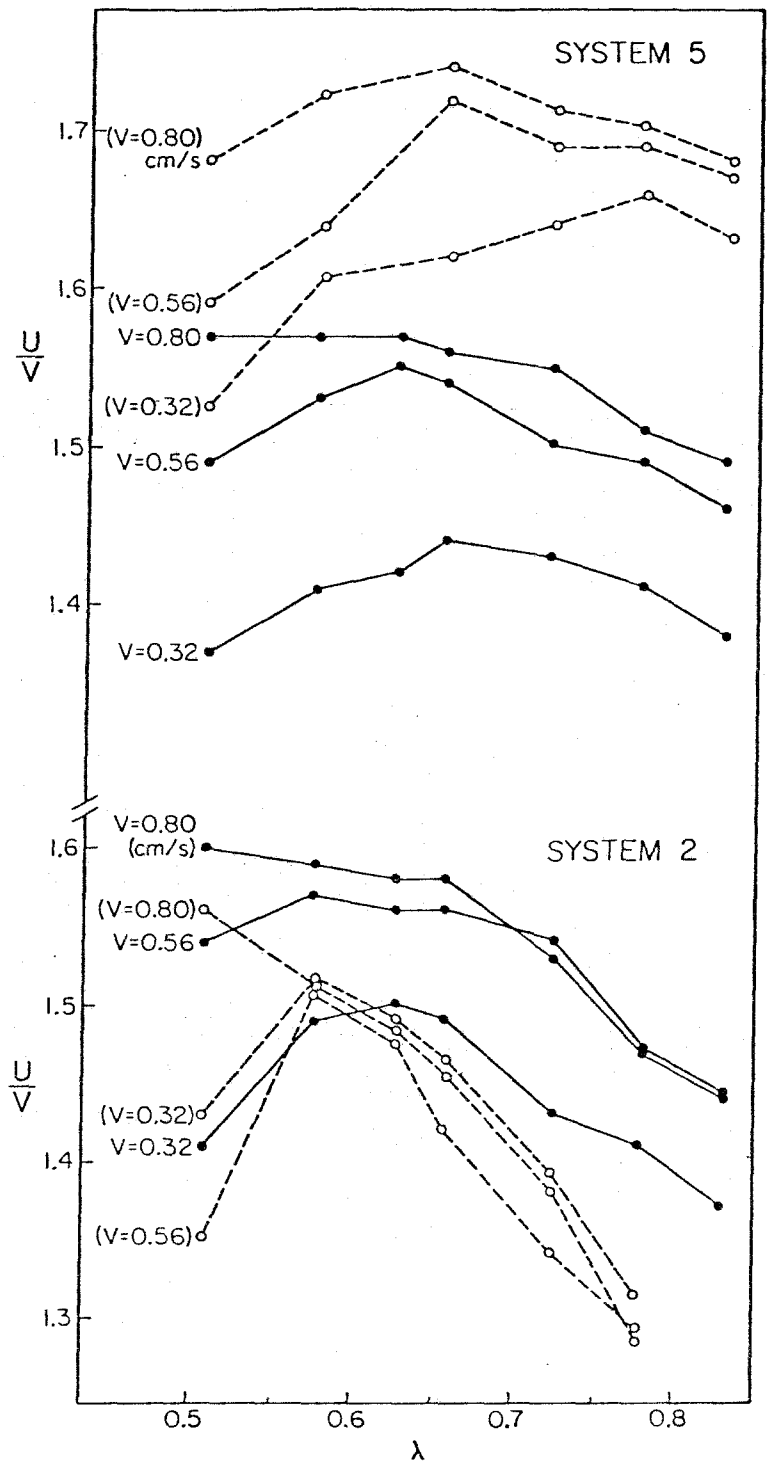
SYSTEM 5
(V=0.80) cm/s
(V=0.56)
V=0.80
(V=0.32)
V=0.56
V=0.32
SYSTEM 2
V=0.80 (cm/s)
(V=0.80)
V=0.56
(V=0.32)
V=0.32
(V=0.56)
U/V
λ
1.7
1.6
1.5
1.4
1.3
0.5
0.6
0.7
0.8

Figure 11.

Chapter 2

"The Creeping Motion of Immiscible Drops Through a Converging/diverging Tube

W. L. Olbricht* and L. G. Leal

Department of Chemical Engineering
California Institute of Technology
Pasadena, California 91125

*Present address: School of Chemical Engineering, Cornell University, Ithaca, New York 14853

In this paper, we report on an experimental study of the motion of an immiscible drop of a Newtonian liquid suspended in creeping flow through a circular tube of periodically varying diameter. We consider both Newtonian and viscoelastic suspending fluids, and are concerned with the mobility of the drop, the additional pressure gradient associated with its presence in the flow, and the deformation and breakup of the drop in the tube. It is shown that the conformation of the drop depends strongly on the value of the inverse capillary number. When this parameter exceeds unity and the suspending fluid is Newtonian, the drop becomes highly elongated, and subsequently breaks into several fragments. In turn, the shape of the drop has a profound effect on its relative velocity and on the additional pressure gradient owing to the presence of the drop in the flow. When the suspending fluid is viscoelastic, elongation of the drop is inhibited under otherwise similar conditions; instead, the drop develops long tails which issue satellite drops. The effect of increasing the suspending fluid polymer concentration is to stabilize these tails. The variety of dispersion processes observed in this experiment appear as onset phenomena at critical values of the relative drop size and the flow rate.

1. Introduction

We report in this paper the results of experiments on the creeping flow of immiscible drops through a horizontal circular tube with periodically varying diameter. This is part of a general study aimed at understanding the dynamics of two-phase flow through porous media at the scale of the individual channels.

Interest in the kinematics and dynamics of multiphase flow through porous media stems, in part, from its application to tertiary oil production methods. It is well known that a large fraction of the oil originally present in a typical reservoir remains unrecovered after conventional production methods including water flooding have been performed. So-called "chemical flooding" methods were proposed as early as 1950 and have more recently been tested in the laboratory and in the field. These methods involve the injection of a "pusher fluid" into the reservoir to displace oil globules trapped in the narrow tortuous pores of the rock matrix by lowering the interfacial tension between the dispersed oil and the aqueous continuous phase, thereby decreasing capillary pressure which holds the oil globules in place. The pusher fluid is often a surfactant-containing microemulsion or miscellar solution which is usually immiscible with the oil-water mixture which initially saturates the porous medium. Even when a more concentrated miscible surfactant solution is used, adsorption of the surfactant on the pore walls usually causes a phase change (Oh and Slattery, 1979). One aspect of the tertiary oil recovery process, then, is multiphase flow through a tortuous channel of rapidly varying cross-section. Miscellar solutions at the concentrations typically employed

in flooding operations characteristically exhibit non-Newtonian rheological properties, including a strongly shear-thinning viscosity in simple shear flow (Dreher and Grogarty, 1979). Although the use of polymer solutions as the pusher fluid has met with only limited success, an attractive variation involves injection of a dilute polymer solution behind a bank of concentrated surfactant for improved mobility control. In either case, the complications of non-Newtonian rheology may prove to be a significant consideration in the design of a successful flooding operation.

The specific problem we study in the present experiment is the motion of immiscible Newtonian drops through a horizontal circular tube with a diameter which varies sinusoidally with axial position. We have conducted experiments for both Newtonian and viscoelastic suspending fluids. The "wavy -wall" configuration is chosen not because of its direct or detailed physical resemblance to a typical channel of a porous medium. Rather, our choice is motivated by a recognition that the geometry of the wavy-wall tube produces two signficant features of the flow kinematics that are expected to be essential to a model of flow in an individual pore, especially for multiphase systems. First, the

undisturbed flow (i.e. no drops present) kinematics differ qualitatively at any given point in the wavy-wall tube from the simple shear flow of the straight-wall tube. Since the cross-sectional area of the wavy-wall tube varies periodically, continuity requires that in the absence of flow separation, a fluid element must experience an acceleration in each convergent region and a corresponding deceleration in each divergent region.

In this case, the velocity varies in the streamwise direction, in marked contrast to steady Poiseuille flow. The class of flows in which the velocity variation is only in the direction of flow is known as pure elongational (or extensional) flows. The velocity field along the tube centerline in the present experiment is irrotational and resembles a succession of two of these elongational flows, namely uniaxial elongation (in the convergent region) and biaxial elongation (in the divergent region). The flow kinematics are, however, known only along the tube centerline. Fluid elements not coincident with the tube centerline experience an additional rotational component, although the magnitude of the straining part of the velocity gradient tensor always exceeds the vorticity, assuming no flow separation. The relative importance of the elongational component of the flow at any given point in the tube increases with the amplitude of the variation in the tube diameter. An additional consideration in this regard is that the rheological behavior of a viscoelastic fluid depends critically on the flow type (i.e. the relative magnitude and form of the velocity gradient tensor). Polymer solutions and polymer melts which show a viscosity that decreases with shear rate in simple shear flow, usually show an increasing elongational viscosity in extensional flows. Some experimental evidence suggests that the increase in elongational viscosity can be so large that flow kinematics change to reduce the magnitude of large extensional stresses, as in flow of a viscoelastic fluid from a large reservoir through an orifice. The dramatic response of the viscosity to the rate of elongation is usually associated with large-scale stretching of the deformable macromolecules

which gives rise to critical changes in the bulk fluid properties (see Leal, Fuller and Olbricht, 1980). Second, flow in a straight tube, without drops present, is steady if the volumetric flow rate is kept constant. For the wavy-wall tube with constant volumetric flow rate, however, the bulk flow is periodic in a Lagrangian sense, with a characteristic period L/V where L is the "wavelength" of the wavy-wall tube and V is the average velocity of the bulk flow. If the suspending fluid is viscoelastic, the intrinsic timescale of the fluid relative to the timescale of the flow can play an important role in determining material behavior.

These two kinematic features of flow through a wavy-wall tube can influence the deformation of an immiscible drop suspended in the flow. The shape assumed by a drop during deformation and hence the resistance to flow depend on the type of flow, which is a consequence of the tube geometry. For a viscoelastic suspending fluid, the response of the drop may also depend critically on the response of the suspending fluid alone to the particular type of flow. Furthermore, because the wavy-wall tube introduces a Lagrangian unsteadiness in the bulk flow and, therefore, an unsteadiness in the shape of the drop, there is an additional timescale for the multiphase problem, namely the intrinsic timescale for drop deformation.

The tube geometry chosen here has been suggested previously as an improved model, relative to the straight-wall tube, for porous media flow of single-phase liquids. As a consequence, numerous results are available for the flow of single-phase, Newtonian fluids through circular tubes with axial variations in cross-sectional area. Many different functional forms

for the variation of the diameter with axial position have been considered. The emphasis in most of these studies has been on the calculation of detailed velocity and pressure fields and the associated pressure drop-flow rate characteristics. Payatakes, Tien and Turian (1973), Payatakes and Neira (1977), Neira and Payatakes (1979), Fedkiw and Newman (1977), and Deiber and Schowalter (1979a) have calculated velocity fields for flow in periodically varying tubes over a wide range of the geometric parameters. These results show consistently that a log-log plot of an appropriately defined friction factor versus Re yields a linear relationship with slope of -1 up to the value of Re at which either flow separation or turbulence occurs. The linear relationship between f and Re is identical to that observed for laminar flow through a straight circular tube. Results for non-Newtonian fluid flow through periodically constricted tubes have been reported by Dodson, Townsend and Walters (1971), Michele (1977), Franzen (1979), and Deiber and Schowalter (1979b). In particular, Franzen (1979) was able to show that the non-Newtonian data for $Re < 1$ also give a linear relationship (log-log) between f and Re with a slope of -1, provided the shear-thinning viscosity of the non-Newtonian fluid is taken into account by using a power-law model for the fluid.

Since an assessment of the applicability of wavy-wall tube flow as a prototype for porous media flow is one motivation for our study, it will be useful to compare our results to available data for flow through actual porous structures. Single-phase non-Newtonian flow through granular beds, packed beds, and beds of capillary tubes has been studied extensively by Marshall and Metzner (1967), Savins (1969), James and McLaren (1975), and Elata et. al., (1977) among others. A friction factor and Reynolds number which

incorporate the shear-thinning behavior of the fluid (as well as the physical structure of the "porous matrix") are used by those various authors to correlate pressure-drop flow rate data. Experimental observations show that dramatic departures from the linear relationship between f and Re occur under certain circumstances. We have already noted that there is a characteristic relaxation time associated with a viscoelastic fluid. If this time is comparable to the characteristic time for the flow, departures from generalized Newtonian behavior can occur since the dynamics of the flow will be governed, in part, by the elastic response of the fluid. A convenient measure of the intrinsic timescale of the fluid relative to the timescale for the Lagrangian unsteady flow is the Deborah number. According to Marshall and Metzner (1967), if De is larger than $\sim$0.05, with the definitions used for the porous medium, large deviations from generalized Newtonian behavior occur. A similar observation was reported by James and McLaren (1975) for dilute polymer solutions where friction factors up to 40 times greater than the comparable generalized Newtonian values were found. The "exact" value of De at which large deviations from purely viscous behavior are observed can vary significantly from problem to problem. Some studies suggest that purely viscous behavior is observed in packed beds up to values of De considerably higher than 0.05 (cf. Schowalter, 1978). For tubes with periodically varying cross-section, Franzen (1979) and Michele (1977) reported deviations from purely viscous behavior at values of De which were an order of magnitude larger than 0.05 (see Section 3).

The creeping motion of immiscible drops in tube flow has been the focus of two previous experimental investigations from this laboratory.

In the first, Ho and Leal (1975) considered the motion of neutrally buoyant drops suspended in Stokes flow through a straight-wall circular horizontal tube. Recently, Olbricht and Leal (1980) examined the effects of a density difference between the drop fluid and the suspending fluid. These papers will be referred to here as (I) and (II), respectively. In both sets of experiments, the size of the drop was comparable to the size of the tube.

In the present experiment, we consider the effects of streamwise variations in the cross-sectional area of a horizontal tube, both for neutrally buoyant and non-neutrally buoyant drops, and for Newtonian and viscoelastic suspending fluids. The drops were Newtonian in all cases. The following dimensionless quantities are determined in the present experiment: f, the friction factor associated with the flow of the suspending fluid alone (i.e. with no drops present); $\Delta P^{+} R_o/\mu_o V$, the additional pressure drop, due only to the presence of the suspended drop, which is scaled by the characteristic viscous pressure (here, R_o is the radius of the tube, μ_o the suspending fluid viscosity, and V the average velocity of the flow); $\frac{U}{V}$, the velocity of the drop relative to the average velocity of the two-phase bulk flow V; and the time dependent shape of the drop which deforms due to the velocity gradient and due to interactions with the tube wall. The material and flow parameters which characterize each experiment are: σ, the viscosity of the drop relative to the viscosity of the suspending fluid; $\Delta\rho/\rho_o$, the difference in density between the drop and suspending fluid relative to the density of the suspending fluid; λ, the undeformed drop radius divided by the tube radius R_o; Γ $(= \mu_o V/\gamma)$ the inverse capillary number, where γ is the interfacial

tension between the drop and suspending fluid; and rheological properties of the suspending fluid. The experiments were all performed with the volumetric flow rate Q held constant, while ΔP^+ varied with time due to the presence of the suspended drop. This is distinct from an associated problem where ΔP, the total pressure drop, is held constant and the flow rate Q varies with time due to the presence of the drop in the flow.

Each of the quantities measured in the present experiment has an important interpretation in the context of the tertiary oil recovery problem. Displacement of trapped residual oil is a necessary but not sufficient condition for a successful chemical flood. Extreme care must be taken to exercise mobility control so that a sweep-efficient oil/water front is formed. The relative velocity of the drop $\frac{U}{V}$ in the convergent/divergent tube is obviously intimately related to the relative mobility of the oil phase during immiscible flooding. By studying flow through an individual channel, we seek, in principle, to determine the conditions (i.e. the optimal choice of the parameters already listed) under which drop mobility is maximized. We are limited, however, by the fact that the ranges of parameters which could be covered by actual chemical flooding operations are enormous. Specifically, the effectiveness of the surfactant-containing fluid in reducing the interfacial tension to ultra-low values, the flow velocity, and the size distribution of the pores can be expected to vary widely. The values of the parameters in the present study suggest that our results would be most applicable under flooding conditions where viscous forces play a significant role, in regions near the injection well, where the sweep velocity is largest, for example. Although the values for the parameters in the present study are realistic, we certainly have not

covered the entire range of technological interest. The additional pressure drop ΔP^+ is related to the accessibility of the individual pores for two-phase flow relative to pores which contain no drops. Payatakes, Flumerfelt and Ng (1978) discussed the possibility that mobilized oil droplets could become trapped within a pore because the pressure drop necessary to force the droplet through the upstream pore neck may be too large. This could result in the blockage of an entire pathway to the collection well. It is therefore desirable to operate in a region of the parameter space where the extra pressure drop due to the presence of the drop is minimal. Factors which influence the value of the extra pressure drop will be identified from the data. The shape of the drop and its possible breakup during the flow is related to dispersion phenomena known to be of fundamental importance in successful flooding operations. Oil segments undergo repeated partitioning and coalescence as they are displaced through the pores. The relative importance of these effects determines the globule size distribution and hence influences the efficiency of oil transport. Payatakes, Flumerfelt and Ng (1978) concluded from the results of a stochastic simulation model that oil segment breakup results in the formation of a dilute oil-in-water emulsion that decreases recovery efficiency. It appears then, that oil drop breakup should be avoided in the design of flooding operations. However, the detailed flow dynamics, including factors which influence drop breakup cannot be deduced from the statistical model. Therefore, another important aspect of our study is the relationship between the experimental system parameters and drop deformation and breakup. Roof (1970) predicted the circumstances under which drop breakup will occur in a porous medium by studying the stability

of the drop shape for a sequence of static (equilibrium) configurations taken to represent the motion of a drop through a pore. The results are dominated by capillary forces which hold the drop in the individual pore. Although "static" calculations of this type (including Oh and Slattery, 1979) account for capillary forces which must be overcome to mobilize the drop, they give no information concerning the effects of viscous (and viscoelastic) forces on the conformation of the suspended drops. These forces are expected to be especially significant when surfactants have been used to lower interfacial tensions. For example, the pressure associated with capillary effects is $O(\gamma/R)$ where γ is the interfacial tension and R is the pore radius. The characteristic viscous pressure is $\mu_o V/R$ where μ_o is the pusher fluid viscosity and V is the velocity in pore. The relative importance of viscous forces relative to interfacial forces is thus $O(\mu_o V/\gamma)$, the inverse capillary number. If the sweep velocity V is taken to be 10 ft/day, with a pusher fluid of 10 cp viscosity, then $\mu_o V/\gamma$ is$O(1)$ if γ is lowered to 10^{-2} dynes/cm, a value which can be easily obtained under many circumstances. An important consideration in the flow problem is the position of the drop in the tube which may be eccentric due to density differences between drop and suspending fluids. Relatively small density differences may produce qualitative differences in ΔP^+ and U/V, as found in (II). Furthermore, of additional interest here is the effect of viscoelasticity on dispersion phenomena. These considerations cannot enter in any "equilibrium" calculations where the effect of flow dynamics is ignored.

In applying the results of the present two-phase flow experiment to immiscible oil displacement methods, it is significant to note that we

consider only the case where the oil droplet does not contact the tube wall. However, this is just one of several possible configurations for the motion of the dispersed (oil) phase through porous structures. Other possible mobilizations take place with the oil remaining in the form of a slug or bolus, moving through the pore while continuously maintaining contact with the wall. Oh and Slattery (1979) compared several modes of displacement and mobilization of oil globules in individual pores to determine the effects of interfacial tension and pore wettability on drop mobility. It was predicted that the porous surface should be water-wet to obtain maximum displacement efficiency. Among a variety of displacement sequences, one predicted mechanism involves the complete detachment of a residual oil globule from the pore wall and its subsequent transport in the pusher fluid. If the pressure gradient is sufficiently large, the droplet will deform to squeeze through the neck of the pore without again contacting the pore wall. This "detached" configuration is the mode of transport which we study in the present experiment. Wasan, et. al. (1979) observed oil detachment and mobilization in an actual sand-packed bed placed under a microscope for in-situ visualization. Two types of detachment occurred, depending on the volume of the residual oil film initially attached to the pore wall. Small-volume films broke from the surface and formed small droplets, but large-volume films were observed to detach and form long, thin filaments or strands. One objective of our work is an understanding of how the mobility of the dispersed phase is influenced by the conformation of the suspended elements in the flow.

The present experiment differs from (I) and (II) in that a systematic study of the effects of viscoelasticity is attempted. The suspending

fluid elasticity was varied by using aqueous polymer solutions of two different concentrations for the suspending fluid. Another difference between this and the previous studies is that the interfacial tension was also varied over a wide range, especially for the Newtonian suspending fluid case where the inverse capillary number, $\Gamma = \mu_o V/\gamma$, is varied by a factor of fifty. (This large variation is important for application of the present results to the oil recovery problem since Γ typically varies over several orders of magnitude depending on operating conditions.) It will be seen that the dynamics of the drop motion through the periodic tube depend strongly on the value of the inverse capillary number.

Although the results for drop deformation and breakup in the present study are mainly qualitative, they may be compared to previous results obtained for kinematically well-characterized flows. Taylor (1934) studied the deformation and breakup of drops suspended in two steady flow fields, simple shear flow generated between parallel bands, and two-dimensional elongation produced in the center of a four-roll mill. Subsequent investigations have confirmed the result that breakup occurs in steady simple shear flow only if the ratio of the drop fluid viscosity to that of the suspending fluid is between $\sim 10^{-3}$ and ~ 4. Within that range, there is a well-defined critical shear rate at which breakup occurs. In steady two-dimensional elongation, breakup can occur at much larger values for the viscosity ratio, and the critical rate of shear is relatively independent of the drop viscosity. Grace (1971) also observed a transient mode of breakup particularly interesting here since flow through channels with varying geometry is inherently an unsteady problem. It was observed that under some conditions, if a droplet was sufficiently deformed

in a two-dimensional straining motion, breakup occurred after the flow was "turned off", even though the drop continued to extend further without breakage if the flow was maintained. More recently, Han and Funatsu (1978) studied the creeping motion of drops suspended in flow through a single abrupt contraction, while Chin and Han (1979) considered the related problem of flow of drops through a tapered tube. Although the geometry of the flow channels differed in those two studies, droplet breakup occurred in both cases downstream of the contraction, i.e. in a region of relaxation of the extensional deformation produced by the constrictions. The rate of extension in these experiments, as in the present experiment, is not known precisely and certainly varies with radial position in the tube. Nevertheless, it can be presumed that the elongational component of the flow resembles a three-dimensional (uniaxial) extension. Since it has proved impossible thus far to generate a kinematically "perfect" uniaxial extensional flow, studies of droplet deformation and breakup in approximate "uniaxial" or "biaxial" flows of the present type are useful, at least in a qualitative sense. Acrivos and Lo (1978) have calculated the conditions for breakup of a slender drop in uniaxial extensional flow. Although the shear field is not as simple in the present experiment, we still seek to make qualitative comparisons with results for drop breakup in homogeneous shear fields. Whether such a comparison is possible is an important practical question since convergent/divergent tube flow of this type may be closely related kinematically to flows encountered in a variety of polymer processing operations.

2. Experimental

2.1 Apparatus

The basic apparatus described in (I) and (II) was modifed for used in the present study. The current configuration is illustrated in Fig. 1. A large reservoir of the suspending fluid was placed above the apparatus. The fluid was then pumped using a Zenith BPB Series metering gear pump. It was necessary to pressurize the upstream side of the pump (i.e. the overhead reservoir) to ∿200 psi when the Newtonian suspending fluid was used in order to prevent the formation of small bubbles in the pump which would otherwise appear at the pump exit. No bubble formation occurred when pumping the viscoelastic suspending fluids, even at atmospheric pressure. The suspending fluid was pumped into a holding section which was immersed in a constant temperature bath maintained at 25 ± 0.1^{o}C. Transit time through the holding section was always sufficiently long to ensure thermal equilibration of the suspending fluid and the constant temperature bath. The suspending fluid then entered a 70 cm long straight circular entry section of internal diameter 0.90 cm.

The test section was comprised of eighteen individual periodic "units" with the shape and dimensions illustrated in Fig. 2. Each unit was bored from a Lucite cylinder using a specially machined tool. The axial variation in radius specified in Fig. 2 (0.45 cm to 0.25 cm) corresponds to a maximum variation in cross-sectional area of a factor of 3.2. Special fittings were machined into the ends of the units so that the pieces could be attached in succession. A rubber gasket of 1 mm thickness was placed between each unit before attachment. The assembled tube

was held in place under compression by two brackets which were attached at the two ends of the tube. Three of the units were fit with pressure ports at the point of narrowest diameter. The pressure ports were connected through the wall of the constant temperature bath to a differential manometer. The design allowed the length of the test section to be varied, along with the position of the pressure taps. Another straight circular section of radius 0.45 cm and length 40 cm followed the test section. This provided a region to observe the relaxation of the deformed drop shape back toward equilibrium. The drops travelled through the relaxation section and were eventually stored in a waste fluid reservoir.

Pressure measurements were made using the identical method detailed in (II). The differential manometer was capable of measuring the pressure difference due only to the presence of the suspended drop in the flow. A variable reluctance transducer with a specially chosen membrane gave a full-scale differential pressure range of 0.3 cm of water. The transducer indicator output was recorded on a strip-chart recorder.

Drops of known volume were injected manually using a Hamilton micrometer syringe (±0.001 ml accuracy) connected to a 17 gauge needle. A typical drop was injected with the pump operating at a very low rate so that the injected drop detached gently from the needle. The pump speed was then increased to the specified flow rate. The detached drop attained an equilibrium lateral position in the straight-wall entry section which was found to be independent of the injection position. The equilibrium position was attained well before the drop entered the

test section except in some special cases discussed later. A detailed discussion of the motion of drops in a straight circular tube is contained in (II). In (I) and (II), up to twenty-four drops were injected in a train to enhance the pressure signal. Here, however, the sensitivity of the transducer was increased and the metering pump improved so that ΔP^+ could be determined for a single drop. This is essential here, because if more than one drop were used, the relative positions of the drops with respect to the period of the tube would constitute an additional parameter for the experiment.

The drops were photographed as they passed through the test section using an RCA TC-1000 video camera equipped with a Kowa 15-75 mm zoom lens fitted with close-up attachments. The camera was mounted on a motorized horizontal rail system so that the drop could be tracked continuously as it passed through the test section. A second video camera photographed the transducer indicator scale. The two images were combined in a split-screen picture which was viewed on a Sanyo video monitor and recorded by a Panasonic Omnivision II videotape recorder. Thus, a record of the shape and position of the drop along with the simultaneous reading of the additional pressure drop was obtained. Since curved surfaces are present in the test section, the refractive indices of the suspending fluid and the constant temperature bath circulating fluid were matched to minimize distortion.

2.2 Materials

Measurements were taken for nineteen fluid systems encompassing a

wide range of material parameters. The specifications for all systems are listed Table 1. The Newtonian suspending fluids were UCON LB-1715 and 95.45% aqueous glycerin solution with viscosities of 7.17P and 3.94P, respectively.

The viscoelastic suspending fluids were aqueous solutions of Dow Separan AP-30, a rheologically well-characterized polyacrylamide. The shear-rate dependent viscosity and primary normal stress difference have been reported by Leal, Skoog and Acrivos (1971). To study the effects of suspending fluid viscoelasticity, two polymer concentrations were used, 0.5% and 1.0%, by weight.

Since the Separan solutions are strongly shear-thinning, there is some arbitrariness in assigning a single value to the suspending fluid viscosity μ_o. In the previous experiments, the viscosity was evaluated at the wall shear rate, but the oscillatory tube radius adds the further complication that the wall shear rate varies with axial position. To maintain some comparison with (I) and (II), the following method has been employed. Pressure drop-flow rate measurements were made for a Newtonian suspending fluid (UCON LB-1715) with no drops present (see Section 3). The data follow the Hagen-Poiseuille law for a straight-wall tube of some particular value of the radius, which is then defined as an "effective" radius r_{HP}. The wall shear rate was calculated assuming that the fluids exhibit power-law dependence of the viscosity on the shear rate $\dot{\gamma}$,

$$\mu = m\dot{\gamma}^{n-1} \tag{1}$$

The appropriate parameters are $n = 0.45$, $m = 12.0$ for 0.5% Separan and

$n = 0.40$, $m = 33.8$ for 1.0% Separan. The effective viscosity is then τ_w/β_w where the wall shear stress τ_w is calculated for any fluid from a force balance as

$$\tau_w = \frac{r_{HP}\Delta P}{2L} \tag{2}$$

and the wall shear rate β_w is given by

$$\beta_w = \frac{3n + 1}{4}\left(\frac{4Q}{\pi r_{HP}^3}\right) \tag{3}$$

It was found that the value of the viscoelastic fluid viscosity depended on the method of solution preparation; although care was taken to treat each solution uniformly, the value obtained for μ_o varied by as much as 10% for different preparations. Typical values of the suspending fluid properties are given in Table 2.

The (Newtonian) drop fluids consisted of various grades of Union Carbide UCON LB-Series lubricant, Dow Corning DC200, and Dow Corning DC510 Series silicone oils. Since $\Delta\rho/\rho_o$ is a parameter of the present experiments, densities were adjusted using clove oil with UCON oils and carbon tetrachloride with the silicone oils. The viscosity of the drop fluid was measured with a Canon-Fenske capillary viscometer. The interfacial tension was measured with a DuNuoy platinum ring tensiometer. Since this method depends on a density difference between the fluids, the value of γ for systems of equal density was determined by extrapolation to $\Delta\rho \to 0$.

2.3 Conditions of the Experiments

The experiments were conducted at two volumetric flow rates, $Q = 4.6$

and 8.7 ml/min. Measurements of ΔP^+, U/V, and drop shape were made for five drop sizes listed in Table 3. To calculate the average velocity V, the (known) volumetric flow rate Q was divided by the effective cross-sectional area, πr_{HP}^2, so that $V = Q/\pi r_{HP}^2$. It may be noted, in this regard, that tracer particles were used to determine that no visible flow separation occurred during the course of the experiments. The non-dimensional drop size λ is also based on the effective Hagen-Poiseuille radius r_{HP}, and this provides a direct comparison with the results of (I) and (II). The dimensionless additional pressure drop is defined as $\Delta P^+ r_{HP}/\mu_o V$.

Values of the inverse capillary number Γ are given in Table I. This parameter varies by a factor of fifty since both the interfacial tension and the flow rate are independently varied in the present experiment.

3. Pressure Drop-Flow Rate Characteristics for Single Phase Flow

The total pressure drop associated with the flow of the suspending fluid alone, i.e. with no drops present, was measured as a function of flow rate in the creeping flow regime. The three fluids used were UCON-LB-1715, 0.5% Separan, and 1.0% Separan.

Newtonian fluid: Pressure drop-flow rate data for flow through conduits are usually correlated in terms of a friction factor and Reynolds number. For flow of a Newtonian fluid through a straight-wall circular tube, the friction factor can be defined by $f = r\Delta P/\ell\rho_o V^2$, where r is the (constant) tube radius, ℓ is the tube length, and V is the average velocity. For laminar flow, the Hagan-Poiseuille law is then expressed as $f = 16/Re$.

A generalization of this correlation for a tube with periodically varying cross-section is complicated by the axial dependence of the tube radius, r(z). For comparison purposes, it is useful to incorporate the tube geometry in definitions of f and Re in a way that data for any circular tube of varying radius can be correlated on the same curve with data for a straight-wall tube. Thus, the varying wavy-wall tube radius is replaced by an "average" or "effective" radius which is independent of axial position. Data correlation will depend on how the effective radius is defined, and there is a degree of arbitrariness no matter how the choice is made. Franzen (1979) proposed a variety of definitions, including one which is based on the assumpotion that the Hagan-Poiseuille law applies over an infinitesmal length dz everywhere along the tube axis. The same type of correlating parameter was considered by Sheffield and Metzner (1976). The effective radius r_{HP} is then expressed as

$$r_{HP} = \left(\frac{LA_o^2}{\pi} \left[\int_o^L \frac{dz}{\varepsilon^2(z)} \right]^{-1} \right)^{1/4} \tag{4}$$

Here, $\varepsilon(z)$ is the function which describes the axial variation in tube cross-sectional area, A_o is the area at $z = 0$, and L is the period of the tube wall oscillation.

We have evaluated r_{HP} for the tube in the present experiments. The tube radius R is given by $R = R_o + a \sin(2\pi z/L)$, where $R_o = 0.35$ cm, $a = 0.1$ cm, and $L = 1.52$ cm. The integral was evaluated numerically to yield the result that $r_{HP} = 0.316$ cm. The nominal velocity V is then taken as $Q/\pi r_{HP}^2$ where Q is the (known) volumetric flow rate. Using these "definitions" for r and V in f and Re, the data are presented in a log-log

plot of f as a function of Re, which is shown in Fig. 3. The data for the wavy-wall tube coincide precisely with the curve for a straight-wall tube with radius r_{HP}. An identical value for the "effective" radius was also determined by calculating the value which gave the best least-squares fit of the wavy-wall tube data to the Hagan-Poiseuille law in its integrated form for a straight-wall tube. It should be pointed out that an average value for the amplitude of the radius, 0.350 cm, and the radius that gives the average cross-sectional area of the tube, 0.357 cm, as well as the other "effective radii" defined by Franzen (1979), give values for r which differ from r_{HP}. Although use of any constant value for the effective radius will give a linear relationship between f and Re, the slope on a log-log plot is -1 only for r_{HP}. For this reason, r_{HP} will be employed also in calculating f and Re for representations of the pressure drop-flow rate data for the viscoelastic suspending fluid.

Neira and Payatakes (1979) have calculated numerically the pressure drop associated with the flow of a Newtonian fluid through a tube of sinusoidally varying diameter. The results apply for all values of the amplitude of the oscillation. The calculated values for f as a function of Re are within 2% of our measured values over the range of Re covered in the present experiment.

Non-Newtonian fluids: Sheffield and Metzner (1976) have shown that the accuracy of the correlation of pressure drop-flow rate data for flow of Newtonian fluids in the wavy-wall tube is not particularly sensitive to the value of the effective radius which is used. Thus, when data for flow of Newtonian fluids through actual porous media are correlated using

a cylindrical capillary model of the pore structure, accurate results are obtained, even though the convergent/divergent nature of the pores is neglected. However, when data for porous media flow are correlated for fluids which exhibit a shear-thinning viscosity, a more accurate representation is obtained if the wavy-wall tube model is employed (cf. Sheffield and Metzner, 1976). This result suggests use of the effective radius (4) and a shear rate dependent viscosity based on the power-law model (1) for correlation of the wavy-wall tube pressure drop data. The Reynolds number is then given by

$$Re_n = 2^{3-n} \left(\frac{3n + 1}{n}\right)^{-n} \frac{(2r_{HP})^n v^{2-n}}{m} \qquad (5)$$

Unfortunately, it is exceedingly difficult to incorporate other rheological features such as normal stress differences and characteristic relaxation times associated with the elastic response of the fluid without solving the equations of motion using a "complete" rheological model to obtain exact velocity and pressure fields for the wavy-wall tube. The usual approach is to temporarily ignore these rheological features. If the only non-Newtonian behavior exhibited in the flow were a shear-thinning viscosity, data for ΔP^+ for non-Newtonian fluid flow "should" follow the same functional relationship as the Newtonian data, $f = 16/Re_n$, where Re_n is the power-law Reynolds number. Deviations from this behavior must therefore be attributed to the neglected rheological features.

The data for the 0.5% and 1.0% aqueous solutions of Separan AP-30 are shown in Fig. 3. The power-law model parameters were evaluated from simple shear flow data over a range of shear rates $0.3 \leq \dot{\gamma} \leq 10\ s^{-1}$. It

can be seen from Table 2 that this range of $\dot{\gamma}$ encompasses the values of the wall shear rate β_w (based on r_{HP}) appropriate to the experiment. It is clear from Fig. 3 that the measured value of f for each of the viscoelastic cases is larger than the value of f for either a power-law or Newtonian fluid at the identical value of Re. The data exceed the "power law" prediction in all cases and by as much as 35%. Similar deviations, both in direction and magnitude, were observed by Michele (1977) for the flow of polymer solutions through a circular tube with abrupt alternate expansions and contractions in diameter. Franzen (1979) observed the same qualitative behavior for a variety of periodic tube geometries. A shear-dependent viscosity alone is apparently insufficient to explain the deviation of the pressure drop/flow rate results (i.e. f vs. Re) from Newtonian behavior.

Under some conditions, the pressure drop may depend substantially on the elastic response of the fluid to the Lagrangian unsteadiness of the flow. In particular, the results may, in part, be governed by an interaction between the characteristic relaxation time of the fluid and the Lagrangian timescale of the flow imposed by the wavy-wall geometry. James and McLaren (1975) have considered a similar problem, specifically the effect of flow unsteadiness on the pressure drop for flow through a packed bed. They suggest that one mechanism which can act to increase the pressure drop involves the effect of the time-dependent flow on the primary normal stress difference. The normal stress acts as a hoop thrust on the curved surface of the tube wall, and is proportional to the square of the shear rate. If

the fluid response time is comparable to the timescale for flow through one period of the tube, the shear rates (and normal stresses) may not be equal at points equidistant upstream and downstream from the throat. In this case, the unsteadiness of the flow coupled with the finite fluid response time results in a net increase in the drag, or equivalently, an increase in the pressure drop for a given flow rate. The contribution of the normal stress effect to ΔP is estimated by James and McLaren to be $O(1)$, i.e. comparable to the Newtonian component. If fluid elasticity plays a role in the deviation of our results from generalized Newtonian behavior, then the data for f should correlate with De which provides a measure of the fluid timescale relative to the timescale of the flow. In estimating the value of De for the present experiment, we have used the results of Marshall and Metzner (1967) who also considered non-Newtonian flow through packed beds. Flow through a convergent (divergent) section of an individual porous channel was modeled by flow toward (away from) the apex of a circular cone. Using this simple geometry for the flow channel, Marshall and Metzner (1967) calculated a timescale over which the deformation rate varies and hence, an expression for De:

$$De = \theta \frac{V}{4} \left(\frac{3}{2} + \frac{1}{4} \left(\frac{L_1}{L_2} \right)^2 \right)^{\frac{1}{4}} \qquad (6)$$

where V is the nominal velocity, θ is the characteristic relaxation time of the fluid, and L_1 and L_2 are the characteristic length and width of the cone. To estimate θ for the Separan solutions, we have used the contravariant form of the convected Maxwell model which relates θ to the normal stress measured in steady simple shear flow. The value of θ is then given by

$$\theta = \frac{1}{2\dot{\gamma}^2}\left(\frac{\tau_{11} - \tau_{22}}{\mu_o(\dot{\gamma})}\right) \qquad (7)$$

where $\tau_{11} - \tau_{22}$ is the primary normal stress difference, μ_o is the viscosity and $\dot{\gamma}$ is the shear rate. Unfortunately, the characteristic time of the fluid estimated in this manner is a function of the shear rate $\dot{\gamma}$. We have evaluated θ at the shear rate contained in (6) to determine De. The product of fRe_n for each point in Fig. 3 is plotted as a function of De in Fig. 4. The data plotted in this fashion show the deviation from "power-law" (or purely viscous) fluid behavior increases with De as expected. It is not possible to determine an "onset" value for De from the present data since even the smallest value of De covered in the present experiment (~ 0.2) shows a measurable deviation from generalized Newtonian behavior. The magnitude of the deviation remains O(1) even as the value of De is increased to unity. Similar results were obtained by Michele (1977) and Franzen (1979) for viscoelastic flow through a variety of oscillatory circular tubes at comparable values of De when estimated in the above manner. However, Marshall and Metzner (1967) and James and McLaren (1975) observed considerably larger deviations for viscoelastic flow through packed beds. Increases in f by as much as a factor of forty were observed for values of De near unity. These larger, i.e. O(10), deviations in the pressure drop appear to occur at critical rates of elongation or stretching. Now, according to the Maxwell model and others in the same rheological class, the stress in a steady purely elongational flow is predicted to become infinitely large as the dimensionless stretch rate $2\theta\dot{E}$ approaches unity. In practice,

however, the stress does not become infinitely large, but dramatic increases in the stress are observed when the rate of extension is increased beyond some critical value. We have calculated the value of the dimensionless stretch rate, at least for fluid elements along the centerline of the model conical geometry, under flow conditions of the present experiment.† The value of $2\Theta\dot{E}$ does, in fact, exceed unity for the higher flow rates covered in Figs. 3 and 4. Nevertheless, O(10) increases in ΔP are not observed in the present experiment. We can suggest two possibilities in light of these remarks. First, perhaps the conical model for the geometry of the wavy-wall tube is insufficient to accurately predict the critical value of stretching necessary to induce "large" increases in ΔP. Alternatively, the flow kinematics may adjust to avoid large-scale stretching of the macromolecules and the accompanying increase in the stress. Specifically, the flow may tend to "channel" through the central portion of the tube and thereby partially ignore the convergent/divergent character of the tube boundary. Sheffield and Metzner (1976) have, in fact, suggested that the effect of channeling alone could account for a deviation in correlations of the type illustrated in Figure 3, without any need to account for viscoelastic flow contributions. Presuming that channeling occurs, they calculated the pressure drop for flow of a purely viscous shear-thinning fluid through an "effective" wavy-wall tube which was intended to mimic the boundary of the central channeling core. Since the

†Michele (1977) observed no "large" increases in ΔP for flow of 1% Separan in a convergent/divergent tube even when the Reynold's number was increased to sufficiently large values for the onset of turbulence.

effective tube is assumed to have the same minimum diameter as the actual tube, the pressure drop for a fixed volumetric flow rate is increased in the effective tube. Calculations based on the Sheffield and Metzner model show that a maximum diameter of 0.58 cm would be required in the effective tube (compared with a minimum and maximum in the actual tube of 0.50 cm and 0.9 cm, respectively) to account for the maximum deviations shown in Figure 3. Although this value appears qualitatively reasonable, the flow visualization studies that we carried out did not exhibit any corroborating evidence of channeling of this magnitude. Furthermore, the existence of some degree of channeling would not eliminate the potential importance of elasticity effects in determining the pressure drop for a viscoelastic liquid, as Sheffield and Metzner suggest. The flow remains Lagrangian unsteady even if the "effective" tube were to reduce to a straight cylinder of diameter equal to the minimum diameter of the wavy-wall tube since the boundary conditions along this "effective" tube wall must vary periodically with axial distance from slip to no-slip. Thus, when the fluid and convective timescales are comparable, De would still be expected to play a role in correlating pressure drop-flow rate data. It may be expected that the degree of fluid channeling would be diminished in any case by the presence of an immiscible drop which is larger than the minimum tube diameter. This expectation is confirmed by photographs which show that the drop can extend well into the widest regions of the tube, especially when the drop is non-neutrally buoyant (cf. Sections 3 and 4).

Although it would be of considerable fundamental interest to conduct two-phase flow experiments in a domain where suspending fluid visco-elasticity induces large deviations from Newtonian behavior in the single-phase flow problem, the regime characterized by O(1) deviations appears to

us to be more important from the standpoint of tertiary oil recovery optimization. Since it appears that O(1) values for De are necessary before large deviations are important, it would require sweep velocities much larger than those usually encountered in chemical flooding operations before large elongational effects occur. Furthermore, the experiments of James and McLaren (1975) suggest that the effect of pusher fluid viscoelasticity in this domain would result in an order-of-magnitude increase in the pressure drop necessary to maintain a constant sweep velocity. This would imply that operation in a regime of large deviations from generalized Newtonian behavior would be highly undesirable. Nevertheless, the experiments reported here show that the effects of non-Newtonian rheology on ΔP^+, mobility and dispersion phenomena may be of considerable interest even at "sub-critical" values of De.

4. Experimental Results for Two-Phase Flow

As the suspended drop moves through the wavy-wall tube, it causes a periodic variation in the pressure drop. A typical output from the transducer indicator is shown in Fig. 5. Each oscillation of the output signal corresponds to the drop's passage through one period of the oscillatory test section. Thus, it is obvious from Fig. 5 that eight wavy-wall units were positioned between the two pressure taps for the particular run illustrated. There are two spurious transient disturbances present in each recording of the pressure signal. As the drop enters the measurement section, the additional pressure drop signal displays a transient disturbance due to the fact that the drop passes directly over the pressure tap. This transient decays before the drop enters the next convergent section, and, hence, the signal associated with the passage of the drop through each of the successive convergent/divergent units is

periodic. The second spurious transient occurs when the drop passes over the second pressure tap as it leaves the measurement section. This additional pressure drop signal decays rapidly to the value with no drops present in the measurement section (zero).

Data for ΔP^+ and U/V as a function of λ are presented in Figs. 6 through 14. The measured values for each suspending fluid are shown in separate figures. The values for ΔP^+ represent an arithmetic average of the maximum and minimum amplitudes of the oscillatory transducer signal. Because the transducer signal was very closely sinusoidal for all the measurements made, this simple average is a good approximation to the time average over several oscillations (indeed, sample comparisons for "typical" systems show these two averages differ by less than 5%). The magnitude of the oscillatory part of the signal, $\delta(\Delta P^+) = \Delta P^+_{max} - \Delta P^+_{min}$, is also shown as a function of λ. Furthermore, the values of U/V reported in the figures also represent "average" velocities. Attributing a single value to the velocity of the drop is meaningful only in the sense of some average, since the axial velocity at any point varies with axial position. As an average velocity, we take simply the inverse of the time for transit between known points separated by an integral number of wavelengths (16) divided by the distance between these points. In practice, we have taken the leading edge of the drop as a reference for determination of the transit time and the average velocity. The average velocity determined in this manner is the same for any point in the drop as long as the shape remains periodic during transit. In some cases, however, the drop exhibits an elongation that increases monotonically

with time while the drop is in the test section. A non-periodic variation in drop shape of this type will be reflected in the value of U/V reported here, and therefore we will consider carefully the effect of deformation on the reported values for U/V whenever appropriate. The measured values of σ, Γ and $\Delta\rho/\rho_o$ for each system and for each flow rate are indicated on the figures and also compiled in Table 1. As in (I) and (II), comparisons between selected systems will help expose the effects of a particular material or flow parameter.

Finally, we have photographed the shape of the drop as it travels through the test section in the manner described in Section 2. We present, in this section, detailed descriptions of deformation and breakup (when applicable) for a wide range of the material parameters. These descriptions are based on the recorded observations and are supplemented with representative "still" photographs shown in Fig. 15. The pictures in Fig. 15 are actual photographs of the video monitor.

4.1 Newtonian Suspending Fluids

Table 1 indicates that the inverse capillary number Γ varies by more than a factor of fifty for the Newtonian suspending fluid systems, $0.043 \leq \Gamma \leq 2.54$. For the purposes of our discussion, we group these systems according to relative magnitudes of Γ. Systems 2a, 2b, 2c and 3 comprise a group of fluid systems which yield "small" values for Γ, $\Gamma < 0.083$; system 1 has values for Γ which are "intermediate", $0.5 < \Gamma < 0.9$; finally, systems 4, 5 and 6 form a group with "large" values for Γ, $\Gamma > 1.3$. The designations "small" and "large" are labels

and do not necessarily imply asymptotic behavior for ΔP^+ or U/V. We will consider the data for each group separately and then make comparisons between the groups to illustrate the effects of the value of Γ.

a. Small-Γ Systems

We consider first the results for the small-Γ systems, i.e. $\Gamma < 0.083$. Since Γ describes the relative importance of the viscous stress which tends to deform the drop compared to the interfacial tension which resists deformation, the small-Γ group contains the "least deformable" drops. Within the group, systems 2a, 2b and 2c vary in the (small) degree of non-neutral buoyancy. System 3 has the same value for Γ and is neutrally buoyant, but varies slightly from 2a - c in viscosity ratio ($\sigma = 0.60$). The additional pressure drop for these small-Γ systems is positive for small drops, attains a maximum as the drop is made larger at a dimensionless drop size which apparently depends on the material and flow parameters, and then decreases, becoming negative as the drop is made sufficiently large. This behavior is reminiscent of a similar trend shown by drops with comparable values of σ, $\sigma < 1$, in the straight-wall tube flow. Indeed, results for system 3a of (I) ($\sigma = 0.58$, $\Gamma \approx 0.075$) show the same qualitative trend as illustrated in Fig. 6. It was shown in (I) and (II) that the value of ΔP^+ is determined by several competing mechanisms including the disturbance of the flow caused by the drop, drop deformation, interactions between the drop and the wall, and the simple replacement of suspending fluid with drop fluid of a different viscosity. It was also shown (cf. (I)) that as the drop is made sufficiently large, the contribution to ΔP^+ from the simple replacement of fluid determines the sign of

ΔP^+. The identical asymptotic behavior is observed in the present results. For values of $\sigma < 1$, the additional pressure drop ΔP^+ is negative in the limit of large λ, because suspending fluid is replaced by the less-viscous drop fluid. Similarly, we shall soon see that when $\sigma > 1$, ΔP^+ is positive in the large-λ asymptote.

We have also studied the effect of an eccentric position of the drop in the tube owing to a difference in density between the drop and suspending fluid for drops within the small-Γ group. It was shown in (II) that relatively small values of $\Delta\rho/\rho_o$ produced asymptotic behavior, as far as the effects of density difference were concerned, for flow through the straight tube. Therefore, we studied the effect of density differences here for the smallest possible values of $\Delta\rho/\rho_o$ that could be measured. The values of $\Delta\rho/\rho_o$ for systems 2a, 2b and 2c are 0.003, 0.000 and 0.001, respectively. Even though these values of $\Delta\rho/\rho_o$ may appear at first glance to be "negligible", they induce an eccentricity in the lateral position of the drop which is clearly visible as the drop travels through the straight-wall tube entry section. The results displayed in Figs. 6 and 9 for systems 2b and 2c show that the value $\Delta\rho/\rho_o = 0.003$ is sufficient to cause a measurable increase in the additional pressure drop and a decrease in drop mobility. The qualitative influence of the eccentric position of the drop is identical to that observed for the straight-wall tube. Furthermore, Fig. 6 shows that the effect of $\Delta\rho/\rho_o$ on ΔP^+ diminishes as the drop is made sufficiently large. A similar result is shown for the drop mobility U/V in Fig. 9. Indeed, for $\lambda > 1.1$, any effect of $\Delta\rho/\rho_o$ on ΔP^+ and U/V is no longer apparent. The identical trend was also observed for the straight-wall tube flow.

The effect of the remaining parameters, namely viscosity ratio σ and dimensionless bulk velocity Γ, have also been studied for systems in the small-Γ group. System 3 differs from 2b only in viscosity ratio (σ = 0.60, compared to 0.40). Figures 6 and 9 show that the effects of an increased drop viscosity relative to the viscosity of the suspending fluid are an increased value for ΔP^+ and a small decrease in drop mobility. The effects of bulk velocity are shown also in Figs. 6 and 9 for system 2b. Since Γ is proportional to the bulk velocity V, the two flow rates covered in this experiment give a variation in Γ of nearly a factor of two for Newtonian fluids. The effect of this variation in Γ on ΔP^+ is a marked increase in ΔP^+, as can be seen in Fig. 6. Furthermore, the same variation in Γ results in a markedly lower drop mobility. The values of U/V for system 2b with Γ = 0.043 are: 1.36, 1.20 and 1.12 for λ = 0.62, 0.91 and 1.14, respectively. These can be compared with system 2b with Γ = 0.065 which gives corresponding values U/V of 1.50, 1.36 and 1.28. The effects of Γ on ΔP^+ and U/V are qualitatively identical to the observations noted in (I) for drops with comparable values of σ in the straight-wall tube.

The drop undergoes relatively small deformation for small values of Γ ($\Gamma < 0.083$), as expected. A dimensionless measure of drop deformation in the wavy-wall tube, albeit an arbitrary one, is the ratio of the longitudinal drop length relative to the undeformed drop diameter. We shall denote this ratio by D. The shape of the drop in the present case varies periodically and, therefore, the length of the deformed drop at any point depends on its axial position in the wavy-wall tube. We calculate

D based on the maximum length attained during the oscillatory deformation. For system 3, which is typical of the small-Γ cases, D increases as the size of the drop is made larger from D = 1.03 at λ = 0.77 to D = 1.24 at λ = 1.15 for V = 0.24 cm/s. The drop undergoes a slightly larger deformation as the average velocity is increased, with D ranging from 1.07 to 1.30 for V = 0.46 cm/s for the same range of λ. The maximum drop length is attained as the drop is midway through the point of narrowest constriction as shown in Fig. 15. This coincides with the point at which the additional pressure drop achieves its maximum value. It is apparent from Fig. 15 that the gap between the drop and the tube wall at this point is very small for these small-Γ drops.

In conjunction with these observations concerning drop deformation, we note that the magnitude of the oscillatory part of the ΔP^+ signal increases monotonically with λ for small-Γ drops. The sensitivity of $\delta(\Delta P^+)$ to λ is relatively weak for small values of λ, showing only a slight increase until λ exceeds $\sim$0.78. Then, $\delta(\Delta P^+)$ increases much more rapidly with further increases of λ. The values of λ at which this change in the sensitivity of $\delta(\Delta P^+)$ occurs correspond to a drop with undeformed radius approximately equal to the smallest radius of the wavy-wall tube. Thus, drops which are smaller (in their undeformed shape) than the tube even at the most narrow constriction show little dependence of $\delta(\Delta P^+)$ on λ. However, when the drop is made larger than the wavy-wall tube "throat", $\delta(\Delta P^+)$ increases rapidly with λ. We note also the effects of other parameters on $\delta(\Delta P^+)$ for small-Γ drops. There is practically no effect of density difference on $\delta(\Delta P^+)$ as is seen in Fig. 6. Also shown in the same figure is an increase in $\delta(\Delta P^+)$ owing to an increase in the viscosity. Not shown in

the figure are the values of $\delta(\Delta P^+)$ for System 2c. At the larger flow rate (Γ = 0.083) the values of $\delta(\Delta P^+)$ coincide with those for System 2b with Γ = 0.083. However, the values of $\delta(\Delta P^+)$ for System 2c with Γ = 0.043, i.e. the smaller flow rate, are substantially larger, and range from 0.42 to 8.4 over the range of λ shown in Fig. 6. Thus, the effect of bulk velocity on $\delta(\Delta P^+)$ is substantial, at least for small-Γ drops.

b. Intermediate-Γ Systems

We consider now the behavior of drops with greater values of the inverse capillary number, specifically system 1 with Γ = 0.50 and 0.94 These values are in the range we have labelled as the "intermediate" values of Γ. The viscosity ratio for system 1 drops, σ = 0.0014, is the smallest value employed in the present experiments. The most striking feature of this system is that most of the drops exhibit breakup in the test section. At the smaller flow rate, breakup occurs for drops with $\lambda > 0.8$. The total number of satellite drops formed during transit through the test section increases with λ. For the larger flow rate, breakup occurs at all values of λ, and the breakup process is periodic, with a maximum of one satellite drop formed for each oscillation of the tube boundary. The first satellite drop, which is always formed in the first oscillation of the test section, is the largest; the sizes of subsequent satellite drops decrease monotonically as the parent drop continues through the test section. The size of a representative satellite drop is larger if the average flow velocity V and/or the size of the parent drop is made larger. In the case of the largest flow rate and drop size, the first satellite drop forms second generation satellites. Drop breakup occurs for System 1 without an extreme increase in the drop's deformed length, as measured by

D. Indeed, the value of D does not vary appreciably with drop size and flow rate (in contrast to the small-Γ cases).

Figure 9 indicates that the relative velocity of a system 1 drop increases with λ for small values of λ at the smaller flow rate ($\Gamma = 0.50$), but becomes insensitive to further changes in λ abruptly at $\lambda \approx 0.8$. This is precisely the value of λ at which onset of drop breakup is observed. Apparently, mobility becomes insensitive to drop size for system 1 drops once the drop is made sufficiently large for breakup to occur. For the larger flow rate ($\Gamma = 0.94$), breakup occurs at all values of λ, and therefore there is no abrupt transition in U/V. The value of U/V for a given drop size increases dramatically with the bulk velocity V, and this effect may be connected with the observed shape of the drop in the tube. If we consider the instantaneous value of the length of the drop along the tube centerline, it is clear that the system 1 drops exhibit qualitatively different deformation for the two flow rates. At the smaller bulk velocity, the drop forms a shape that resembles a right circular cone as the leading edge enters a convergent section. At this instant the axial drop length is approximately 0.8 of its undeformed diameter, and the pressure drop signal is a maximum, which indicates that this configuration of the drop offers the largest resistance to motion. Photographs of the same drop for the larger bulk velocity ($\Gamma = 0.94$) show that the axial length of the drop is considerably larger and always exceeds the undeformed drop diameter. The shape of the drop as the leading edge enters the convergent section resembles a prolate spheroid with major axis along the tube center. Although this point corresponds also

to the maximum value for ΔP^+ obtained during the oscillatory deformation, the value of ΔP^+ is considerably less than the value obtained at the lower bulk velocity. This result is reflected in Fig. 8 which shows that ΔP^+ and therefore the resistance to flow owing to the presence of the drop is smaller for the larger bulk velocity, with the effect of V becoming larger with increasing λ. Figure 8 indicates that the additional pressure drop for system 1 drops is negative for all values of λ, decreasing monotonically as the drop size is made larger. It should be noted that the satellite drops which are formed during the breakup process described above are apparently not large enough to perturb the pressure drop signal as they trail the parent drop through the test section.

c. Large-Γ Systems

We consider now the remaining Newtonian systems, that is, the group with values of the inverse capillary number which are designated as "large", $\Gamma > 1$. A qualitatively different type of deformation is observed for the large-Γ Newtonian systems (4, 5 and 6), and this difference influences the values obtained for ΔP^+ and U/V. When a system 4 drop is made sufficiently large, $\lambda > 0.8$, the drop experiences a "permanent" elongation during its passage through the test section. The length of the drop increases steadily during the first five or six oscillations. The rate of elongation suddenly increases when the drop becomes sufficiently long that the leading edge of the drop begins to invade the next constriction before the trailing edge of the drop has completely evacuated the preceding one. This behavior is illustrated in Fig. 7 where D is plotted as a function of the number of oscillations through which the drop has passed for λ = 1.04 and V = 0.24 cm/s. Elongation continues until an equilibrium

"length" is attained, D = 1.9 for this particular case. Photographs of the drop are shown in Fig. 15. The drops formed from systems 5 and 6 are mroe viscous, and they exhibit even larger deformation, attaining a length equal to four tube wavelengths while still in the test section. The degree of deformation for a given viscosity ratio increases when the size of the drop and/or the average velocity are made larger. In the cases of larger V and λ, the highly elongated drops are observed to break in the straight tube following the test section. The drops which result from breakup in the relaxation section are considerably larger than the satellite drops which form in the test section for system 1. Qualitative results for deformation and dispersion for systems 4, 5 and 6 are summarized in Table 3.

When permanent elongation takes place, the value reported for the average velocity of the drop must be considered carefully. In this case, the velocity of the drop varies with axial position,not over a timescale L/V, but instead over the time associated with the permanent elongation of the large-Γ drop. Therefore, changes which take place over this timescale should be accounted for in the data. Specifically, the length of the drop changes, but because we have taken the leading edge of the drop as a reference for determination of the average velocity, the values for U/V in Fig. 9 for systems 4, 5 and 6 reflect a component of the velocity owing to increasing drop length. To identify this component and separate it from the velocity of the center-of-mass of the drop, we have used the videotape recordings to <u>estimate</u> the velocity of the center of the drop. Within the limits of an estimate, it was found that the velocity of the

center of the drop did not vary systematically among the systems for a fixed value of V and λ. Therefore, a single set of the average values of U/V with respect to the drop center is reported in Table 3.

In view of these remarks, the values of U/V shown in Fig. 9 reflect the effect of viscosity ratio and drop size on the average rate of extension during transit through the test section. The data confirm the qualitative observations already reported. System 4 drops (σ = 0.070) show no permanent elongation for the smallest value of λ for both flow rates. In these cases, the value of U/V in the figure agrees closely with the value of the center of the drop reported in Table 3. However, when the viscosity of the drop is made larger, the value for U/V becomes larger than the value for the center of the drop. The difference between the values for U/V in Fig. 9 and Table 3 is proportional to the average rate of elongation of the drop in the test section. It is clear from Fig. 9 that drop extension increases with σ, Γ and weakly with λ in the ranges of these parameters which was covered. It is obvious, however, that this result cannot be extrapolated to $\sigma \to \infty$.

The magnitude of the average rate of extension of the drop is important to the degree of dispersion, at least in a qualitative sense. The number of drops which result from breakup in the relaxation section is very roughly proportional to the degree of extension of the original drop. Furthermore, the difference between U/V and the velocity of the center of the drop is related to the degree of axial separation of the fragment drops that result from breakup.

Several other features of the data for ΔP^+ for large-Γ systems merit

comment here. The pressure drop ΔP^+ appears to be most closely related to the viscosity ratio σ. Furthermore, the profiles of ΔP^+ as a function of λ are relatively insensitive to changes in the values of Γ, as can be seen easily by comparing ΔP^+ for system 4 to similar data for the small-Γ systems. Large deformation and elongation of the drop over multiple wavelengths of the tube tends to diminish the magnitude of the oscillatory part of the pressure drop signal. Indeed, the oscillation is completely absent in some cases. Consequently, data for $\delta(\Delta P^+)$ for the large-Γ systems are not reported. It is interesting to note, however, that the pressure drop signal does not vary significantly over a timescale associated with the elongation of the drop in the test section. That is, the extreme deformation of the drop does not appear to affect ΔP^+ even though $\delta(\Delta P^+)$ is reduced or eliminated.

The effect of an eccentric position of the drop owing to non-neutral buoyancy was studied also for the large-Γ systems 7 and 8. The values of $\Delta\rho/\rho_o$ were relatively small (0.022 and 0.024, respectively) so that comparisons could be made with straight-wall tube data from (II). It was shown in (II) that asymptotic behavior for "large" $\Delta\rho/\rho_o$ occurs at values which are comparable to the values of $\Delta\rho/\rho_o$ employed here. The effects of density differences noted here and in (II) are likely to apply to many industrial and biological processes, at least qualitatively, since values of $\Delta\rho/\rho_o$ of at least this magnitude are likely to be common. A non-neutrally buoyant drop formed from systems 7 or 8 exhibits a greater degree of deformation than that noted for the large-Γ neutrally buoyant cases. The elongated drop deviates far from the tube centerline, well into the

bowed sections of the tube, and extends over many wavelengths of the test section. Furthermore, system 7 drops exhibit breakup into small drops while still in the test section for $\lambda > 1.05$ with $V = 0.24$ cm/sec, and for all values of λ with $V = 0.46$ cm/sec. The drops spend a large fraction of time in the low mobility regions near the tube wall in the regions of large cross-sectional area. Further breakup occurs in the relaxation section, resulting in the formation of many droplets of various sizes. System 8 drops exhibit breakup within the test section for all values of V and λ. It is interesting to note that the more viscous drops break up at smaller values of λ and V. It was impossible to determine appropriate values for ΔP^+ and U/V in some cases. When breakup was substantial in the test section, the signal for ΔP^+ did not attain a steady-state value before the leading edge of the drop reached the downstream pressure tap. Similarly, a unique value for the velocity was also impossible to determine.

4.2 Viscoelastic Suspending Fluid, 0.5% Separan

The data for the viscoelastic suspending fluids are now considered, beginning with 0.5% Separan AP-30, the smaller of two polymer concentrations employed in the present study. Data for ΔP^+ for neutrally buoyant and non-neutrally buoyant drops are presented in Figs. 10 and 11, respectively. The relative velocities U/V for this case are shown in Fig. 12.

The value of ΔP^+ appears to be strongly dependent on the value of the drop viscosity for all values of Γ. The additional pressure drop ΔP^+ is positive when $\sigma > 1$ and negative when $\sigma < 1$. The only exception to this general rule is the non-neutrally buoyant system 12. In this case, ΔP^+

remains positive for all drop sizes although $\sigma < 1$. However, it should be pointed out that $\Delta\rho/\rho_o$ is relatively large (0.037) in this case, and it is known from the results of (II) that drop eccentricity owing to a density difference between the drop fluid and suspending fluid can make a significant positive contribution to ΔP^+, especially for viscosity ratios near unity. On the other hand, the effect of drop eccentricity appears secondary to the effect of σ when σ is large, as can be seen from a comparison of system 11 ($\Delta\rho/\rho_o = 0.0$, $\sigma = 18.2, 12.6$) and system 13 ($\Delta\rho/\rho_o = 0.036$, $\sigma = 23.2, 16.1$) which show nearly equal values for ΔP^+. The additional pressure drop increases with flow rate for most viscoelastic fluid systems studied, the non-neutrally buoyant system 12 excepted.

Although the value of ΔP^+ appears to be dominated by σ for the range covered here, the drop deformation and mobility depend on the value for Γ as well. As in the case of the Newtonian suspending fluids, the systems can be divided into groups based on the relative values for Γ. Systems 11 - 13 are in the "small-Γ" range, $0.05 < \Gamma < 0.096$, while systems 9, 10 and 14 have values for Γ which are in the range we have labeled for this discussion as "intermediate-Γ", $0.24 < \Gamma < 0.43$.

a. Small-Γ Systems

The dependence of drop mobility on λ for small-Γ drops in 0.5% Separan shows behavior which is similar to that observed for the Newtonian suspending fluids. The relative velocity is a monotonically decreasing function of drop size. The actual values of U/V are roughly the same for "equivalent" cases of Newtonian and viscoelastic suspending fluids, i.e. for comparable values of Γ and σ. The effect of drop eccentricity is to decrease the value of U/V, as can be seen by comparing systems 11 and 13, but the sensitivity of U/V to eccentricity is diminished compared to the Newtonian result.

For $\Gamma < 0.096$, the drops show a deformation pattern which differs qualitatively from the Newtonian suspending fluid shape. The small-Γ drop in 0.5% Separan assumes the shape of a prolate spheroid as it passes through the narrow constrictions. The maximum pressure drop is attained in this configuration when the drop is approximately half-way through the throat of the constriction. However, unlike the case of the Newtonian suspending fluid, small-Γ drops in 0.5% Separan tend to maintain the shape well after the leading edge of the drop has passed through the throat. We shall return to this point in Section 5. The effect of non-neutral buoyancy on the drop shape is barely visible especially in the narrow regions of the tube, and the eccentric drops show little asymmetry in shape.

b. Intermediate-Γ Systems

The intermediate-Γ group for 0.5% Separan, systems 9, 10 and 14, $0.24 < \Gamma < 0.43$, show trends for drop mobility as a function of λ that are qualitatively different than those exhibited by small-Γ systems. The importance of Γ is made apparent by a comparison of systems 9 and 12 which are shown in figure 12. Although U/V is a strong function of λ for system 12 ($\Gamma \approx 0.06$), it is nearly independent of λ for system 9 ($\Gamma \approx 0.40$). We find also that the value of U/V for these intermediate-Γ cases is dominated by the value of the viscosity ratio. The mobilities of systems 9, 10 and 14 drops increase as the viscosity ratio is made smaller. This effect of the viscosity ratio is sufficiently strong to dominate the effect of eccentric position which usually retards drop mobility if all other parameters are unchanged. Thus, system 14 drops have a greater mobility than the neutrally buoyant, but more viscous drops of systems 9 and 10. It must be emphasized that the behavior of the drop mobility described above

cannot be attributed to permanent elongation of the drops (as in the large-Γ Newtonian cases), since no such change in length during drop transit was observed for the intermediate-Γ groups in 0.5% Separan.

However, drops in the intermediate-Γ group in 0.5% Separan do undergo greater deformation than the small-Γ drops. Unfortunately, it was impossible to generate values for Γ in the "large-Γ" class which were covered for the Newtonian systems (there Γ was as large as 2.54), although this point will be reconsidered for 1.0% Separan suspending fluid in Section 4.3. Consequently, permanent elongation and drop breakup in the relaxation section, which were observed for Newtonian systems 4, 5 and 6 ($\Gamma > 1$), are not observed for the 0.5% Separan suspending fluid systems studied. However, another important dispersion process occurs for the 0.5% Separan suspending fluid. System 9, 10 and 14 drops develop tails which are shown in Fig. 15. The tail is observed to break up at its end, issuing a satellite drop which trails the parent drop. Tail breakup occurs at "critical" values of both the average velocity and the drop size. The width of the tail, and therefore, the size of the satellites, increases with V and λ, but decreases slightly as the parent drop continues through the test section. Furthermore, for smaller drops at the small flow rate, the tail forms as the drop passes through each constriction and "recoils" completely before the drop encounters the next convergent section. As the drop is made larger and/or the flow rate is increased, the tail is unable to retract completely in the divergent section before the leading edge of the drop enters the next con-constriction. When this occurs, the drop develops a "permanent" tail which grows in length as the drop passes through the test section. In every case,

these "permanent" tails are shed in the relaxation section following the test section. The satellite drops that are formed by these systems are smaller than the drops formed in the Newtonian system 1. Not surprisingly then, they are insufficient to affect the pressure drop during the course of the experiment. Of course, this does not imply that ΔP^+ would remain unchanged if the length of the wavy-wall tube was made larger.

The drop viscosity influences tail formation and breakup; drops with a lower viscosity evolve tails and shed satellite drops at lower values of the flow rate and drop size than their more viscous counterparts. Non-neutral buoyancy, on the other hand, is not a factor, except to skew the tail toward the tube wall.

4.3 Viscoelastic Suspending Fluid, 1.0% Separan

The effects of suspending medium viscoelasticity were studied further by varying the concentration of the aqueous polymer solution. The data for ΔP^+ and U/V for neutrally buoyant drops suspended in a 1.0% Separan AP-30 solution are shown in Fig. 12; corresponding data for non-neutrally buoyant drops are illustrated in Fig. 13. The characteristic time of the manometer-transducer system response was significantly longer in this case than the time for drop transit through one oscillation of the test section owing to the large zero-shear rate viscosity of the suspending fluid which also fills the manometer legs. When a drop entered the test section with 1.0% Separan as the suspending fluid, the pressure signal responded to the presence of the drop slowly, and the drop passed through

several wavelengths of the tube before a steady-state periodic signal was obtained. The value of ΔP^+ shown is the "average" of that signal. However, it is impossible to compare the magnitude of the oscillatory part of the signal for the 1.0% Separan cases with the other suspending fluids since the response time appears comparable to the period of the oscillation.

The additional pressure drop appears to be slightly reduced as the viscoelasticity of the suspending medium is increased. However, the sign and relative magnitude of ΔP^+ are dominated, as in previous cases, by the magnitude of σ, especially for large drops. The presence of small drops in 1.0% Separan produces little change in the pressure drop, as was also the case for the 0.5% Separan suspending fluid. In addition, drop eccentricity makes little contribution to the additional pressure drop.

a. Intermediate-Γ Systems

With 1.0% Separan as the suspending fluid, systems 17, 18, and 19 produced values for Γ which are in the "intermediate-Γ" range, according to our designation, $0.19 \leq \Gamma \leq 0.37$. No systems gave values of Γ in the small-Γ range owing to the larger nominal viscosity of the 1.0% Separan suspending fluid. Data for neutrally-buoyant system 17 show only a slight decrease in U/V as the drop is made larger. However, drop mobility for non-neutrally buoyant drops, systems 18 and 19, shown in Figure 13, exhibits a unique minimum as λ is increased. A comparison between these intermediate-Γ systems shows that U/V appears to be unaffected by σ or Γ at small values of Γ. However, for large values of Γ, U/V increases with decreasing viscosity ratio. The same qualitative dependence on σ was observed for 0.5% Separan suspending fluid for comparable values of Γ.

Indeed, the values of U/V are comparable for the two cases.

Drop deformation for the intermediate-Γ drops in 1.0% Separan is similar to the behavior noted for 0.5% Separan for intermediate values of Γ. The "magnitudes" of deformation, i.e. the values of D, are nearly equal for comparable values of Γ and λ. Furthermore, a tail forms and breaks off in the relaxation section, but only for the largest drop size and the highest flow rate. The drop location at the maximum pressure reading is shifted downstream slightly from the 0.5% Separan suspending fluid. A maximum pressure reading is attained when roughly two-thirds of the drop has passed the point of minimum tube diameter. In addition, an increase in the gap width between the drop surface and the tube wall was also noted.

b. Large-Γ Systems

System 15 and system 16 feature values for Γ ($0.86 \leq \Gamma \leq 1.12$) which are considerably greater than the 1.0% Separan systems already described. In terms of our previous designations, this range of values for Γ overlaps the "intermediate" and "large" classes. The drop mobilities for these two systems are large, with values for U/V in excess of 1.6 for system 15. In addition, the mobility increases with λ, especially for system 15, even though no "permanent elongation" of the drops is observed. The data for these two systems indicate that drop mobility is a strong function of viscosity ratio if all other parameters remain fixed, as was also noted for the intermediate-Γ cases. However, a notable difference between systems 15 and 16 and the intermediate-Γ cases is that the drop mobility appears to be independent of V and hence Γ for the larger values of Γ. A comparison of systems 14 and 9 with system 15 shows

this effect.

There are significant qualitative differences in the dispersion phenomena for drops suspended in the 1.0% viscoelastic medium. First, the drops show increased deformation over the 0.5% solution, although this is probably a consequence of the larger viscosity of the more concentrated polymer. More importantly, the formation and breakup of the tail for system 15 and system 16 drops exhibit different characteristics than those previously noted for the 0.5% Separan solution. It was noted that when a tail formed in the 0.5% Separan solution, a satellite drop broke from the end during passage through each of the wavy-wall tube oscillations. Although a tail forms just as readily in the 1.0% solution, breakup is drastically inhibited. The tail is capable of surviving several (three to ten) oscillations intact before issuing a satellite drop from its end. The thickness of the tail varies over its length by more than a factor of three without breakup. This observation holds for eccentrically positioned drops as well. They show gross asymmetry in the shape of the tail, yet do not breakup. The result of inhibited tail breakup is that a greatly reduced number of satellite drops forms during passage through the test section, usually four or five, compared to eighteen (one per oscillation) in 0.5% Separan. The satellites which do form, though, are larger than those which form in the 0.5% Separan and the Newtonian suspending fluids, suggesting that the total volume of the satellite drops which are formed may be comparable for the different suspending fluids. Furthermore, as in the earlier case, the tail which remains attached as the drop exits the test section breaks

from the drop in the straight tube relaxation section.

No gross elongation of drops is observed for the 1.0% viscoelastic suspending fluid, even though values for the inverse capillary number are nearly as large as those for Newtonian suspending fluid systems 4, 5, and 6 (1.12 presently, compared to 1.34 for the Newtonian systems). It should be recalled that drops in these Newtonian systems were extremely extended in the flow direction, occupying up to four periods of the test section (see Section 3.1).

Finally, drops suspended in 1.0% Separan solution exhibit tip-streaming in the straight tube entry section if the drop size and the average velocity are sufficiently large. These concentric drops form pointed ends from which drops, smaller than the usual satellite drops which are formed in the test section, issue continuously until the drop reaches the test section. The onset of tip-streaming occurs at $\lambda = 0.64$ for $V = 0.46$ cm/s for system 15 and at $\lambda = 0.80$ for $V = 0.24$ cm/s, and occurs at all sizes for $V = 0.46$ cm/s for system 16.

5. Discussion

5.1 Newtonian suspending fluid.

The most striking consequence of the wavy-wall tube geometry is that the additional pressure drop is periodic in most cases. We have presented results in terms of the average value ΔP^+ of the maximum and minimum amplitudes of the oscillatory signal, along with the difference $\delta(\Delta P^+)$ between these two values, which gives the magnitude of the oscillatory part. The data show that $\delta(\Delta P^+)$ can be considerably larger than ΔP^+, especially for viscosity ratios near unity. The instantaneous resistance to flow owing only to the presence of the suspended drop increases

steadily as the leading edge of the deformed drop passes through a convergent section of the wavy-wall tube. The resistance then decreases rapidly as the drop evacuates the "throat" and fills the wide region of the tube. It is important to emphasize that the instantaneous value of ΔP^+ increases as the drop is forced through a convergent section, even when the drop fluid is much less viscous than the suspending fluid, i.e. $\sigma << 1$.

The magnitudes of both the average additional pressure drop ΔP^+ and the oscillatory part $\delta(\Delta P^+)$ depend on the dimensionless bulk velocity Γ for the Newtonian systems with small values for Γ. The values of ΔP^+ and $\delta(\Delta P^+)$ decrease as Γ is increased for given values of λ and σ. The identical trend was observed in (I) and (II) for ΔP^+ (a constant, since $\delta(\Delta P^+)=0$), and was attributed to increased deformation of the drop which lowers resistance to flow. A similar explanation seems appropriate here. The deformation of the drop, measured roughly by the drop's axial length at any point in the tube, increases with Γ for small-Γ Newtonian systems. This observation would suggest a decrease in the average additional pressure drop ΔP^+. However, the effect of Γ on deformation, i.e. axial drop length, is greatest when the drop is in the narrow throat of the wavy-wall tube. This observation suggests that the effect of V on $\delta(\Delta P^+)$ should also be significant, since the value of $\delta(\Delta P^+)$ is dominated by the increase in resistance as the drop passes through the narrow regions.

As the value of Γ is made larger, an important dispersion process occurs. Although the intermediate-Γ drops do not elongate, drop breakup is observed for system 1 (σ = 0.0014, Γ = 0.50 and 0.94).

It is of interest to estimate the rate of extension which induces breakup in this case for comparison with the results of Grace (1971) for hyperbolic flow, where breakup occurs at a critical value of the dimensionless extension rate $G\mu_o a/\gamma$ (where a is the undeformed drop radius), which is a function of the viscosity ratio. The dimensional extension rate G for wavy-wall tube flow is estimated as $G = \frac{Q}{\pi}\left[\frac{r_{max}^2 - r_{min}^2}{r_{max}^2\, r_{min}^2}\right]\frac{2}{L}$ based upon the change in the average velocity between points of maximum and minimum cross-section. The values of $G\mu_o a/\gamma$ calculated in this fashion are $0.3 < G\mu_o a/\gamma < 0.9$ for $V = 0.24$ cm/s, and $0.5 < G\mu_o a/\gamma < 0.9$ for $V = 0.46$ cm/s. From observations reported in Section 4, we estimate that breakup occurs when the dimensionless extension rate exceeds 0.4. This value compares to a measured critical value of 0.5 in hyperbolic flow. Although it must be admitted that a strict comparison between steady hyperbolic extension and flow through the wavy-wall tube neglects both the rotational component of motion and the wall interactions for the latter case, this result shows that the dimensionless extension rate is at least approximately sufficient to cause breakup of the drop, when interpreted in terms of Grace's criterion. However, some features of the deformation and breakup process in the wavy-wall tube suggest that this interpretation should not be taken too literally. Drop breakup for system 1 drops tends to occur at values of the draw ratio (dimensionless length D at breakup) which are approximately one-half those observed in the four-roller device for the identical viscosity ratio. Also, breakup occurs in a time which is also one-half the time for breakup in hyperbolic flow. A possible explanation for this is that the drop is already appreciably deformed in the straight-wall tube entry

section before entering the first constriction of the wavy-wall test section. However, photographs of the drop shape during breakup suggest a fundamental difference between the breakup processes for the two flows. In the wavy-wall tube, the shape of the drop is clearly asymmetric in the streamwise direction near the point of breakup, whereas a fore-aft symmetry occurs at the point of breakup in the four-roll mill. The width of the drop at a given axial distance downstream from the breakup point is considerably greater than the width at the same distance upstream, and there is a concomitant decrease in the downstream length of the drop compared to the length upstream of the breakup point. This asymmetry of the shape may reflect the fact that the undisturbed flow type varies between the convergent and divergent regions. Hence, the breakup process may be determined in part by the variation of flow type rather than simply the existence of a critical rate of extension. Effects of unsteadiness in the velocity gradient are known to influence breakup in simple shear flow, and it is possible that the Lagrangian unsteadiness of the flow also plays an important role in determining the conditions for breakup in the wavy-wall tube. Such a conclusion is supported by the fact that system 1 drops exhibit breakup without the extreme elongation which they would show in hyperbolic flow, especially since the latter is a kinematically "stronger" flow than the rotational wavy-wall tube flow.

The situation changes for the larger values of Γ. A direct comparison of the present data for large-Γ with results for the straight-wall tube is impossible because the maximum value for Γ employed in (I) and (II) was 0.2. However, larger values are of interest in chemical flooding.

Perhaps the most significant observation in the case of large-Γ drops is the elongation of the whole drop to form long strands or filaments under certain conditions. The elongated drop resembles the mobilized strip of oil photographed by Wasan, et. al. (1979), and cited there as one possible mode of oil globule transport. It is particularly important to note that strand formation occurs without regard to the actual oil detachment process, since the drops never contact the pore (tube wall) surface in this experiment. Instead, the formation of strands seems to occur with the drop suspended freely in the flow, and depends only on the material parameters, specifically λ, V, and σ. These strands have particularly large values for U/V and hence, represent an extremely attractive mode of oil transport. Once displacement is accomplished, formation of a concentrated oil bank is crucial to a successful flooding operation. Our results suggest that strand formation enhances the formation of a front, because oil that is displaced behind the front is carried at a velocity much greater than the average pusher fluid velocity. Hence, strands migrate in the flow toward the front where coalescence with the oil-water bank can take place. It is also significant to note that Payatakes, et. al.(1978) have suggested that the fastest traveling drops are those which are smaller than the narrowest portion of the pore constriction. However, the data indicate that extended strands have a larger velocity than the smallest drops in the present study, which are smaller than the narrowest diameter of the wavy-wall tube.

Although strand formation thus tends to enhance drop mobility in the test section, the effect may be of dubious value since gross elongation of the drop is also a precursor to breakup. The neutrally buoyant

strands, once extended over multiple periods, exhibit an axial variation in radius which is in-phase with the oscillatory tube boundary, although small compared to the amplitude of the wall oscillation. This shape is apparently stable, insofar as the drops do not exhibit breakup while still in the test section; however, when the drop enters the relaxation section, the periodic disturbances grow, and breakup into several small drops follows readily. This breakup process bears a closer resemblance to breakup in the four-roll mill as described by Grace (1971) than to the break-up of system 1 drops, at least in the sense that breakup occurs during stress relaxation. We can compare the critical draw ratio for breakup in hyperbolic extension, which depends on the viscosity ratio, with the estimated draw ratio at the point of breakup in the straight-wall relaxation section of the present system. The values for hyperbolic extension, taken from the data of Grace for viscosity ratios, σ, comparable to systems 4, 5, and 6, are 5, 9, and 20, respectively. For wavy-wall tube flow, we have estimated the critical draw ratio by determining the smallest value of the deformed dimensionless drop length for which breakup occurs in the relaxation section. The minimum draw ratios observed for systems 4, 5, and 6 were 3, 6, and 10, respectively. It is evident that these are not "critical" draw ratios, but rather just the lowest values which were observed for the combinations of drop sizes and flow rates used in our study. Nevertheless, the values obtained show that breakup definitely occurs at smaller values of the draw ratio in the wavy-wall tube flow than in a steady hyperbolic flow. The difference between the draw ratios for the two flows may be a consequence of the disturbances in drop shape induced by

the wavy-wall geometry. The extended drop enters the relaxation section with "finite-amplitude" wave-like disturbances in shape already present, and these disturbances simply grow during stress relaxation. On the other hand, deformed drops in hyperbolic extension show no capillary waves until the flow ceases.

The mechanism by which drops are drawn into strands has been identified in Section 4. Drops tend to elongate when the leading edge of the drop begins to invade the next convergent region before the trailing edge of the drop has "recoiled" from the preceding divergent region. Equivalently, we may say that strand formation occurs for a given suspending fluid when the time scale associated with deformation is greater than the characteristic time of the flow, or

$$\frac{\lambda r_{HP} \mu_i}{\gamma} > \frac{L}{U}$$

where μ_i is the drop viscosity. The data show that increased values of the average velocity or drop viscosity, and decreased values of the interfacial tension tend to enhance the formation of strands, in qualitative accord with this inequality.

It was also noted in Section 4 that non-neutrally buoyant drops exhibit a greater degree of elongation than concentric ones for fixed values of the other parameters. Indeed, in many cases, drop breakup of eccentrically positioned drops occurs in the test section, in marked contrast to neutrally buoyant drops which breakup only in the straight-wall relaxation tube. A definition of flow strength based on the ability of the flow to deform a suspended drop (e.g. Olbricht, Rallison,

& Leal, 1980) would imply that a purely extensional flow, which exists only along the tube centerline, is most efficient at producing drop deformation. It may thus appear surprising, at first, that eccentrically positioned drops exhibit a greater degree of deformation than neutrally buoyant ones, all other factors being equal. However, the flow field in the convergent-divergent tube geometry is not homogeneous, and the magnitude of the velocity gradient, defined as $(\nabla v:(\nabla v)^T)^{1/2}$, increases monotonically with distance from the tube centerline. Thus, it is possible that the flow strength may be greatest away from the tube centerline despite the fact that fluid elements off the centerline experience a rotational component to the flow.

In order to test this possibility, we have examined the detailed kinematics of the undisturbed flow (i.e. no drops present) of a Newtonian fluid through a wavy-wall tube using available numerical solutions of the creeping flow equation at a cross-section (radius 0.35 cm) which is midway between maximum and minimum tube diameters. The estimated flow strength first decreases as the distance from the tube centerline increases, but eventually attains a minimum and then monotonically increases as the wall is approached. Indeed, for this particular cross-section, the flow strength at distances from the centerline greater than one-half the tube radius actually exceeds the flow strength at the tube centerline. This result may qualitatively differ for a tube with a substantially greater amplitude of wavy-wall oscillation. However, the increasing flow strength which occurs near the tube wall in

the present study is apparently responsible for the increased deformation which is observed for eccentrically positioned drops, relative to neutrally buoyant drops under otherwise similar conditions.

The periodicity of the pressure signal disappears, i.e. $\delta(\Delta P^+) = 0$ when strand formation occurs. This occurs apparently because the drop is able to deform easily to lower its resistance to passage through the narrowest throat of the tube. Also, the drop quickly extends to occupy more than one period of the tube at any specified time. Consequently, the simple oscillatory nature of the flow is not apparent. The value of ΔP^+ is still determined primarily by the viscosity ratio σ. However, the facile deformation of the drop diminishes the importance of V on ΔP^+ as compared to the small-Γ cases.

5.2 Viscoelastic Fluid Systems

The effect of suspending fluid viscoelasticity was studied by employing two concentrations of aqueous Separan as the suspending fluid. Unfortunately, in a viscoelastic fluid, quantitative results for the dimensionless additional pressure drop $\Delta P^+ r_{HP}/\mu_o V$ are somewhat ambiguous because they inevitably reflect the manner in which the nominal suspending fluid viscosity is assigned in the non-Newtonian fluid. This problem was also encountered for viscoelastic flow through the straight-wall tube (cf. (I) and (II)), but the situation is even more complicated in the present case because of the wavy-wall geometry. We have evaluated the suspending fluid viscosity, somewhat arbitrarily, in a fashion analogous to the method of (I) and (II) by using the shear-rate at the wall of the "equivalent" circular tube with radius r_{HP}.

We have already discussed (cf. Section 3) the role of viscoelasticity in wavy-wall tube flow of the suspending fluid alone, i.e. with no drop present. In that case, the effect of suspending fluid elasticity is to increase the pressure drop over that which would be expected based on shear-thinning considerations alone. It was found that the difference in magnitude was correlated with the value of De which is the ratio of the characteristic relaxation time of the fluid relative to the time scale of the Lagrangran unsteady flow in the wavy wall tube. The presence of a drop in the flow not only causes a disturbance of the flow which may be large (in view of the fact that the size of the drop is comparable to the size of the tube), but also introduces an additional time scale, namely the intrinsic time for drop deformation.

The significance of this latter observation is that the dependence on the viscosity ratio, or other parameters which control the rate of drop deformation in a Newtonian fluid, may be at least partially suppressed in a viscoelastic suspending fluid if the characteristic time scale for drop deformation in the wavy wall tube is much less than the characteristic relaxation time for the fluid. One indication of this can be seen in the magnitude of the oscillatory part of the additional pressure drop $\delta(\Delta P^+)$ in the viscoelastic fluids. We observed earlier that the value of $\delta(\Delta P^+)$ is sensitive to the viscosity ratio for fixed values of Γ and λ for the case of a Newtonian suspending fluid (cf. system 2c and system 3 in Fig. 6). This observation is consistent with the results of Rallison (1980) who showed, for Newtonian systems with

small values of Γ, that the time scale for drop deformation scales with σ in any type of flow. However, data for small-Γ drops suspended in 0.5% Separan, which are shown in Figs. 10 and 11, suggest that $\delta(\Delta P^+)$ is independent of σ when the suspending fluid is viscoelastic. Indeed, the data show that there is little difference in $\delta(\Delta P^+)$ for fixed λ and small values of Γ even though σ varies by a factor of 100. There are also qualitative changes in the drop shape in the viscoelastic fluid which suggest the inhibiting effect which a finite fluid response time can have on the drop dynamics. It was shown earlier that the shape of a typical drop in a Newtonian suspending fluid follows the contours of the wavy-wall tube for small and intermediate values of Γ. Specifically, the leading edge of the drop typically expands into the wider regions of the tube almost immediately after it has passed through the throat of the convergent section. In the viscoelastic fluid, on the other hand, the drop remains pointed during its passage through the throat, and the leading edge expands into the wider regions of the tube only after the drop front has passed well into the divergent region. Furthermore, there is a visible gap between the tube wall and the drop surface at the point of smallest diameter, even for small values of Γ. For the Newtonian suspending fluid, there was no visible gap for the small-Γ drop (though this obviously does not mean the drop contacts the wall in those cases). Apart from the qualitative differences in shape for drops in a viscoelastic suspending fluid, the other crucial consideration here is the sensitivity of the shape to σ for a given suspending fluid,

Although there is a strong dependence of the shape on σ for the Newtonian cases, photographs of the drop in the two viscoelastic fluids show only a weak dependence on σ. This observation and the relative independence of $\delta(\Delta P^+)$ to changes in σ are both apparently manifestations of the fact that the Langrangian unsteady deformation of the drop is dominated by the characteristic response time of the suspending fluid for small values of Γ. Indeed, the ratio of the characteristic relaxation time for the viscoelastic fluid to the intrinsic time for drop deformation is approximately De/Γ. For small values of Γ in the present experiment, this parameter is O(10) which indicates that the dominant time scale is, indeed, the response time for the suspending fluid.

The decreased sensitivity of drop deformation to the dimensionless velocity Γ does help to explain the variation of ΔP^+ with Γ that was observed in the present study. In the Newtonian case, ΔP^+ decreased as the average velocity was made larger. This was attributed to increased deformation of the drop, as in the straight wall tube case. However, for viscoelastic suspending fluids, the reverse trend is observed. We believe that this is a consequence of the fact that the deformation of the drops is not as sensitive to the average velocity as in the Newtonian case, especially for large drops. As a result, the value of ΔP^+ is probably more strongly affected by the value of σ, which is larger for the larger flow rate, than it is by drop deformation. As Γ is increased, the average velocity gradient is increased and the viscosity of the suspending fluid thus decreases due to shear-thinning, causing ΔP^+ to

increase. It should be noted that it is only ΔP^+ which is increased as σ increases; as the suspending fluid viscosity decreases, the overall pressure drop in the tube will also decrease.

The situation changes when we consider the behavior of $\delta(\Delta P^+)$ for intermediate values for Γ. In these cases, the parameter De/Γ is O(1), indicating that the relaxation time of the suspending fluid and intrinsic time for drop deformation are comparable. There appears to be substantial deviation from the small-Γ curves for $\delta(\Delta P^+)$ as a function of λ most notably for system 10 and system 9 shown in Fig. 10. The videotape recordings show substantial differences in the degree of deformation between the intermediate-Γ systems. Although the shape resembles that observed for the small-Γ drops, including the gap between the drop and tube wall, the length of the drop is larger in the intermediate-Γ cases, and increases with σ. Indeed, system 9 is sufficiently deformed that the leading edge invades the next throat before the trailing edge of the drop has evacuated the preceding one. When this occurs, it has a profound effect on $\delta(\Delta P^+)$, as already discussed. This behavior is observed for all values of λ for systems 9 and 10 (for the large value of Γ) and also for system 14, but only for the largest drop size, which accounts for the curious sign change of the slopes of the $\delta(\Delta P^+)$ versus λ curves in Figure 11. The effect of σ on the deformation of intermediate-Γ drops in a viscoelastic suspending fluid is also reflected in the mobility of the drops U/V which increases with decreasing σ. Thus, it appears that the time scale for deformation of intermediate-Γ drops is at least comparable to the viscoelastic

characteristic time, as suggested by the fact that $De/\Gamma = O(1)$. These results suggest collectively that the relevant time scale for intermediate-Γ drops is the intrinsic time for drop deformation and not the viscoelastic time scale of the suspending fluid.

In addition to a dependence on σ, the drop mobility U/V for non-neutrally buoyant large-Γ drops in 1.0% Separan, system 18 and system 19, shown in Figure 13 exhibits a minimum as λ is increased. This behavior is not a consequence of the viscoelasticity of the suspending fluid. Small non-neutrally buoyant drops give values for U/V approximately equal to that for concentric drops from system 17. As the drops are made larger, neutrally buoyant drops in system 17 show a definite tendency to "permanently" elongate as they flow through the test section. This appears to enhance the mobility of the drop, but actually reflects the increased velocity of the leading edge of the drop as it elongates. Non-neutrally buoyant drops of intermediate size do not show any permanent elongation because of their eccentric position in the tube. These drops tend to migrate toward the wall in the regions of larger diameter. When near the wall, they occupy slower pathlines of the undisturbed flow. This allows time for the drop to "recoil" before the next constriction is encountered, thus preventing permanent elongation. The net effect is to decrease the apparent value of the mobility for intermediate sized eccentric drops compared to the concentric case. However, like many other features resulting from drop eccentricity, the effect is diminished as the drop size exceeds 0.9 because the drop effectively occupies the entire cross-section of the tube. Permanent elongation of large non-

neutrally buoyant drops is possible and is, in fact, observed. Therefore, the velocity of large drops is unaffected by density differences. This results in the apparent minimum in the U/V-profile at intermediate sizes.

The importance of dispersion phenomena to the efficiency of chemical flooding operations has already been mentioned, and we now review the various dispersion processes that were observed under the range of conditions covered in the present experiment. No breakup was observed for "small" values of Γ for either the Newtonian or viscoelastic suspending fluids, although the shape of the drop differed for the two types of suspending fluid. At intermediate values of Γ, Newtonian system 1 exhibited breakup in the test section, although the drop did not undergo elongation before breakup. Drops with intermediate values of Γ in the 0.5% Separan solution formed tails which under some conditions issued satellite drops in the test section and broke away from the main part of the drop in the relaxation section. A maximum of one drop per oscillation formed once the tail had grown sufficiently long and disturbances to the shape in the form of waves appeared on the tail surface. None of the intermediate-Γ drops exhibited breakup in the test section without tail formation for the 0.5% suspending fluid. Breakup occurred for the drops with large values of Γ in both Newtonian and viscoelastic suspending fluids, although the actual breakup process differed for the two types of suspending fluid. In the Newtonian fluid, large-Γ drops undergo a gross elongation and breakup in the relaxation section into several (usually four to six)

drops of various sizes. Breakup occurs as disturbances in the extended drop shape grow, roughly resembling the breakup process in the four-roll mill. For the large drops in 1.0% Separan, breakup occurs only in conjunction with tail formation, even though the value of Γ is comparable to that at which permanent elongation takes place for the Newtonian suspending fluid. Furthermore, the effect of the visco-elasticity of the suspending fluid is clearly to stabilize the tail which permits large disturbances of the tail shape without breakup. As a consequence, fewer and larger drops are formed as the elasticity of the suspending fluid increases. This result is in agreement with the prediction of Chin and Han (1980) for breakup of a Newtonian jet in a viscoelastic continuous phase. For large wavelength disturbances breakup of the jet is inhibited by the elasticity of the suspending fluid, and when breakup occurs, the resulting fragment drops are larger when compared to the Newtonian suspending fluid. Since the disturbances of the shape of the deformed drop in the present experiment are roughly comparable to the length of a wavy-wall tube wavelength, the large wavelength prediction of Chin and Han (1980) should be at least qualitatively relevant.

6. Conclusions

Experimental data have been reported for two-phase creeping flow through a tube with periodic cross-section. The additional pressure drop owing only to the presence of an immiscible Newtonian drop is periodic as the drop travels through the successive convergent/divergent regions of the wavy-wall tube. Data for the additional pressure drop

are reported in terms of the "average" value ΔP^+ over typical period and the magnitude $\delta(\Delta P^+)$ of the oscillatory part. The undeformed radius of the suspended drop is comparable to the radius of the tube and exceeds the smallest tube radius in most cases. Consequently, we observe that the drop must undergo substantial deformation in order to move through the "throat" of each convergent section. Even when the drop viscosity is small, the additional pressure drop accompanying flow in the convergent region can be relatively large.

The conformation of the drop and therefore the additional pressure drop and drop mobility U/V depend crucially on the value of the inverse capillary number, $\Gamma = \mu_o V/\gamma$. When the suspending fluid is Newtonian, the drop shows relatively little deformation for small values of Γ, but exhibits substantial deformation which leads to eventual drop breakup for intermediate and large values of Γ. Perhaps the behavior of the large-Γ systems is most significant, however, since our observations for this case appear to resemble deformation behavior of oil globules in actual porous media. We find that for large values of Γ, the drop elongates in the flow and finally breaks into many fragment drops either in the test section or in the straight-wall relaxation section depending on whether or not the drop is concentrically located. Elongation, and breakup occur as "onset" phenomena at critical values of Γ and λ for fixed σ. The kinematics of the flow field in the wavy-wall tube are significantly extensional in nature, which is particularly efficient for drop deformation. Consequently, elongation of large-Γ drops in the Newtonian suspending fluid, occurs in the wavy-wall tube for values of

Γ, σ, and λ which would fail to produce elongation in a straight-wall tube. The fact that breakup is observed after the extensional deformation is relaxed suggests an analogy between the wavy-wall tube flow and the four-roll mill, as far as drop deformation and breakup are concerned. Although the tube flow studied here is important as a prototype for a number of industrial processes, our results suggest that it would be useful to reconsider deformation and breakup in the simpler (kinematically) flow of the four-roll mill, especially for time-dependent straining motions of magnitudes greater than the critical strain rate.

The effect of suspending fluid viscoelasticity has been systematically studied. As a preliminary to studying the two-phase problem, total pressure drop--flow rate data were obtained for creeping flow of Newtonian and viscoelastic fluids with no suspended drops present. The data for the viscoelastic fluid show a deviation from generalized Newtonian (i.e. purely viscous fluid) behavior which is correlated with the value of De. The magnitude of the deviation is comparable to the Newtonian contribution to the pressure drop, and this is consistent with other results for flow through periodically varying tubes.

The role played by suspending fluid viscoelasticity with drops present apparently depends on the value of Γ. For small values of Γ, the deformation of the drop and hence the oscillatory part of the additional pressure drop ΔP^+ is influenced by σ, which indicates that ΔP^+ probably depends most on the replacement of suspending fluid by drop fluid in this case. For intermediate and large values of Γ, suspending

fluid viscoelasticity appears to inhibit the elongation of drops relative to that observed for the Newtonian suspending fluid. However, the formation of tails from the trailing edge of the drop are characteristic of the viscoelastic suspending fluids for larger values of Γ. These tails issue a number of satellite droplets, up to one per oscillation of the wavy-wall tube. It was found by varying the concentration of the polymer solution, that increasing suspending fluid elasticity tends to stabilize the tail to disturbances associated with the periodicity of the flow. This has the practical effect of increasing the size of the satellite drops and decreasing the number that are issued. Unfortunately, we are unable to specify the mechanism of viscoelastic action without a more detailed analysis of the flow field with drops present.

References

Acrivos, A. & Lo, T. S. 1978 Deformation and breakup of a single drop in an extensional flow. J. Fluid Mech., 86, 641.

Chin, H. B. & Han, C. D. 1979 Studies on droplet deformation and breakup. I. Droplet deformation in extensional flow. J. Rheol., 23, 557.

Chin, H. B. & Han, C. D. 1980 Studies on droplet deformation and breakup. II. Breakup of a droplet in non-uniform shear flow. J. Rheol., 24, 39.

Deiber, J. A. & Schowalter, W. R. 1979a Flow through tubes with sinusoidal axial variations in diameter. A.I.Ch.E. J., 25, 638.

Deiber, J. A. & Schowalter, W. R. 1979b Flow of Newtonian and viscoelastic fluids through tubes with sinusoidal axial variations in diameter. Presented at A.I.Ch.E. Annual Meeting, San Francisco, Ca., Nov., 1979.

Dodson, A. G., Townsend, P. & Walters, K. 1971 On the flow of Newtonian and non-Newtonian liquids through corrugated pipes. Rheol. Acta., 10, 508.

Dreher, K. D. & Grogarty, W. B. 1979 An overview of mobility control in micellar/polymer enhanced oil recovery processes. J. Rheol., 23, 209.

Elata, C., Burger, J., Michlin, J. & Takserman, U. 1977 Dilute polymer solutions in elongational flow. Phys. Fluids, 20, S49.

Fedkiw, P. & Newman, J. 1977 Mass transfer at high Peclet numbers for creeping flow in a packed-bed reactor. A.I.Ch.E. J., 23, 255.

Franzen, P. 1979 Zum Einfluss der Porengeometrie auf den Druckverlast bei der Durchströmung von Porensystemen. I. Versuche an Modellkanälen mit variablem Querschnitt. Rheol. Acta., 18, 392.

Grace, H. P. 1971 Dispersion phenomena in high viscosity immiscible fluid systems and application of static mixers as dispersion devices in such systems. Engng. Foundation 3rd Res. Conf. on Mixing, Andover, New Hampshire.

Han, C. D. & Funatsu, K. 1978 An experimental study of droplet deformation and breakup in pressure-driven flow through convergent and uniform channels. J. Rheol.,22, 113.

Ho, B. P. & Leal, L. G. 1975 The creeping motion of liquid drops through a circular tube of comparable diameter. J. Fluid Mech., 71, 361.

James, D. F. & McLaren, D. R. 1975 The laminar flow of dilute polymer solutions through porous media. J. Fluid Mech., 70, 733.

Leal, L. G., Skoog, J. & Acrivos, A. 1971 On the motion of gas bubbles in a viscoelastic fluid. Can. J. Chem. Engng., 29, 569.

Leal, L. G., Fuller, G. G. & Olbricht, W. L. 1980 Studies of the flow-induced stretching of macromolecules in dilute solution. Progress in Aeronautics, AIAA, to appear.

Marshall, R. J. & Metzner, A. B. 1967 Flow of viscoelastic fluids through porous media. Ind. Engng. Chem. Fund., 8, 393.

Michele, H. 1977 Zur Durchflusscharakteristik von Schüttungen bei der Durchströmung mit verdünnten Lösungen aus langkettigen Hochpolymeren. Rheol. Acta., 16, 413.

Neira, M. A. & Payatakes, A. C. 1979 Collocation solution of creeping Newtonian flow through sinusoidal tubes. A.I.Ch.E. J., 25, 725.

Oh, S. G. & Slattery, J. C. 1979 Interfacial tension required for significant displacement of residual oil. Soc. Pet. Eng. J. (Apr., 1979), 83.

Olbricht, W. L. & Leal, L. G. 1980 The creeping motion of immiscible drops through a straight circular tube: the effects of density differences between the fluids, in press.

Olbricht, W. L., Rallison, J. M. & Leal, L. G. 1980 A criterion for strong flow based on microstructure deformation, in press.

Payatakes, A. C., Flumerfelt, R. W. & Ng, K. M. 1978 On the dynamics of oil-ganglia populations during immiscible displacement. Presented at A.I.Ch.E. 84th National Meeting, Atlanta, Ga., Feb., 1978.

Payatakes, A. C. & Neira, M. 1977 Model of the constricted unit cell type for isotropic granular porous media. A.I.Ch.E. J., 23, 922.

Payatakes, A. C., Tien, C. & Turian, R. M. 1973 A new model for granular porous media. A.I.Ch.E. J., 18, 58.

Rallison, J. M. 1980 Appendix. The effects of shear and vorticity on deformation of a drop, by Hakimi, F. S. & Schowalter, W. R., in press.

Roof, J. G. 1970 Snap-off of oil droplets in water-wet pores. Soc. Pet. Eng. J. (Mar., 1970), 85.

Savins, J. G. 1969 Non-Newtonian flow through porous media. Indust. Engng. Chem., 81, 18.

Schowalter, W. R. 1978 Mechanics of Non-Newtonian Fluids, Pergamon Press, Oxford, England.

Sheffield, R. E. & Metzner, A. B. 1976 Flows of non-linear fluids through porous media. A.I.Ch.E. J., 22, 736.

Taylor, G. I. 1934 The formation of emulsions in definable fields of flow. Proc. Roy. Soc., A146, 501.

Wasan, D. T., McNamara, J. J., Shah, S. M., Sampath, K. & Aderansi, N. 1979 The role of coalescence phenomena and interfacial rheological properties in enhanced oil recovery: an overview. J. Rheol., 23, 181.

TABLE 1. MATERIAL PROPERTIES OF THE SYSTEMS STUDIED

System	Suspending Fluid Newtonian:	Drop Fluid Newtonian:	γ (dynes/cm)	$\Delta\rho/\rho_o$	V= 0.24 σ	V= 0.24 Γ	V= 0.46 cm/s σ	V= 0.46 cm/s Γ
1	UCON LB-1715	water	3.5	0.000	0.0014	0.50	0.0014	0.94
2a	95.45% glycerin	DC200+CCl_4	22.0	0.003	0.40	0.043	0.40	0.083
2b	"	"	22.0	0.000	0.40	0.043	0.40	0.083
2c	"	"	22.0	0.001	0.40	0.043	0.40	0.083
3	"	"	22.0	0.000	0.60	0.043	0.60	0.083
4	"	DC510	1.3	0.000	0.70	1.34	0.70	2.54
5	"	"	1.3	0.000	7.52	1.34	7.52	2.54
6	"	"	1.3	0.000	14.6	1.34	14.6	2.54
7	UCON-LB 1715	DC200	2.5	0.024	0.070	0.70	0.70	1.31
8	"	"	2.5	0.022	17.9	0.70	17.9	1.31
	Viscoelastic:	Newtonian:						
9	0.5% Separan	UCON LB	5.3	0.000	0.20	0.34	0.30	0.43
10	"	UCON LB-X	5.3	0.000	0.94	0.34	1.42	0.43
11	"	DC510	18.5	0.000	12.6	0.073	18.2	0.096
12	"	DC200	24.5	0.037	0.29	0.050	0.42	0.066
13	"	DC200	18.1	0.036	16.1	0.069	23.2	0.091
14	"	UCON LB	5.0	0.026	0.10	0.24	0.14	0.33
15	1.0% Separan	UCON LB-X	5.1	0.000	0.081	0.86	0.12	1.10
16	"	UCON LB-X	5.1	0.000	0.38	0.89	0.57	1.12
17	"	DC510	16.0	0.000	3.63	0.29	5.46	0.37
18	"	DC200	21.7	0.039	0.085	0.19	0.13	0.24
19	"	DC200	16.1	0.038	4.77	0.26	7.17	0.33

TABLE 2. PROPERTIES OF THE SUSPENDING FLUIDS

	V = 0.24 cm/s			V = 0.46 cm/s		
Suspending fluid	β_w (s^{-1})	μ_o (P)	N_1 (dynes/cm^2)	β_w	μ_o	N_1
95.45% glycerin	3.09	3.94	0	5.81	3.94	0
UCON LB-1715	3.09	7.17	0	5.81	7.17	0
0.5% Separan	4.03	7.48	35	7.66	4.95	45
1.0% Separan	4.36	18.39	55	8.25	12.31	85

TABLE 3. SUMMARY OF DISPERSION PHENOMENA (NEWTONIAN LARGE-Γ SYSTEMS)

λ	System 4 (σ=0.70)	System 5 (σ=7.52)	System 6 (σ=14.6)
(V = 0.24 cm/s)			
0.61	periodic shape	periodic shape	periodic shape
0.77	periodic shape	elongation	elongation
1.04	elongation	elongation	elongation
1.15	elongation	elongation	breakup
(V = 0.46 cm/s)			
0.61	periodic shape	elongation	elongation
0.77	elongation	elongation	elongation
1.04	elongation	breakup	breakup
1.15	breakup	breakup	breakup

λ	(V = 0.24 cm/s) U/V (drop center)	(V = 0.46 cm/s) U/V (drop center)
0.61	1.62	1.62
0.77	1.61	1.64
0.91	1.60	1.65
1.04	1.60	1.64
1.15	1.58	1.62

Figure Captions

Figure 1. Schematic diagram of experimental set-up (not to scale). (1) Constant temperature bath. (2) Micrometer syringe. (3) Suspending fluid storage section. (4) Test section. (5) Pressure port. (6) Auxiliary pressure port. (7) Videocamera. (8) Videomonitor. (9) Videotape recorder. (10) Manometer by-pass valve. (11) Pressure transducer. (12) Transducer Indicator. (13) Gear pump. (14) Variable speed motor. (15) Pressurized suspending fluid reservoir. (16) Compressed nitrogen.

Figure 2. Scale drawing of a test section unit.

Figure 3. Friction factor f vs. Re for Newtonian and viscoelastic flow. Re_n is defined in terms of the power-law parameters. x-Newtonian data.

Figure 4. Data for fRe_n as a function of Deborah number De for the viscoelastic fluids.

Figure 5. Typical tracing for the additional pressure drop ΔP^+. The additional pressure drop is always negative for this particular case.

Figure 6. Dimensionless average additional pressure drop and dimensionless magnitude of the oscillatory part as a function of dimensionless drop size for small-Γ systems in a Newtonian suspending fluid. System 2b values for (ΔP^+) (not shown) increase monotonically with λ from 0.8 to 12.1

Figure 7. Maximum dimensionless drop length D versus the number of oscillations of the wavy-wall tube through which a drop (System 4; λ = 1.04, V = 0.24 cm/s) has passed.

Figure 8. Dimensionless average additional pressure drop as a function of dimensionless drop size for intermediate-Γ and large-Γ systems in a Newtonian suspending fluid. "1" indicates System 1, etc.

Figure 9. Relative drop velocity as a function of dimensionless drop size for all systems with a Newtonian suspending fluid. System 2c for Γ = 0.043 is not shown (see text).

Figure 10. Dimensionless average additional pressure drop and dimensionless magnitude of the oscillatory part as a function of dimensionless drop size for neutrally buoyant intermediate-Γ systems with 0.5% Separan.

Figure 11. Dimensionless average additional pressure drop and dimensionless magnitude of the oscillatory part as a function of dimensionless drop size for non-neutrally buoyant intermediate-Γ systems with 0.5% Separan.

Figure 12. Relative drop velocity as a function of dimensionless drop size for all systems with 0.5% Separan.

Figure 13. Dimensionless average additional pressure drop and relative drop velocity as a function of dimensionless drop size for neutrally buoyant drops in 1.0% Separan.

Figure 14. Dimensionless average additional pressure drop and relative drop velocity as a function of dimensionless drop size for non-neutrally buoyant drops in 1.0% Separan.

Figure 15. Photographs of the videomonitor: a) system 3, $\lambda = 0.912$, $\Gamma = 0.065$ (at maximum ΔP^+); b) system 3, $\lambda = 1.15$, $\Gamma = 0.065$; c) system 4, $\lambda = 1.04$, $\Gamma = 1.05$, after passing through two periods; d) same as in (c), after twelve periods; e) system 9, $\lambda = 0.912$, $\Gamma = 0.34$ (at minimum ΔP^+); f) system 14, $\lambda = 1.15$, $\Gamma = 0.26$; g) system 16, $\lambda = 0.912$, $\Gamma = 0.88$.

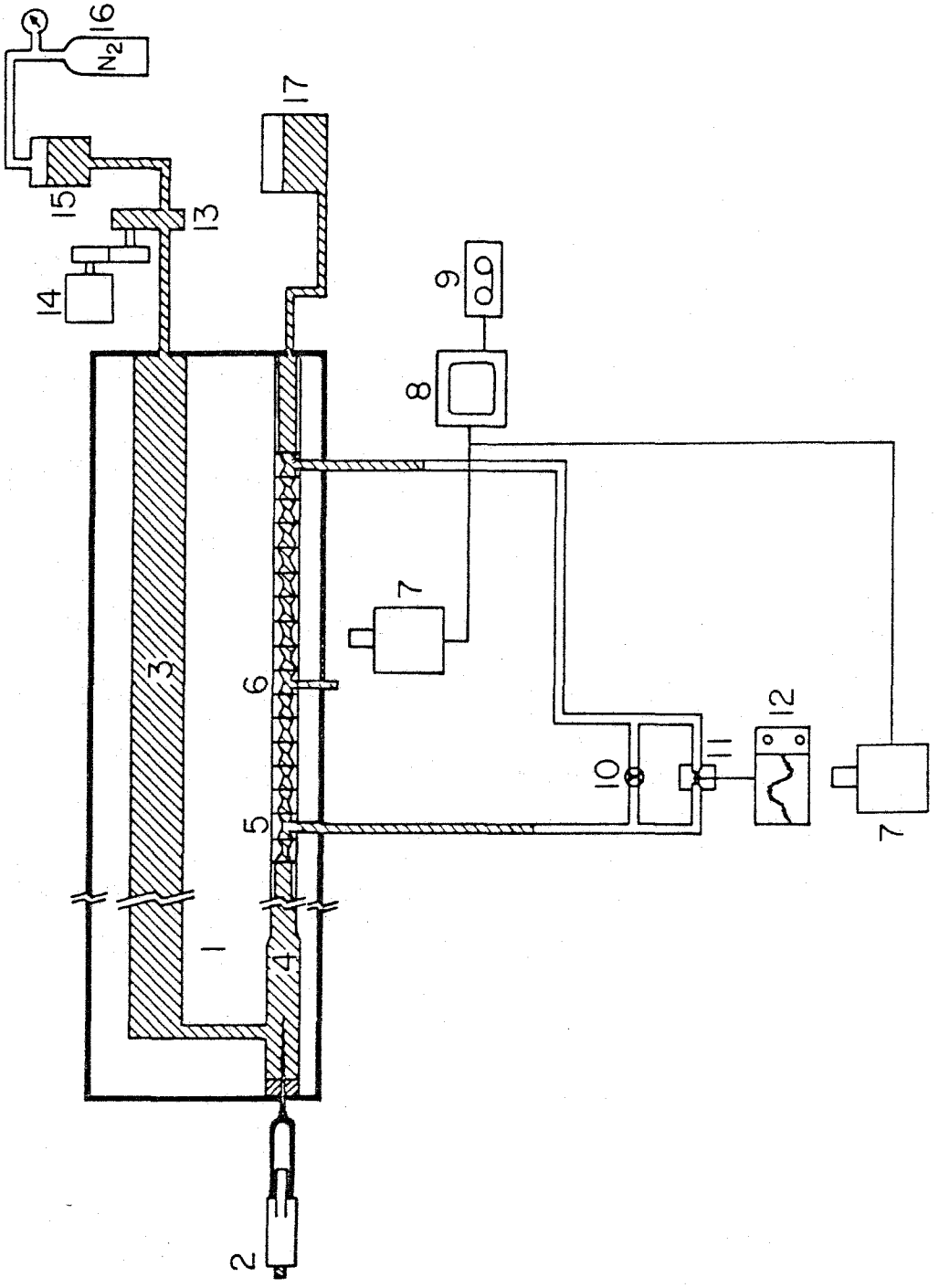

Figure 1.

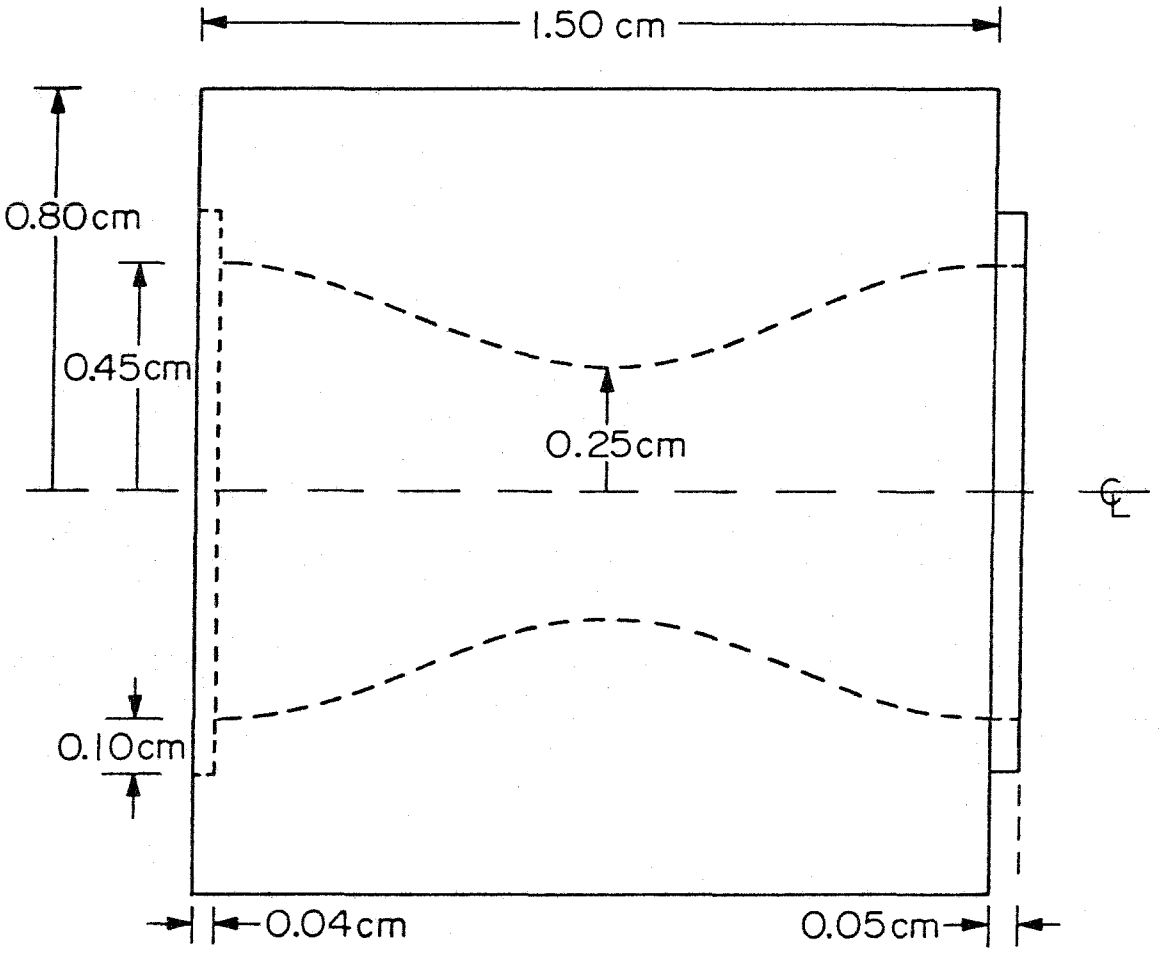

Figure 2.

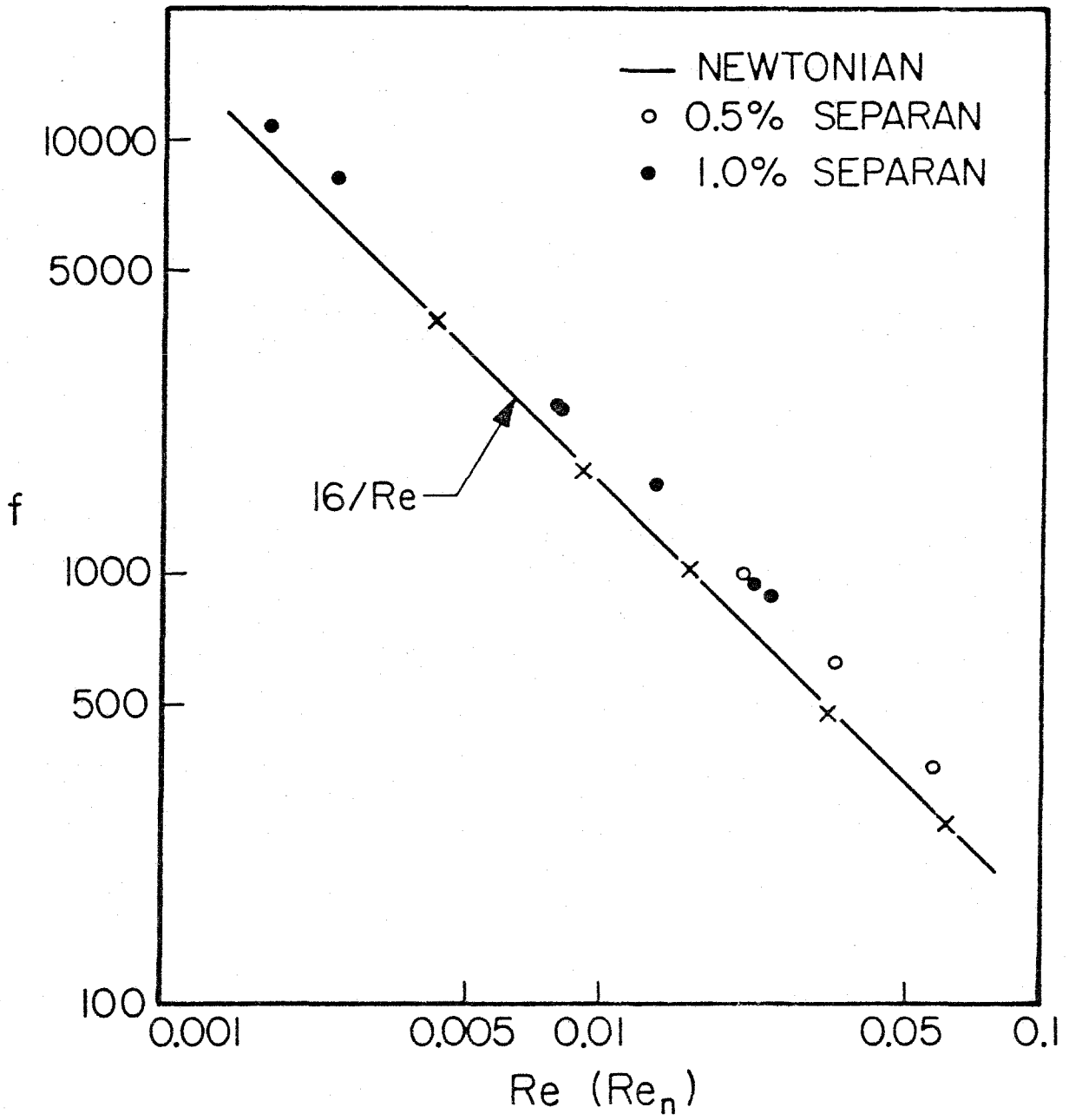
NEWTONIAN
0.5% SEPARAN
1.0% SEPARAN
16/Re
f
10000
5000
1000
500
100
0.001
0.005
0.01
0.05
0.1
Re (Re$_n$)

Figure 3.

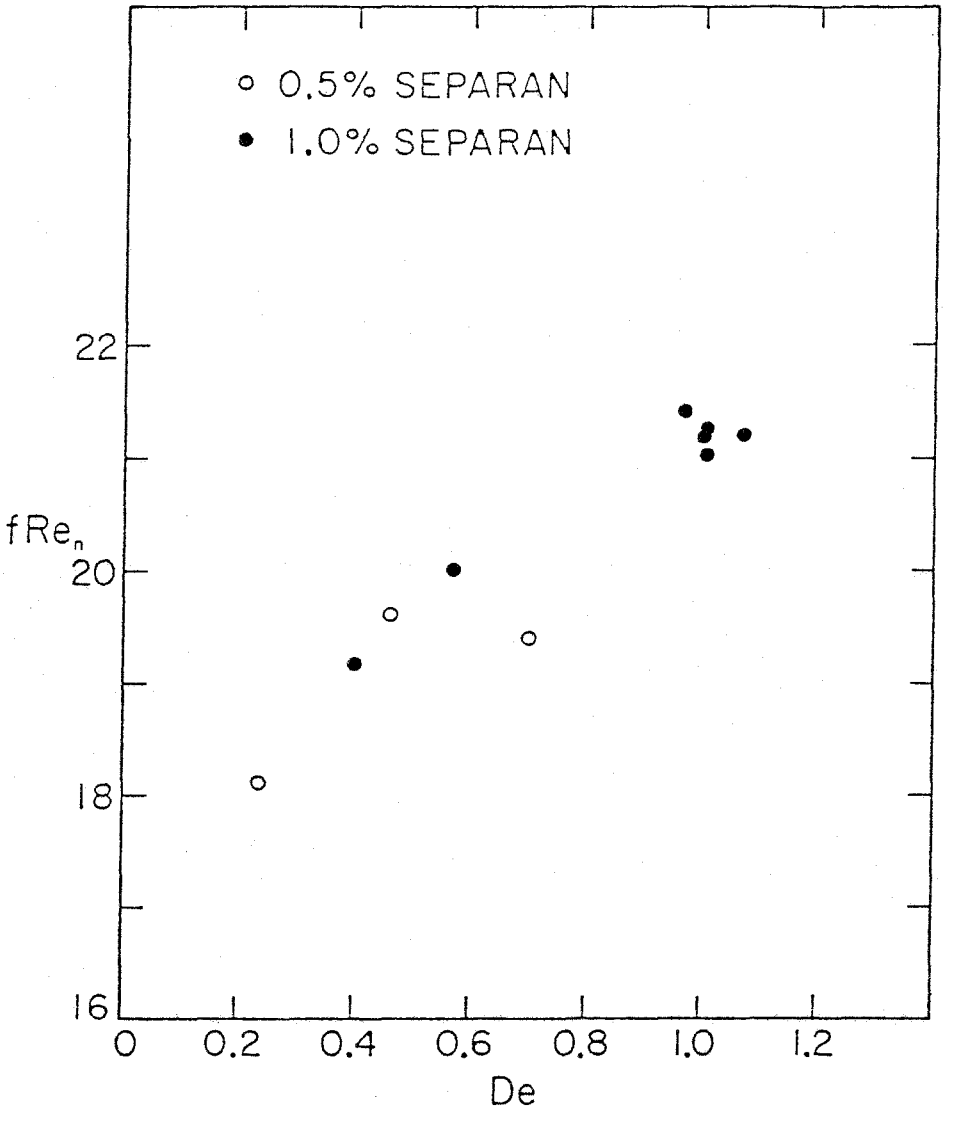

Figure 4.

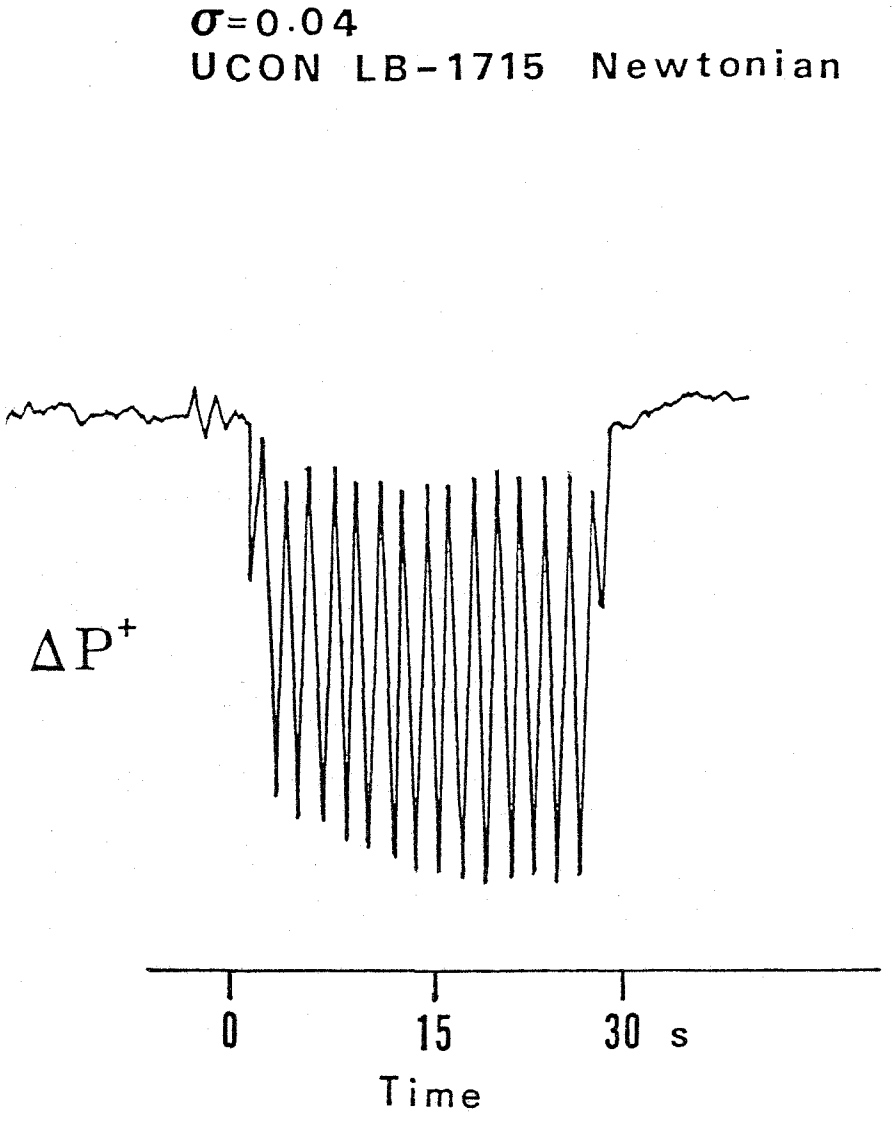

Figure 5.

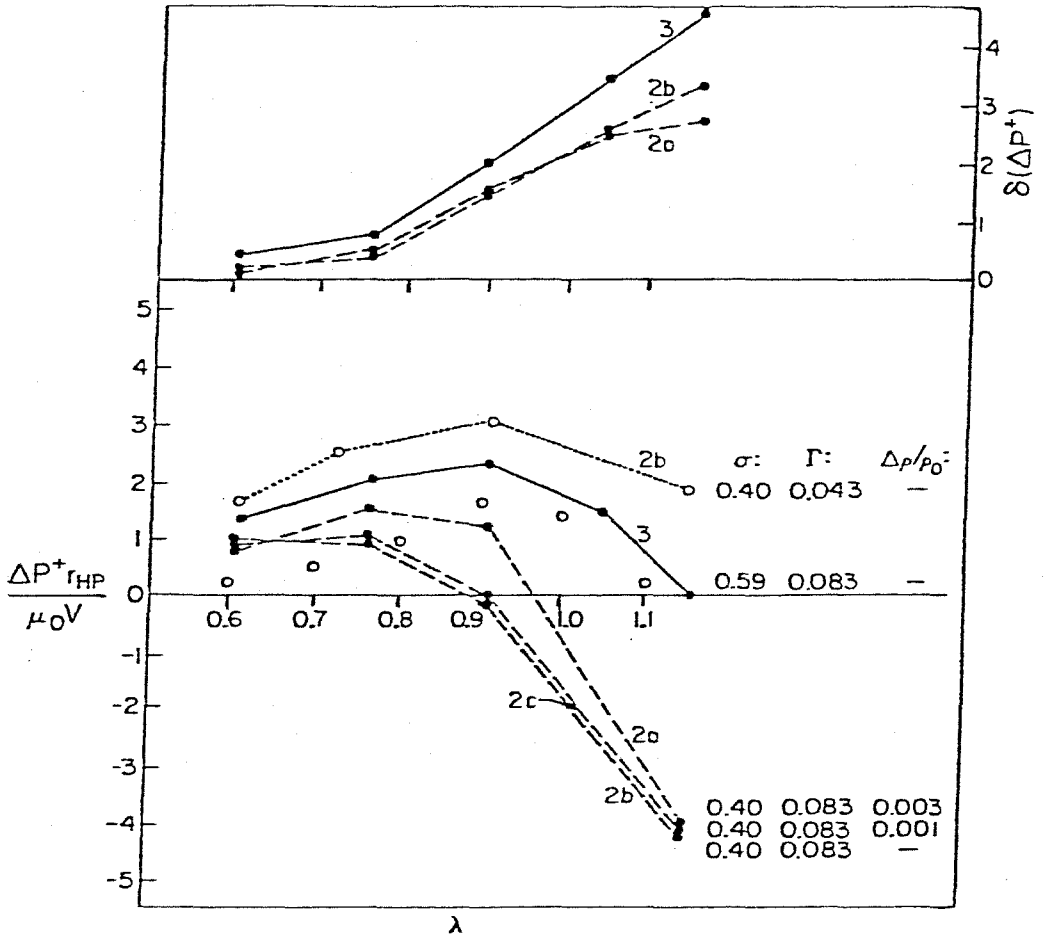
3
2b
2a
δ(ΔP+)
ΔP+rHP / μ0V
2b σ: Γ: Δp/p0:
0.40 0.043 —
3
0.59 0.083 —
2c
2a
2b
0.40 0.083 0.003
0.40 0.083 0.001
0.40 0.083 —
λ

Figure 6.

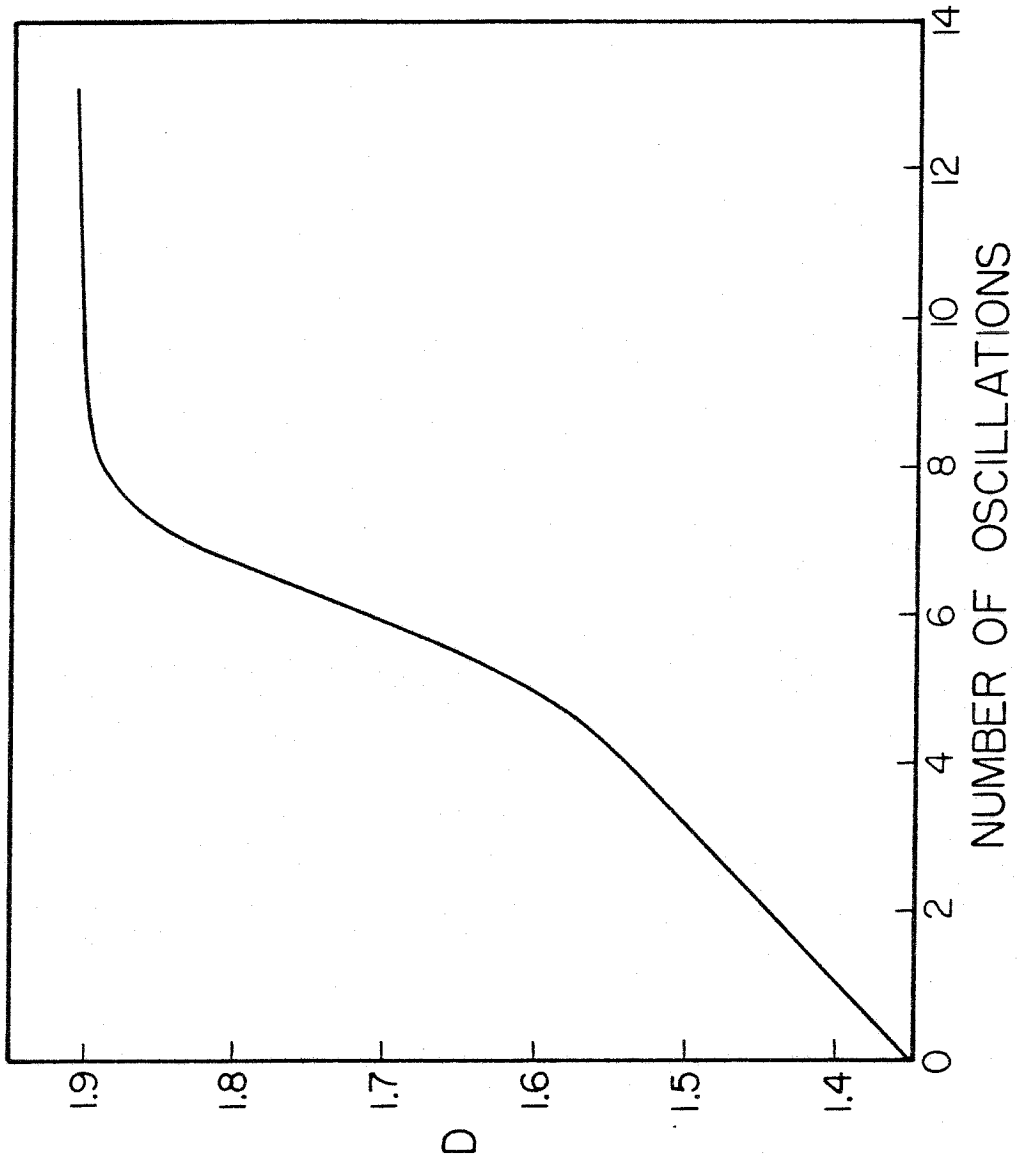

Figure 7.

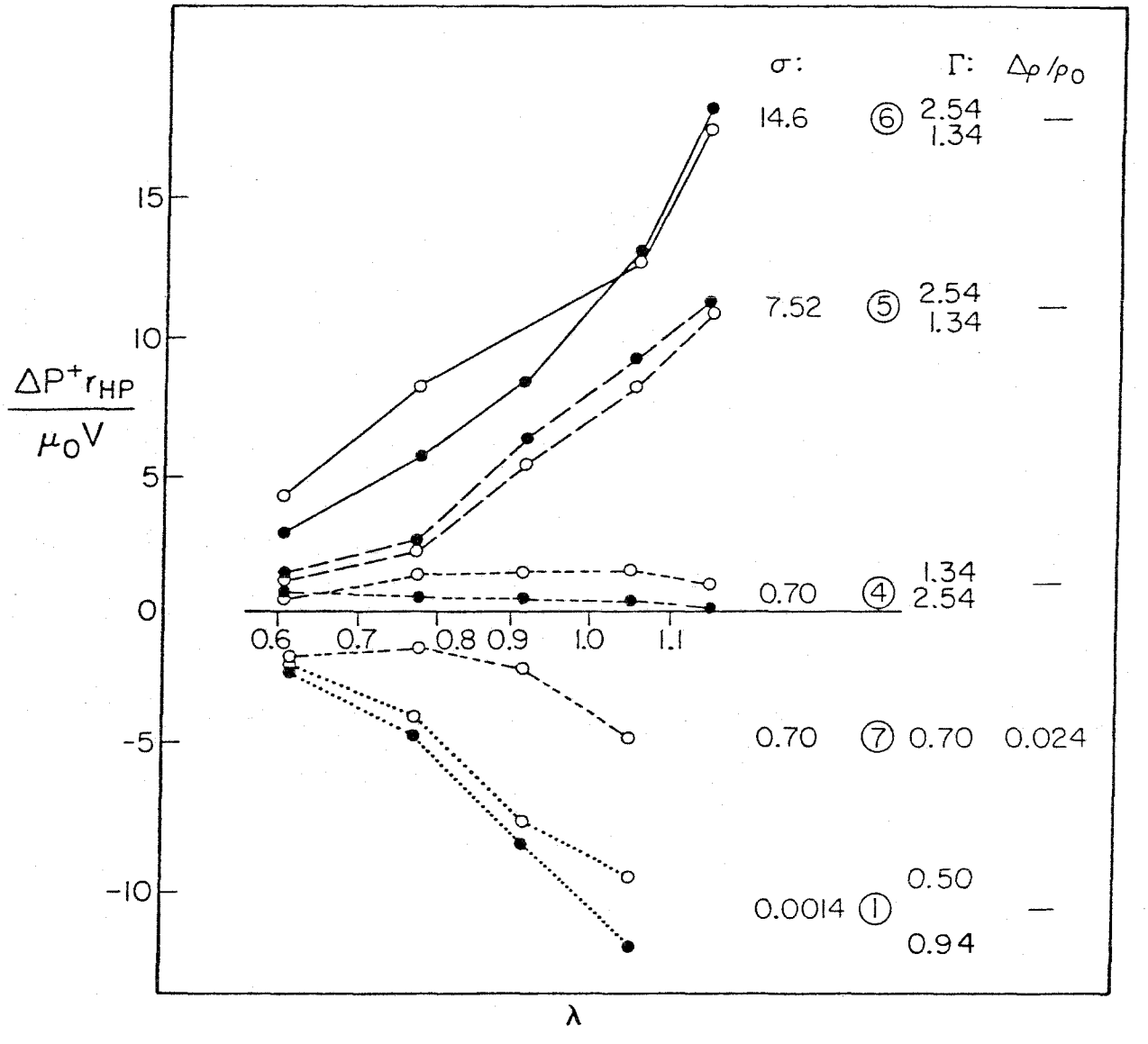
σ:
Γ:
Δρ/ρ0
14.6
⑥ 2.54
1.34
—
7.52
⑤ 2.54
1.34
—
0.70
④ 1.34
2.54
—
0.70
⑦ 0.70
0.024
0.0014
① 0.50
0.94
—
15
10
5
0
-5
-10
0.6
0.7
0.8
0.9
1.0
1.1
λ
ΔP+rHP / μ0V

Figure 8.

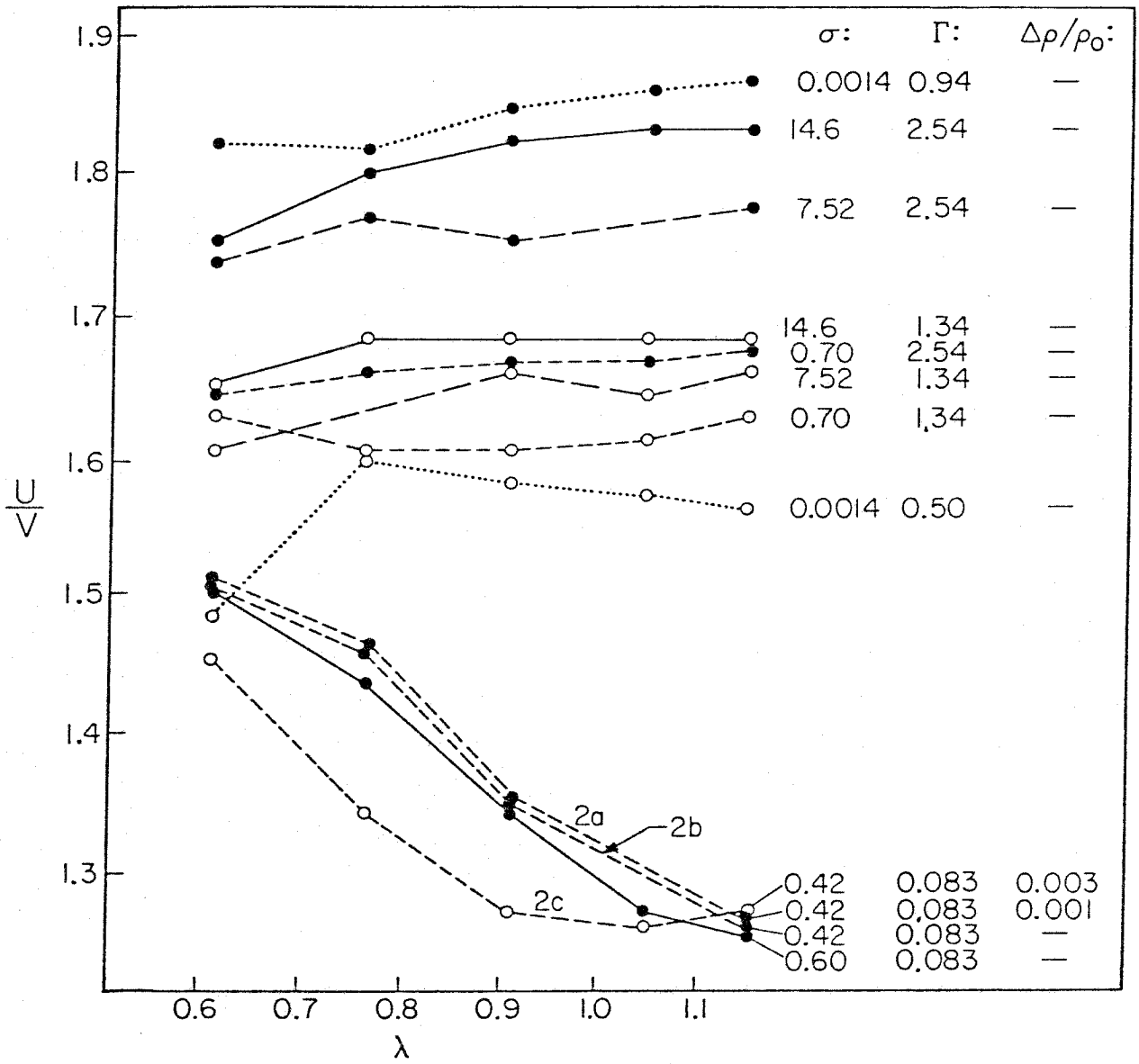
σ: Γ: Δρ/ρ₀:
0.0014 0.94 —
14.6 2.54 —
7.52 2.54 —
14.6 1.34 —
0.70 2.54 —
7.52 1.34 —
0.70 1.34 —
0.0014 0.50 —
0.42 0.083 0.003
0.42 0.083 0.001
0.42 0.083 —
0.60 0.083 —
2a
2b
2c
U/V
λ
1.9
1.8
1.7
1.6
1.5
1.4
1.3
0.6
0.7
0.8
0.9
1.0
1.1

Figure 9.

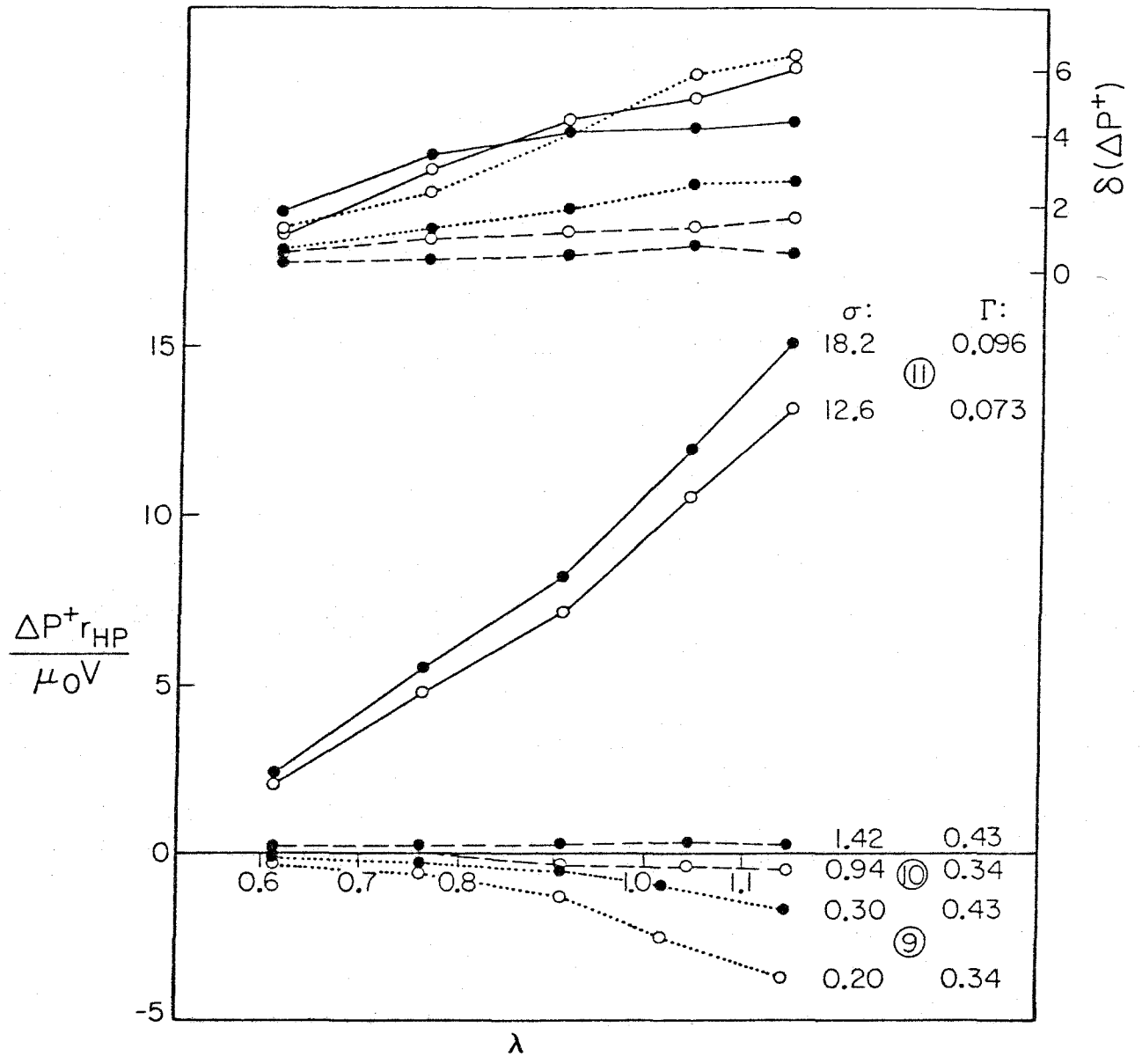
$\frac{\Delta P^+ r_{HP}}{\mu_0 V}$
$\delta(\Delta P^+)$
λ
σ:
Γ:
18.2
0.096
⑪
12.6
0.073
1.42
0.43
0.94
⑩
0.34
0.30
0.43
⑨
0.20
0.34
15
10
5
0
-5
6
4
2
0
0.6
0.7
0.8
1.0
1.1

Figure 10.

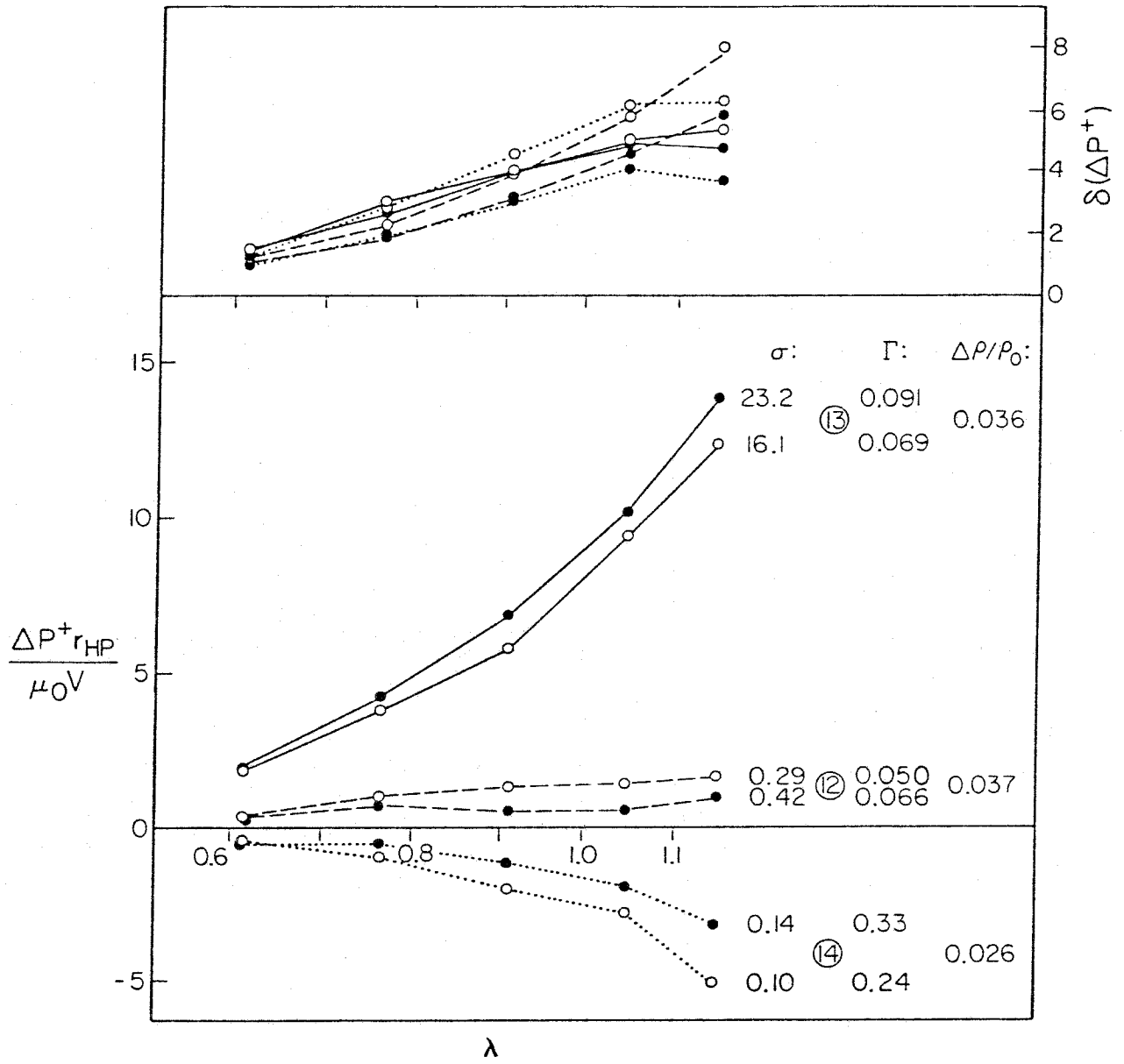
8
6
4
2
0
δ(ΔP⁺)
σ:
Γ:
Δρ/ρ₀:
15
23.2
0.091
⑬
0.036
16.1
0.069
10
ΔP⁺r_HP / μ₀V
5
0.29
0.050
⑫
0.037
0.42
0.066
0
0.6
0.8
1.0
1.1
0.14
0.33
⑭
0.026
-5
0.10
0.24
λ

Figure 11.

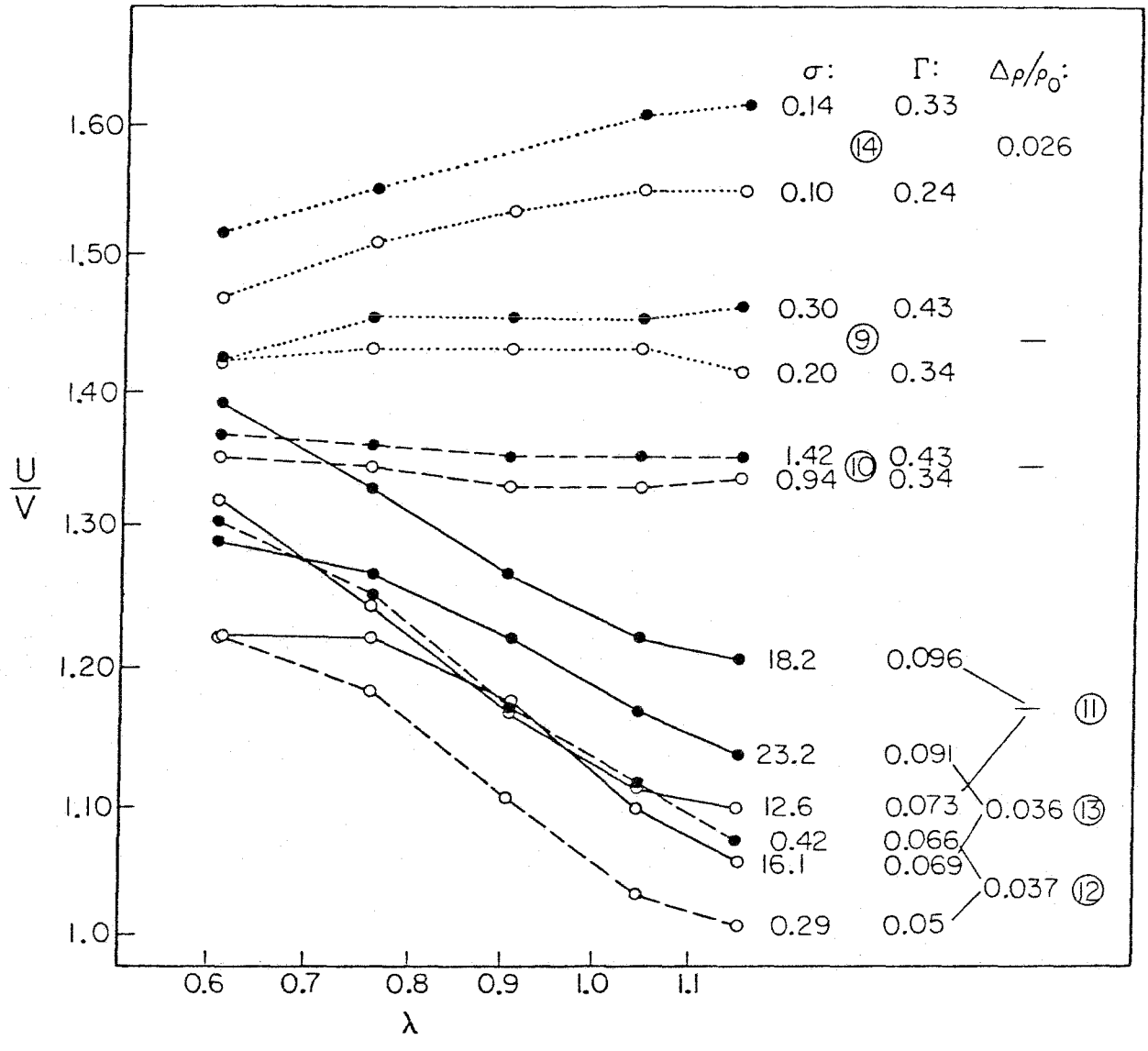
σ:
Γ:
Δρ/ρ0:
0.14
0.33
⑭
0.026
0.10
0.24
0.30
0.43
⑨
—
0.20
0.34
1.42
0.43
⑩
—
0.94
0.34
18.2
0.096
⑪
23.2
0.091
12.6
0.073
0.036
⑬
0.42
0.066
16.1
0.069
0.037
⑫
0.29
0.05
U/V
1.60
1.50
1.40
1.30
1.20
1.10
1.0
0.6
0.7
0.8
0.9
1.0
1.1
λ

Figure 12.

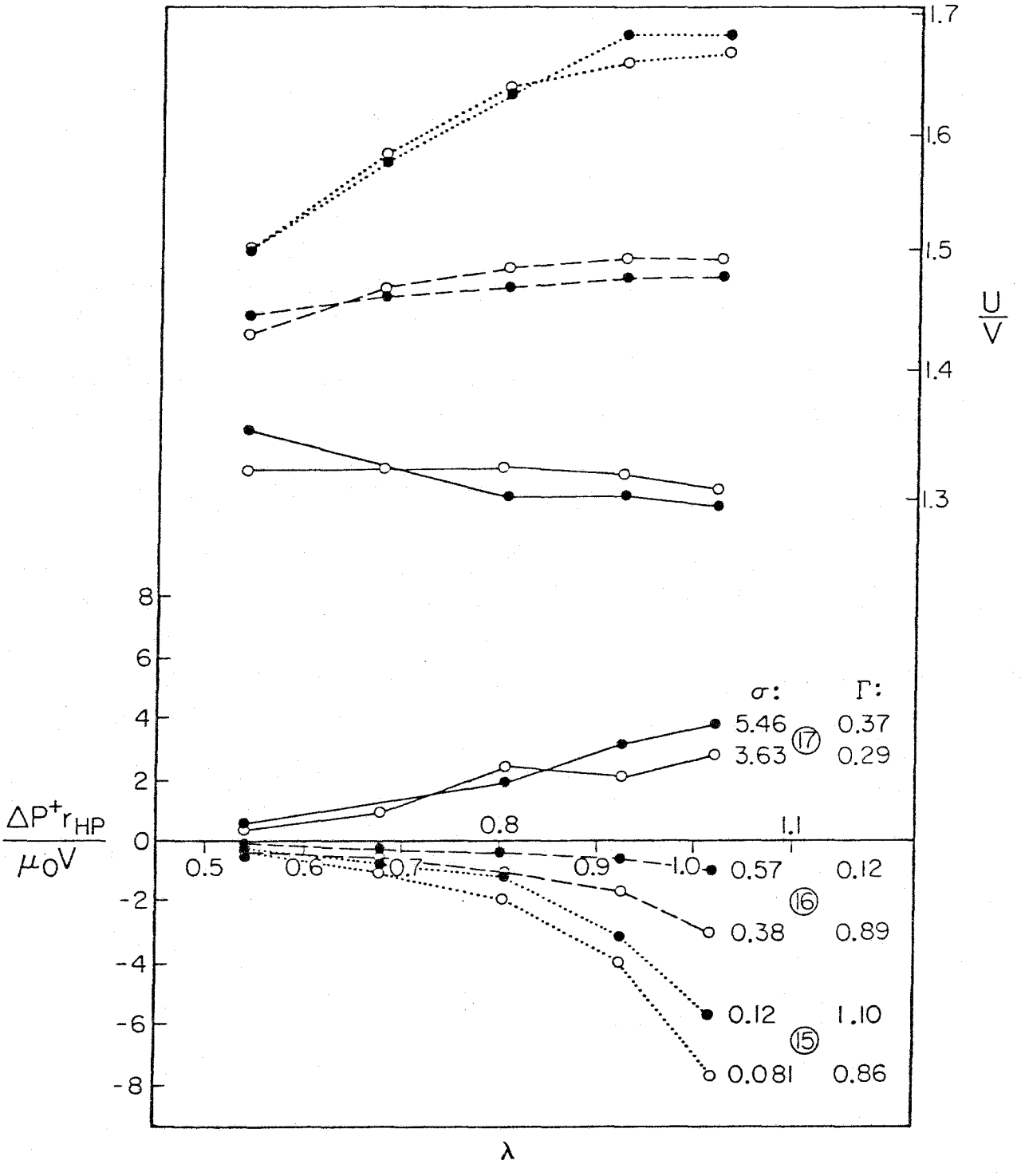
1.7
1.6
1.5
1.4
1.3
U/V
8
6
4
2
0
-2
-4
-6
-8
ΔP⁺r_HP / μ₀V
σ:
Γ:
5.46
0.37
17
3.63
0.29
0.8
1.1
0.5
0.6
0.7
0.9
1.0
0.57
0.12
16
0.38
0.89
0.12
1.10
15
0.081
0.86
λ

Figure 13.

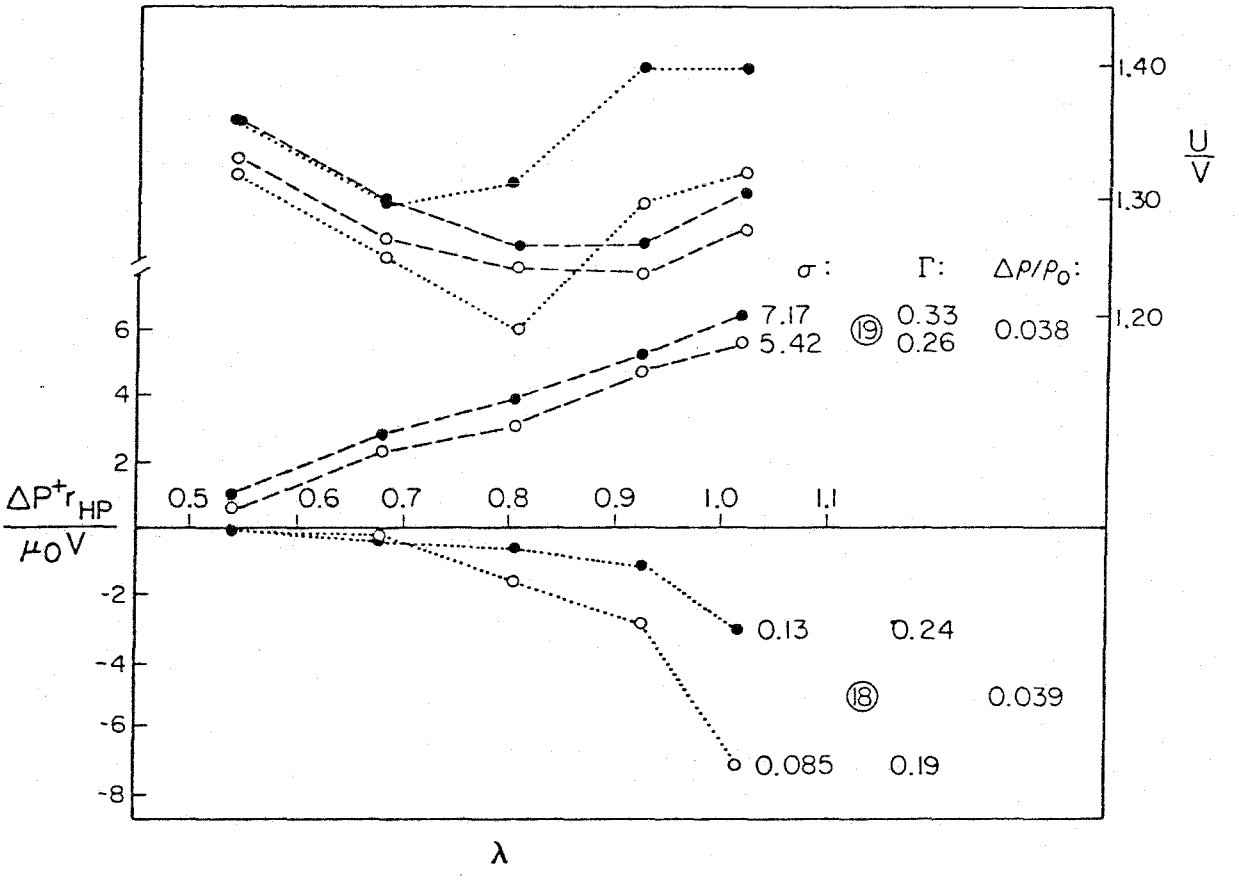
1.40
1.30
1.20
U/V
σ:
Γ:
Δρ/ρ0:
7.17
5.42
⑲
0.33
0.26
0.038
6
4
2
ΔP+rHP / μ0V
0.5
0.6
0.7
0.8
0.9
1.0
1.1
-2
-4
-6
-8
0.13
0.24
⑱
0.039
0.085
0.19
λ

Figure 14.

a b

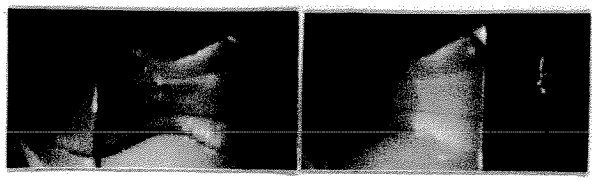

c d

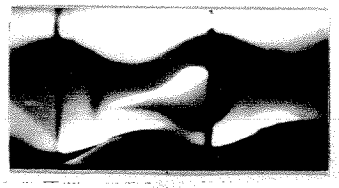

e

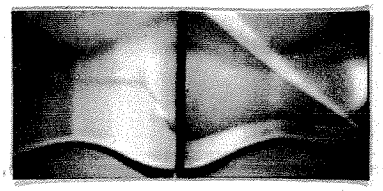

f

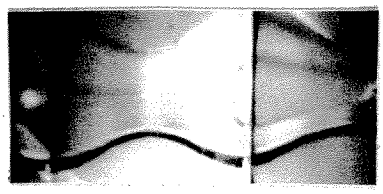

g

Figure 15.

Chapter 3

"Strong Flow Criteria Based on Microstructure Deformation"

W. L. Olbricht*, J. M. Rallison**, and L. G. Leal

Department of Chemical Engineering
California Institute of Technology
Pasadena, California 91125

*Present address: School of Chemical Engineering, Cornell University, Ithaca, New York 14853

**Present address: Department of Applied Mathematics and Theoretical Physics, Cambridge University, Silver Street, Cambridge, Great Britain

Abstract

The dynamics of fluid systems which consist of a suspended material in a Newtonian continuous phase is investigated theoretically. Criteria are derived to predict conditions under which the strength of a flow, i.e. a measure of the form and magnitude of the velocity gradient tensor, is sufficient to induce significant deformation and/or orientation of the fluid microstructure, that is, the elements which collectively comprise the suspended phase. The development relies upon the choice of a model to describe the microstructure, and the form of the criteria reflects this choice. Once the choice is made, however, the detailed material properties of a particular fluid system enter only as parameters in the resulting equations, and thus, the results encompass a large class of fluid systems, including particulate suspensions and macromolecular solutions. Two microstructure models are investigated here. When the microstructure is characterized by a vector, the flow strengths of all linear flows are displayed in a single figure from which the strength of a particular flow can be evaluated directly. A comparison is then made for selected flows between these results and those for the case where an irreducible second order tensor is employed to describe the microstructure. A significant difference between the two models derives from the

fact that the "volume" of the microstructure must be conserved in the second order tensor case. The criteria are finally used to predict the degree of macromolecular stretching in a model turbulent flow and the breakup of immiscible liquid drops in simple shear flow. A comparison between the flow strength predictions and experimental data yields good qualitative agreement in the latter case.

I. Introduction

The dynamics of fluid systems consisting of a Newtonian continuous phase and a second, suspended material, constitutes an important class of problems which has been extensively studied, both experimentally and theoretically. The present paper is an attempt to construct a theoretical framework which can be used to understand certain common features of the relationship between motion of the system as a whole, and the conformation of the suspended phase.

We consider both particulate systems, in which the suspended material may be a drop or a solid particle, and macromolecular solutions in which the macromolecules are modelled as deformable particles insofar as mean dynamic interactions with the solvent are concerned. Thus, we use the word "conformation" to denote the instantaneous shape and orientation of the "particles", either individually, as would be relevant to single-particle systems, or collectively, as would usually be appropriate for a suspension or solution where a meaningful description of conformation necessarily involves a statistically averaged statement of "shape" and/or "orientation", cf. Hinch and Leal (1975, 1976). For convenience, we will refer collectively to the suspended material as microelements, and the appropriate conformational information as the microstructure.

In many problems, the conformation of the microelement (or elements) is the most important parameter of the system for theoretical prediction. Specifically, we are concerned with the prediction of flow-induced changes in the conformation of microelements (either collectively or individually,

as appropriate) since these can be dramatic, and are almost always responsible for macroscopically important dynamical phenomena. At the level of an individual particle, for example, the flow-induced deformation and subsequent breakup of liquid drops are essential components of emulsification processes, and have been studied extensively (Grace, 1971). In suspensions or solutions, flow-induced changes in microstructure are directly related to the macroscopically observable properties of the material as a whole (Barthés-Biesel & Acrivos, 1973a). The existence of drag reduction in turbulent motions of extremely dilute polymer solutions is thought by many investigators to be a consequence of a high level of flow-induced extension of the macromolecules (cf. Hinch, 1977). Finally, the flow-induced deformation and breakup of aggregates of solid particles, studied recently by Kao (1975), has a clear practical significance in flocculation processes.

Obviously, the details of interaction between the continuous and suspended phases will vary considerably from system to system (a point which we shall discuss shortly). Thus, it would be unrealistic to expect to develop a theory, common to all systems, which would be capable of predicting the detailed dynamics of flow-induced conformation changes in any particular case. A characteristic feature of the examples cited above, however, is the importance of the degree of flow-induced deformation of the microstructure. Specifically, in each case, a critical question is the possible existence of flow conditions in which the microstructure is highly distorted relative to its rest configuration. Such large distortion leads generally to "breakup" or "rupture" of deformable microelements, or

to regimes in which the effect of the microelements on bulk properties is maximized in the case of suspensions or solutions. The thesis of our present paper is that a general criterion can be developed for the existence of highly distorted microstructure states which is relevant to a wide class of two-component fluid systems. In particular, we consider the development of a classification scheme for steady, spatially homogeneous flows based on their ability to "deform" the fluid microstructure (i.e. the conformation of either a suspension or solution). A flow which is capable of producing a large deformation in finite time will be called "strong", following the precedent of Tanner (1976); otherwise, the flow will be called "weak". The meaning of this distinction will be made exact in the course of the development of a specific criterion for strong (or weak) flows.

Most previous approaches to the development of a flow-classification scheme have been strictly kinematical in nature (cf. Tanner & Huilgol, 1975); that is, the properties of the "suspending" fluid and of the microelements are not considered. Rather, the development of a strong flow criterion has consisted of determining whether the eigenvalues of the velocity gradient tensor have positive real parts. If this is the case, two adjacent fluid elements in the undisturbed flow will move apart at an exponential rate, and so will points of a "particle" which deforms exactly with the undisturbed flow. The kinematic criterion thus prescribes a necessary condition for the existence of large microstructural deformations, but is not a sufficient condition for real systems of particles or macromolecules. Neither the properties of the two phases, nor the

instantaneous state of the microstructure enters the criterion, and these play an important role as indicated above.

Any improvement, relative to a kinematic criterion for strong (or weak) flow, must therefore result from the inclusion of further information about the microstructure. However, the fundamental idea of a general criterion for strong flows will be lost unless this information can be included in a parametric fashion which encompasses all (or the majority) of the class of systems of interest. In order to determine whether such a formulation is possible, and, if so, what form it should take, it is necessary to examine the specific two-component systems which were mentioned before. Two types of considerations are relevant: first, we must decide upon a convenient and efficient description of a system for characterization of its microstructural state; and second, we must determine the form for an equation which describes the time-dependent evolution of this microstate. The variations in microstructure with time consist both of changes in orientation and shape. For deformable microelements, we are most directly interested in changes of the latter type and these are reflected by changes in the length scale(s) of the microelements. The magnitude(s) of the length scale(s) of the microelements can be described by an appropriate invariant which will reflect the properties of the particular system under consideration. It will be seen that the strong flow criterion indicates, in effect, the conditions under which unbounded growth of the invariant, and thus unbounded growth of the length scale(s), occurs. The rotational component of the flow field influences indirectly the length scale growth rate, and it is

possible to describe the dynamics of orientation from the analysis which leads to the strong flow criterion.

The resulting flow classification is then applied to two illustrative examples. First, we examine the degree of microstructure deformation (or "stretching"), which is predicted in a random velocity field of known (specified) statistics. Macromolecular stretching is generally regarded as a prerequisite for drag reduction in turbulent flow. Early work on this problem (e.g. Lumley, 1969) was restricted to two-dimensional flow fields, but there are important qualitative differences between two- and three-dimensional flow fields for molecular extension. Second, we investigate the breakup of a liquid drop which is suspended in a second liquid that is undergoing an arbitrary linear motion of the type $\underline{u} = \underline{\Gamma}\cdot x$. In this case, we examine the dynamics of a vector microstructure which provides a crude model of the deformation dynamics (except in an axisymmetric straining flow where it is exact), but is relatively simple to use.

II. Basic Equations

A. Variables for Characterization of Microstructure

We consider throughout systems which are spatially homogeneous, thereby insuring that spatial position is not a significant microstructural variable. Time variations are permitted, however, so this restriction may be relaxed by considering Lagrangian time variations as seen by a microelement.

It seems at first sight that the description of the microstructure of a suspension will depend strongly on the material under investigation. In particular, there is a clear distinction between those systems of identical non-Brownian particles when it suffices to consider the deformation and orientation of a single element, and those (involving Brownian or interaction effects) where a statistical average over different particles is involved. Notwithstanding this complexity, Hinch and Leal (1975) have noted that for both small and large departures from isotropy, the microstructure of a wide class of suspension-type materials may be described to a good approximation by means of irreducible tensors of ranks zero, one and two. Furthermore, the grossest and hence dynamically most significant feature tends to be represented by the lowest harmonic present. We consider first the class of materials where description of a single microelement is sufficient.

The simplest case under this classification is exemplified by a dilute suspension of rigid spheres in which case the volume of the spheres is the only (scalar) variable. This case is trivial, however, in that the structure is unaffected by the applied (linear) flow. The next case of interest in order of complexity is that of a permanently axisymmetric particle, such as a "dumbbell" or a spheroid; the structure may then be specified by a single vector $\underline{R}$ which incorporates both overall deformation and orientation. (The special case of a rigid axisymmetric particle involves only a unit orientational vector $\underline{p}$). In general, however, a description of the shape of a deformable microelement requires second and/or higher order tensor(s) with components which vary

in magnitude with time. For instance, for small deviations from sphericity the surface distortion of a liquid drop may be written

$$R = a(1 + \underline{R}\cdot\underline{\underline{A}}\cdot\underline{R}/R^2)$$

where the undisturbed shape is $R=a$, and $\underline{\underline{A}}(t)$ is an irreducible second rank tensor. The formula is in fact reasonably accurate for $O(1)$ values of $\underline{\underline{A}}$, but is formally valid only when $||\underline{\underline{A}}||$ is small (further corrections involve fourth harmonics).

We suppose following Hinch and Leal that the first departures from isotropy can commonly (as above) be described by tensors of order no higher than two, and limit our subsequent considerations to systems which allow either a vector or irreducible second order tensor description of the microstructure. In view of the presumed "smallness" of $|\underline{R}|$ or $||\underline{\underline{A}}||$, the dynamical equations for $\underline{R}$ and/or $\underline{\underline{A}}$ can be linearized about their equilibrium values. The flow classification scheme which we derive in subsequent sections is then based effectively on a stability analysis ("stability" meaning that the appropriate invariant characterizing particle length scales remains bounded for all values of t as $t \to \infty$) using these equations in which we search for combinations of $||\nabla\underline{u}||$ and $||\underline{\underline{E}}||/||\underline{\underline{\Omega}}||$ which lead to unbounded growth in $|\underline{R}|$ or in the principal values of $\underline{\underline{A}}$ with time. We regard such growth as indicative of the onset of <u>finite</u> deformation of the microstructure, analogous to the exponential growth of disturbances in conventional linear stability theory. Such onset conditions may coincide with the existence of <u>large</u> distortions or even critical (breakup) phenomena. This is known to be the case, for example,

for the linear dumbbell model of a macromolecule in solution where the condition for unbounded growth of the end-to-end distance has been shown by additional analysis to coincide with the condition for large extensions of the corresponding nonlinear dumbbell models (Fuller, 1980). However, the linearized dynamical equations relevant in the small deformation limit $|\underline{R}|$ or $||\underline{\underline{A}}|| << 1$ cannot alone provide any information about the final, "finite-amplitude" distortion which results from an initial unbounded growth. Indeed, the connection implied between unbounded growth of small initial disturbances and the existence of large deformations in the final state must be regarded as a hypothesis, to be tested by comparison either with exact solutions of the corresponding nonlinear dynamical equations, or preferably with experiments.

If we turn to suspensions or solutions, rather than single particle systems, a meaningful description of the microstructure will generally require the specification of statistical distributions of the conformation variables appropriate to a single, microelement e.g. $\underline{R}$ or $\underline{\underline{A}}$. These statistical distributions are directly related to the bulk properties of the suspension or solution, the prediction of which is the primary goal of most theoretical analyses. In this regard, however, it should be noted that the prediction of bulk rheological properties generally requires second (and higher) order tensors even when the microelements are axisymmetric and individually specified by the axial end-to-end vector $\underline{R}$. Specifically, the bulk constitutive equation in this case is found to depend on $\langle \underline{\underline{RR}} \rangle$, $\langle \underline{\underline{\underline{\underline{RRRR}}}} \rangle$, etc. Similarly, when the specification of a single element requires a second (or higher) order tensor, the bulk constitutive equations require statistical averages of these tensors,

e.g. $\langle \underline{\underline{A}} \rangle$, $\langle \underline{\underline{A}} \cdot \underline{\underline{A}} \rangle$. Thus, in either case, a complete determination of the bulk constitutive relationship for mechanical properties of the material requires a statistical description of microstructure which involves at least second rank tensors. We will consider solutions or suspensions with microstructures that are statistically isotropic in the rest state, and specifiable via a second order tensor when the structure is modified by flow. This generally limits our analysis to "small" departures from isotropy. The philosophy of basing a "flow classification scheme" on the exponential growth of small "departures" from a statistically isotropic state is identical to that described earlier for single microelements.

Thus, the unifying feature which underlies our present work is the fact that all of the dynamical equations which describe the time evolution of single particle conformation, as well as the time-dependent variation in statistically averaged conformation variables for model suspensions or solutions, can be expressed in one of two common forms depending upon whether it is the vector or second order tensor description which is required. Thus, a unified stability analysis and resulting "flow classification scheme" can be carried out, and the general features of this analysis are independent of the nontrivial differences both of detail, and of the physical meaning of the microstructural variables, which exist from case to case.

B. Dynamical Equations for Evolution of Microstructure

In the case of a microstructure which can be characterized by a vector, say $\underline{R}$, a general equation describing flow induced variations in $\underline{R}$

(for $|\underline{R}| << 1$) can be proposed which encompasses all of the exact microdynamical equations that have been derived either for axisymmetric single particles, or for suspensions or solutions with axisymmetric microelements. This equation is

$$\dot{\underline{R}} = \underline{\underline{\Omega}}\cdot\underline{R} + G\left[\underline{\underline{E}}\cdot\underline{R} - \frac{F}{F+1}(\underline{r}\cdot\underline{\underline{E}}\cdot\underline{r})\underline{R}\right] - \frac{\alpha}{F+1}\underline{R} \qquad (1)$$

where $\underline{r} \equiv \underline{R}/R$ with $R \equiv |\underline{R}|$, and $\underline{\underline{E}}$ and $\underline{\underline{\Omega}}$ are the rate-of-strain and vorticity tensors, respectively, of the local undisturbed bulk motion of the suspending fluid. The coefficients G, α and F are parameters which depend upon the properties of both the microelements and the suspending fluid. Specific values which reduce (1) to the linearized version of the exact dynamical equations for specific model systems will be discussed shortly. First, however, it is useful to examine (1) from a qualitative point of view. The first two terms on the right-hand side derive from the mean hydrodynamic effect of the suspending fluid's motion on the microstructural vector, $\underline{R}$, and are thus regarded as the "driving force" for distortion of the microstructure from its rest configuration. The third term is then seen to represent a "restoring mechanism", tending to return the system to the rest state, $\underline{R} \equiv 0$.

The equation (1) describes exactly the rotation of the axis of revolution for an axisymmetric rigid particle in a homogeneous, linear flow of the type $\underline{u} = (\underline{\underline{E}} + \underline{\underline{\Omega}})\cdot x$, with G a shape factor of magnitude generally less than unity (Bretherton, 1962), $F/(F+1) = 1$ and $\alpha/(F+1) = 0$. In addition, (1) is of the same form as the evolution equation for the end-to-end vector in the axisymmetric

"elastic ellipsoid" model of a macromolecule in solution which was recently discussed by Hinch (1977). The equation (1) is also identical in form to that describing the rotation and extension/compression of the linear elastic dumbbell model which originated with Kuhn and Kuhn (1945). The latter had $G = 1$, $F = 0$ and $\alpha = H/6\pi\mu a$ where H is the linear spring constant and $6\pi\mu a$ is the Stoke's resistance factor for spherical beads. The inclusion of bead-bead hydrodynamic interactions in the dumbbell model modifies the restoring constant, α, but does not change the form of the equation for the linear elastic dumbbell. Finally, if the connector law in the dumbbell model is modified to include "internal viscosity", as well as a linear spring, the resulting microdynamical equation for the end-to-end vector is precisely (1), with $G = 1$ and $\alpha = H/6\pi\mu a$ as before, but with $F = K/6\pi\mu a$ where K is the coefficient of internal viscosity (Bird et al., 1977).

A relevant question is whether one may apply (1) in some approximate sense even if the microstructure is not axisymmetric. In this regard, it is perhaps worth noting that the dumbbell particle, which is strictly axisymmetric,is nevertheless intended to model the main features of orientation and deformation of a "random-coil" macromolecule in solution and the latter would not, in general, exhibit an axisymmetric structure. In this sense, then, there is a strong precedent for suggesting that the vector model may also provide a crude representation of the orientational and deformational characteristics of other nonaxisymmetric microelements. We shall, in effect, test this hypothesis for liquid drops in section VI of this paper. The linear elastic dumbbell limit (i.e. $G = 1$, $\alpha = \text{const.}$,

F = 0) was used by Tanner (1976) to develop a strong flow criterion. Although the linear dumbbell is restricted to small $|\underline{R}|$, Tanner assumed, as here, that the existence of unbounded growth of $|\underline{R}|$ is indicative of the condition for "onset" of large values of $|\underline{R}|$. However, by basing his analysis on the linear elastic dumbbell limit, Tanner seriously restricted the applicability of his results. Specifically, G = 1 is indicative of a "particle" which would deform and rotate identically to a line element of the fluid where $\alpha = 0$. In addition, the fact that F = 0 for the linear dumbbell means that it exhibits no "rigidity" regardless of the rate at which its end-to-end separation changes. In both of these features, the linear dumbbell is special and (we believe) not necessarily representative of the behavior of real particles or molecules, which inevitably have a finite aspect ratio and an internal rigidity to deformation. These features of real particles or molecules yield an inefficiency in the ability of a steady straining motion to rotate the particle relative to a line element with the same orientation, and a limit on attainable rates of deformation or stretching in any given flow field. In general, a real rigid particle spins with the full vorticity, but only a part of the steady straining motion. In the context of the model equation (1), this physical effect corresponds to values of G different from unity. Almost all rigid axisymmetric particles exhibit values of $G < 1$ (with the exception of particles of peculiar shape — cf. Bretherton, 1962). The parameter $G \to 1$ from below for particles of infinite major to minor axis ratio, while a particle of spherical shape has G = 0. Elastic particles and viscous drops in axisymmetric straining

flow (where (1) is relevant) both exhibit values of $G \neq 1$. Even the elastic dumbbell shows a value of $G < 1$ if the "beads" are constrained from rotating freely as they do in the usual formulation of the model.[†] The coefficient F can vary between 0 and ∞, corresponding to a particle with an elastic (nondissipative) resistance to deformation and a rigid particle, respectively. As indicated earlier, nonzero values of F in the dumbbell model arise from the inclusion of "internal viscosity" in the connector. All real particles will exhibit nonzero values of F.

It may also be noted that a comparison between the predicted rheological (and birefringent) behavior of a solution (or suspension) of linear dumbbells with $G = 1$ and $F = 0$, and the observed behavior in real solutions provide further indirect support for the relevance of values of $G \neq 1$ and $F \neq 0$. Specifically, a solution of linear dumbbells ($G = 1$, $F = 0$) is predicted to exhibit a constant viscosity in steady shear flow, as well as a first normal stress difference, N_1, which increases quadratically with shear rate (thus becoming unbounded for very large shear rates) and a second normal stress difference, N_2, which is identically zero. In contrast, a modification of the model to values of $G < 1$ and/or values of F which are nonzero leads to a shear thinning

[†]When the spheres of the dumbbell are allowed to rotate freely, as is usually assumed, the effective "particle shape" can only be a line element (with the consequence that $G = 1$) regardless of any other features which may be incorporated into the model, or of the assumed ratio of sphere radius to separation distance. This is most easily seen by noting that a dumbbell with freely rotating spheres will experience no torque in a simple shearing flow when the axis of the dumbbell is aligned with the undisturbed velocity — this is a distinguishing characteristic of a particle with an effective axis ratio of infinity, for which $G = 1$.

viscosity, a first normal stress difference with a high shear rate plateau, and a second normal stress difference which has the same form as N_1 but which is negative and of magnitude $(1 - G)/2$ relative to N_1 (cf. Gordon and Schowalter, 1972). In addition, in flows starting from rest, the model with $G < 1$ and /or $F > 0$ yields a nonzero initial stress and oscillatory overshoots. The fact that the latter predictions are in close qualitative agreement with observation, coupled with an understanding of the fluid mechanics of real particle motions, provides strong motivation for considering the microdynamical equation (1) with $G \neq 1$ and $F > 0$ Indeed, Gordon and Schowalter (1972) suggest, on the basis of the rheological predictions, that a model of the form (1) may also apply in relatively concentrated polymer solutions where it is proposed that values of $G < 1$ may arise from hydrodynamic or other interactions between the macromolecules.

It should be reiterated that the equation (1) is to be regarded as the linearized version, for small R, of the full dynamic equation for evolution of a vector microstructure. In the context of the dumbbell, for example, a more "complete" model of a real macromolecule has been suggested by Hinch (1977) and Tanner (1975), among others, to properly contain a nonlinear spring, and a nonlinear hydrodynamic resistance of the beads — i.e. the magnitudes of both α and F should be dependent on R — as well as values of G different from unity. In general, each of the constant parameters in (1) is thus to be regarded as the asymptotic limiting value appropriate for small departures of the microstructure from its rest configuration, $R = 0$. The important point is that the

specific values, G = 1, F = 0, used by Tanner (1975) in his earlier "flow classification" analysis are not consequences of the approximation to microstructural distortions of small magnitude, as is true of the linearity of the model equation, but rather correspond to particular combinations of "shape" and "rigidity" of the microelements.

We have noted, in the previous section, that a more general description of microstructure is required for systems in which the microconfiguration is not either individually or statistically axisymmetric. We restrict our attention to microstructures which are describable via an irreducible symmetric second order tensor, a form which is relevant to the first departures of the structure from isotropy owing to the action of a general undisturbed steady linear flow of the form $\underline{u} = \underline{\underline{\Gamma}}\cdot\underline{x} = (\underline{\underline{E}} + \underline{\underline{\Omega}})\cdot\underline{x}$. The requirement of symmetry derives from the observation that the first departures from isotropy (of the shape of the microelements, or of the statistical distribution of orientations, say) are quadratically small (Hinch and Leal, 1975). A particular case which is included within this framework has already been cited, namely $\underline{\underline{A}} = \underline{\underline{R}}\,\underline{\underline{R}}$ where $\underline{\underline{R}}$ satisfies (1). In this case,

$$\dot{\underline{\underline{A}}} = \underline{\underline{A}}\cdot\underline{\underline{\Omega}} - \underline{\underline{\Omega}}\cdot\underline{\underline{A}} + G\left(\underline{\underline{E}}\cdot\underline{\underline{A}} + \underline{\underline{A}}\cdot\underline{\underline{E}} - \frac{2F}{F+1}\frac{(\underline{\underline{E}}:\underline{\underline{A}})}{\mathrm{tr}\,\underline{\underline{A}}}\,\underline{\underline{A}}\right) - \frac{2\alpha}{F+1}\underline{\underline{A}} \qquad (2)$$

and the conditions under which $R = (\mathrm{tr}\,\underline{\underline{A}})^{1/2}$ becomes unbounded will be determined in Section III. The interesting new case is that in which the physics of the microstructure requires $\mathrm{tr}\,\underline{\underline{A}} = 0$. In the case in which $\underline{\underline{A}}$ describes the first departure in the shape of a single particle from a sphere, the volume of the microelements is proportional to

$1 + \mathrm{tr}\,\underline{\underline{A}} + O(\underline{\underline{A}}^2)$ and the condition $\mathrm{tr}\,\underline{\underline{A}} = 0$ thus requires that the particle volume be conserved as it is deformed. If $\underline{\underline{A}}$ describes the first departure of some statistical distribution from isotropy for an assembly of particles, the condition of conservation of total probability requires $\mathrm{tr}\,\underline{\underline{A}} = 0$. The linearized version of the general dynamics equation for $\underline{\underline{A}}$ which guarantees $\mathrm{tr}\,\underline{\underline{A}} = 0$ is

$$\dot{\underline{\underline{A}}} = \underline{\underline{A}}\cdot\underline{\underline{\Omega}} - \underline{\underline{\Omega}}\cdot\underline{\underline{A}} + G\left(\underline{\underline{E}}\cdot\underline{\underline{A}} + \underline{\underline{A}}\cdot\underline{\underline{E}} - \frac{2}{3}(\underline{\underline{E}}:\underline{\underline{A}})\underline{\underline{I}}\right) - \alpha\underline{\underline{A}} + \beta\underline{\underline{E}} \tag{3}$$

An evolution equation of this general form has been investigated previously in the context of microstructural constitutive equations of state by Hand (1962), Barthés-Biesel and Acrivos (1973a), and Hinch and Leal (1975, 1976). Such an equation can also be rigorously derived for small deviations of viscous drops (Frankel and Acrivos, 1970) or elastic particles (Goddard and Miller, 1967) from sphericity. It may be noted, however, that the first deviations of a slightly deformed rigid ellipsoid from rotation with the local vorticity of the fluid (as is true for a sphere) occurs at $O(\underline{\underline{A}}^2)$. Indeed, an exact expression for rotation of a slightly deformed ellipsoid was shown by Goddard and Miller (1967) to be given by

$$\dot{\underline{\underline{A}}} = \underline{\underline{\Omega}}\cdot\underline{\underline{A}} - \underline{\underline{A}}\cdot\underline{\underline{\Omega}} - 2(\underline{\underline{A}}\cdot\underline{\underline{E}}\cdot\underline{\underline{A}}) + (\underline{\underline{A}}\cdot\underline{\underline{A}})\cdot\underline{\underline{E}} + \underline{\underline{E}}\cdot(\underline{\underline{A}}\cdot\underline{\underline{A}}) + O(\underline{\underline{A}}^3)\ . \tag{4}$$

Thus, unlike the vector equation (1), which describes exactly the rotation in the linear flow $(\underline{\underline{E}} + \underline{\underline{\Omega}})\cdot\underline{x}$, the linearized equation (3) can only yield rotation of a sphere in the limit of a rigid particle, where $G \to 0$ (an example is a viscous drop, which we will consider in section V, in the limit as the viscosity ratio approaches infinity). This does not, however,

affect the utility of (3) for the investigation of a criterion for "strong flow" based on an exponential increase in the anisotropy of the microstructure with time.

Indeed, apart from the condition that $\underline{\underline{A}}$ remain traceless, the tensor model (3) is similar to the vector model. The parameter α measures the strength of the restoring mechanism which causes the structure to return to its rest state in the absence of motion. Further, G provides a measure of the relative efficiency of the straining motion, compared to vorticity, in changing $\underline{\underline{A}}$. The material properties of the particular system under consideration are incorporated in the model through the parameters α and G. In the case of a deformable drop, for example, these parameters are functions of the interfacial tension, drop size and viscosity ratio (cf. Barthés-Biesel and Acrivos, 1973a).

III. A Strong Flow Criterion for Microstructures Characterized by a Vector

We have seen that the equation (1) describes the time evolution of microstructure for axisymmetric microelements. We now obtain a criterion for strong flow from (1) by determining the conditions which yield exponential growth of the length scale, R.

Of course, any prediction of $\underline{R}$ as a function of time includes information both on the rotation of the particle axis and flow-induced stretching along the axis of symmetry. It is thus instructive to separate the stretching and rotation contributions in (1) by obtaining evolution equations for R and $\underline{r}$ separately. It is straightforward to show that

$$\dot{R} = \frac{1}{F+1}\{G(\underline{r}\cdot\underline{\underline{E}}\cdot\underline{r})R - \alpha R\} \tag{5}$$

and

$$\dot{\underline{r}} = \underline{\underline{\Omega}}\cdot\underline{r} + G[\underline{\underline{E}}\cdot\underline{r} - (\underline{r}\cdot\underline{\underline{E}}\cdot\underline{r})\underline{r}] \tag{6}$$

The latter equation is identical to that analyzed by Bretherton (1962) and others (cf. Leal and Hinch, 1972) for rotation of a rigid, axisymmetric particle in a linear flow $\underline{u} = (\underline{\underline{E}} + \underline{\underline{\Omega}})\cdot\underline{x}$. The equations (5) and (6) show that the vorticity directly affects the rate of particle rotation but only indirectly influences the variation in length scale, R. Furthermore, the rate of rotation is independent of the degree of particle "rigidity" and "elasticity". The rate of microelement stretching is determined at any instant by its orientation relative to the principal axes of strain, as well as its present level of stretch relative to the rest state. The presence of finite internal "rigidity" in the particle

is seen from (5) to play the nonessential role, insofar as the criterion for unbounded stretch is concerned, of scaling the time for microelement extension (or compression).

Now, Bretherton (1962) and Leal and Hinch (1972) have analyzed the nature of the solutions for rotation of a rigid particle. Specifically, Bretherton has shown that a vector $\underline{p}$, satisfying the linear equation

$$\dot{\underline{p}} = \underline{\underline{\Omega}}\cdot\underline{p} + G\underline{\underline{E}}\cdot\underline{p} \tag{7}$$

will rotate exactly as $\underline{r}$, but also vary in magnitude. The solution of (7) is of the form

$$\dot{\underline{p}} = \sum_n a_n e^{\lambda_n t}\hat{\underline{p}}_n \tag{8}$$

where λ_n are the eigenvalues and $\underline{p}_n$ are the corresponding eigenvectors of the characteristic equation

$$\det[\underline{\underline{\Omega}} + G\underline{\underline{E}} - \lambda\underline{\underline{I}}] = 0. \tag{9}$$

The three eigenvalues are either all real, or else there is one real eigenvalue and a complex conjugate pair. Before proceeding further, however, let us reconsider the dynamical equation (5) for evolution of the lengthscale, R.

The unit vector, $\underline{r}$, required in (5) is obtained from $\underline{p}$ by simply dividing by the magnitude of $|\underline{p}|$, i.e.

$$\underline{r} \equiv \underline{p}/(\underline{p}\cdot\underline{p})^{\frac{1}{2}} .$$

Thus

$$\underline{r}\cdot\underline{\underline{E}}\cdot\underline{r} = \frac{1}{(\underline{p}\cdot\underline{p})}\,[\underline{p}\cdot\underline{\underline{E}}\cdot\underline{p}]$$

But, it is evident from (7) that

$$\underline{p}\cdot\underline{\underline{E}}\cdot\underline{p} \equiv \underline{p}\cdot\left[\underline{\underline{\Omega}}\cdot\underline{p} + G\underline{\underline{E}}\cdot\underline{p}\right]\frac{1}{G}$$

$$= \frac{1}{G}\,\underline{p}\cdot\dot{\underline{p}} \quad .$$

Thus, the dynamic equation (5) can be rewritten in the form

$$(F + 1)\dot{R} = \frac{\underline{p}\cdot\dot{\underline{p}}}{\underline{p}\cdot\underline{p}}\,R - \alpha R \tag{10}$$

The geometric coefficient G, which appears explicitly in (6), is finally seen in equation (10) to influence the rate of microelement stretching only indirectly through its effect on the rate of rotation, i.e. $\dot{\underline{p}}$. Finally, introducing (8), equation (10) becomes

$$(F + 1)\dot{R} = \frac{\sum_m \sum_n \lambda_m\cdot(\underline{p}_n\cdot\underline{p}_m)}{\sum_m \sum_n \underline{p}_n\cdot\underline{p}_m}\,R - \alpha R$$

where $p_i = \alpha_i \hat{p}_i e^{\lambda_i t}$. This can be written

$$(F + 1)\dot{R} = \left[f(t) - \alpha\right]R \tag{11}$$

where f(t) is the appropriate function of time containing all the eigenvalues and corresponding eigenvectors. The solution of (11) can be written formally

$$R = R_o \exp\left[\int_o^t \frac{f(t') - \alpha}{F + 1}\,dt'\right] .$$

We associate "strong flows" with the existence of unbounded growth of R.

This occurs for any F when $f(t) > \alpha$. A strong flow criterion is now determined by finding the maximum value attained by f(t) and comparing it with α.

We consider first the case when all eigenvalues are real, say $\lambda_1 > \lambda_2 > \lambda_3$. In this case it is easily shown that $\max[f(t)] = \lambda_1$ and that $f(t) \to \lambda_1$ as $t \to \infty$. The other possibility is that one eigenvalue is real, say μ, and the others form a complex conjugate pair, $\zeta \pm i\xi$. In this case, too, the maximum value of f(t) is the largest real part of the eigenvalues, either μ or ζ. In both cases, this is also the asymptotic value for f(t) as $t \to \infty$. Thus, the strong flow criterion is seen to reduce to the condition that the real part of (λ) be larger than α for at least one of the eigenvalues of (9). If this condition is not satisfied, the flow is called weak. We note the possibility that f(0) may be less than α, but $\max[f(t)] > \alpha$. In this case, the particle first compresses, but as it rotates toward the principal extension axes, it reverses this trend and grows exponentially in length. The reversal occurs at the point when $f(t) = \alpha$. We also note that the existence of a complex eigenvalue, in the rotation problem, say $\lambda = \zeta + i\xi$, will introduce an oscillatory modulation of the magnitude of the end-to-end distance, R. The condition for strong flow

$$\mathrm{Re}(\lambda) > \alpha \tag{13}$$

is, in fact, identical to that used earlier by Tanner (1976) but without the insight which is afforded by the decomposition of (1) into separate equations for particle rotation and extension. With this justification in hand, we may now return to the eigenvalue problem defined by the equations

(7) - (9) in order to determine the conditions on $\underline{\underline{E}}$ and $\underline{\underline{\Omega}}$ for existence of a strong flow.

The eigenvalues of $(G\underline{\underline{E}} + \underline{\underline{\Omega}})$, and hence the classification of a specific flow as weak or strong, are affected by both the form and magnitude of the velocity gradient tensor. In order to develop a flow classification scheme which depends only on the flow type, it is necessary to separate these two effects. This can be accomplished by introducing the magnitude of the velocity gradient tensor, defined as $(\nabla\underline{u}:\nabla\underline{u}^T)^{\frac{1}{2}}$ which is a positive scalar quantity that is invariant under orthogonal transformations, as a scaling factor for $(G\underline{\underline{E}} + \underline{\underline{\Omega}})$. Thus, we examine the eigenvalues of the normalized tensor

$$\underline{\underline{L}} = \frac{G\underline{\underline{E}} + \underline{\underline{\Omega}}}{(\nabla\underline{u}:\nabla\underline{u}^T)^{\frac{1}{2}}}$$

The strong flow criterion (13) then becomes

$$\lambda^+ \equiv \max \mathrm{Re}(\lambda_i) > \lambda(\nabla\underline{u}:\nabla\underline{u}^T)^{-\frac{1}{2}}$$

where the λ_i are the eigenvalues of $\underline{\underline{L}}$. The normalization clearly does not change the fundamental nature of the strong flow criterion, but facilitates the comparison of different flow types for velocity gradients of constant magnitude.

Since the fluid is incompressible, $\mathrm{tr}\underline{\underline{L}} = 0$, and hence $\underline{\underline{L}}$ has seven independent components. The magnitude of λ^+ depends only on the invariants of $\underline{\underline{L}}$, however, corresponding to the fact that the strength of the flow must be invariant to overall rotations of the axes. Furthermore,

since $\underline{\underline{L}}$ is normalized, the domain of all possible flow fields forms a subset of the $(\mathrm{tr}\underline{\underline{L}}^2, \det \underline{\underline{L}})$ plane. The eigenvalues for any flow, which will be represented by a single point in the accessible region of this plane, are the roots of the characteristic equation

$$\lambda^3 - (\tfrac{1}{2}\mathrm{tr}\underline{\underline{L}}^2)\lambda - \det\underline{\underline{L}} = 0 \ . \tag{15}$$

Accessible Domain

To determine the accessible region of the $(\mathrm{tr}\underline{\underline{L}}^2, \det\underline{\underline{L}})$ plane, it is permissible, in view of the rotational invariance of $\mathrm{tr}\underline{\underline{L}}^2$ and $\det \underline{\underline{L}}$, to choose the principle axes of $\underline{\underline{E}}$ as coordinate axes so that the general linear flow, $\underline{u} = (\underline{\underline{E}} + \underline{\underline{\Omega}})\cdot\underline{x}$, can be represented as

$$\underline{\underline{E}} = \begin{pmatrix} a & & \\ & b & \\ & & -(a+b) \end{pmatrix} ; \ \underline{\underline{\Omega}} = \begin{pmatrix} 0 & g & -h \\ -g & 0 & j \\ h & -j & 0 \end{pmatrix} \tag{16}$$

The magnitude of the vorticity vector ω is given by $\omega^2 = g^2 + h^2 + j^2$, and

$$\underline{\underline{L}} = \frac{1}{(2M)^{\frac{1}{2}}} \begin{pmatrix} Ga & g & -h \\ -g & Gb & j \\ h & -j & -G(a+b) \end{pmatrix} \tag{17}$$

where the magnitude of the velocity gradient tensor is $(2M)^{\frac{1}{2}}$ with $M = (a^2 + b^2 + ab + \omega^2)$. The invariants of $\underline{\underline{L}}$ are

$$\begin{aligned} \text{tr } \underline{\underline{L}} &= 0 \\ \text{tr } \underline{\underline{L}}^2 &= \frac{1}{M}\left[G^2(a^2 + b^2 + ab) = \omega^2\right] \\ \det \underline{\underline{L}} &= -(2M)^{-3/2}\left[G^3 ab(a + b) + G\{g^2(a + b) - j^2 a - h^2 b\}\right] \end{aligned} \tag{18}$$

Now, since $\text{tr } \underline{\underline{L}}^2$ is an even function of G, while $\det \underline{\underline{L}}$ is odd, we can restrict our attention to positive values of G and use symmetry to determine the accessible domain when $G < 0$. It may be seen directly from (18) that

$$-1 \leq \text{tr } \underline{\underline{L}}^2 \leq G^2$$

with the minimum value attained for a purely rotational flow (a=b=0), and the maximum value occurring in a pure straining motion with $\omega^2 = 0$. The simplicity of this result is due to the fact that only the magnitude of the vorticity appears in $\text{tr } \underline{\underline{L}}^2$. This is not true for $\det \underline{\underline{L}}$, but then the range of possible values may be found by noting that $\det \underline{\underline{L}}$ is determined, for a fixed value of $\text{tr } \underline{\underline{L}}^2$, by a and b with the only constraint among all possible choices of g, h and j being that $g^2 + h^2 + j^2 = \omega^2$, i.e. the orientation of the vorticity vector remains arbitrary. The extremal values of $\det \underline{\underline{L}}$ are plainly attained by choosing the orientation to be parallel to one of the principal axes of $\underline{\underline{E}}$. Thus, at the extremum of $\det \underline{\underline{L}}$, one of a^2, b^2 or $(a+b)^2$ is ω^2 and the other two vanish. For instance, if $a > 0$, $a > b$, then the largest value of $\det \underline{\underline{L}}$ (for fixed $\text{tr } \underline{\underline{L}}^2$) is obtained for $c^2 = \omega^2$, $a^2 = b^2 = 0$. The extremum of $\det \underline{\underline{L}}$ is thus found

by determination of

$$\text{Max}\left\{\frac{-G^3ab(a+b) - G\omega^2}{2(\omega^2 + a^2 + b^2 + ab)^{3/2}}\right\} \quad \text{subject to the condition}$$

$$\text{tr}\,\underline{\underline{L}}^2 = \frac{G^2(a^2 + b^2 + ab) - \omega^2}{\omega^2 + a^2 + b^2 + ab} = \text{constant.}$$ This is a simple maximization problem and yields a = -2b which corresponds, for each value of $\text{tr}\,\underline{\underline{L}}^2$ (i.e. for each ω^2), to uniaxial extension for $\underline{\underline{E}}$. (There are two other extrema for a/b; however, these do not correspond to maxima, and have no physical significance in view of the nonanalytic nature of the extrema in the full (a/b,g,h,j) space.) The boundary of the accessible domain corresponding to a maximum in $\det \underline{\underline{L}}$ for each value of $\text{tr}\,\underline{\underline{L}}^2$ is given by

$$\det \underline{\underline{L}}\Big|_{\max} = f(\text{tr}\,\underline{\underline{L}}^2) \equiv \frac{\text{sgn}(b)2G^3(1 + 3K)}{6^{3/2}(1 + KG^2)^{3/2}} \tag{19}$$

where $K = \frac{1}{G^2}\,\frac{G^2 - \text{tr}\,\underline{\underline{L}}^2}{1 + \text{tr}\,\underline{\underline{L}}^2}$. It can be demonstrated by a similar analysis that the minimum value of $\det \underline{\underline{L}}$, for a given value of $\text{tr}\,\underline{\underline{L}}^2$, is

$$\det \underline{\underline{L}}\Big|_{\min} = -f(\text{tr}\,\underline{\underline{L}}^2) \tag{20}$$

which occurs when the straining part of the flow is biaxial in form (i.e. a = -b). The accessible domain is shown in Figure 1 as the region ABCD for a typical case, G > 0. Provided $G^2 \geq 3$, the boundaries BA (or BC) will exhibit a maximum (or minimum) in $\det \underline{\underline{L}}$ as we have shown in Figure 1, with the maximum given by $G(6 - G^2)/\sqrt{2}(9 - 2G^3)^{3/2}$ and occurring at

$\omega^2 = 2(3 - G^2)$. Otherwise, for $G^2 < 3$, $\det \underline{\underline{L}}$ increases (or decreases) monotonically along BA (or BC) with increase in $\mathrm{tr}\, \underline{\underline{L}}^2$.

Various points on the diagram can be identified with particular flow fields. First, consider the class of two-dimensional flows. For these, $\det \underline{\underline{L}} = 0$ and $\mathrm{tr}\, \underline{\underline{L}}^2$ varies from G^2, corresponding to hyperbolic extension, to -1, corresponding to pure rotation. The segment DB contains all two-dimensional flows. The special case of simple shear flow is located on this segment at $\mathrm{tr}\, \underline{\underline{L}}^2 = \frac{1}{2}(G^2 - 1)$. Another important class of flows are purely extensional flows, i.e. $\underline{\underline{\Omega}} = \underline{\underline{0}}$. The two invariants are given in this case by $\mathrm{tr}\, \underline{\underline{L}}^2 = G^2$ and $\det \underline{\underline{L}} = \frac{-1}{(2M)^{3/2}} G^3 ab(a + b)$. All vorticity-free flows thus lie on the segment CA. It is a simple matter to determine that the point A corresponds to uniaxial extension with $\det \underline{\underline{L}} = G^3/3\sqrt{6}$. The curve AB has already been identified as the boundary of the accessible domain. It corresponds to a uniaxial extension for $\underline{\underline{E}}$ with the vorticity aligned in the direction of the principal strain axis and increases in magnitude as the point B is approached. The opposite curve CB corresponds to a biaxial extension with vorticity aligned in the direction of a principal compression axis and again increasing in magnitude as B is approached. All pure rotations, i.e. $\underline{\underline{E}} = 0$, are represented by the single point B. The situation is summarized in Figure 2.

Domain of Stability

Any flow of the type $\underline{u} = (\underline{\underline{E}} + \underline{\underline{\Omega}}) \cdot \underline{x}$ can thus be represented by a point on the $(\det \underline{\underline{L}}, \mathrm{tr}\, \underline{\underline{L}}^2)$ plane, and the eigenvalues which determine the rate of

stretching of the microstructure, R, for that flow are given by the solution of the characteristic equation (15). The three roots of (15) are

$$\lambda_1 = s_1 + s_2$$

$$\lambda_2 = -\frac{1}{2}(s_1 + s_2) + \frac{\sqrt{3}}{2} i(s_1 - s_2)$$

$$\lambda_3 = -\frac{1}{2}(s_1 + s_2) - \frac{\sqrt{3}}{2} i(s_1 - s_2)$$

where

$$s_1 \equiv \left[\frac{\det \underline{\underline{L}}}{2} + \sqrt{D}\right]^{1/3} \quad ; \quad s_2 = \left[\frac{\det \underline{\underline{L}}}{2} - \sqrt{D}\right]^{1/3}$$

and

$$D \equiv (\det \underline{\underline{L}})^2 - \frac{1}{54}(\mathrm{tr}\, \underline{\underline{L}}^2)^3$$

The discriminant, D = 0, is shown in Figure 1 as two dotted lines OA and OC in the $(\det \underline{\underline{L}}, \mathrm{tr}\, \underline{\underline{L}}^2)$ plane, and marks the position at which the nature of the roots changes from the real roots in the region AOC, to one real and two complex conjugates in the region BOC and BOA. In BOA, D < 0 and the maximum real part of these roots is, in fact, just given by λ_1, i.e. $\lambda^+ = \lambda_1$. In AOC, where D > 0 and all roots are real, λ_1 is again the largest. Thus $\lambda^+ = \lambda_1$ in the whole region ACOB, excluding the discriminant OC, and the characteristic equation (15) then provides a <u>linear</u> relationship between $\mathrm{tr}\, \underline{\underline{L}}^2$ and $\det \underline{\underline{L}}$ for each constant value of λ^+ in this region. Typical contours for arbitrarily chosen constant values of λ^+ are sketched in Figure 1. The minimum value, $\lambda^+ = 0$, occurs on the OB axis. Along the discriminant OA, the value of λ^+ <u>increases</u> monotonically as a function of $\det \underline{\underline{L}}$

$$\lambda^+ = 2^{2/3}(\det \underline{\underline{L}})^{1/2}$$

with the maximum of λ^+ occurring at the single point A

$$\lambda^+_{max} = 2G/\sqrt{6} \ .$$

In the region COB, on the other hand, $D < 0$ and the largest real part occurs in the complex conjugate roots of (19) so that

$$\lambda^+ = \mathrm{Re}(\lambda_2,\lambda_3) = -\frac{1}{2}\lambda_1 \ .$$

In this case, a second linear relationship holds between $\det \underline{\underline{L}}$ and $\mathrm{tr}\, \underline{\underline{L}}^2$ namely

$$-8(\lambda^+)^3 + (\mathrm{tr}\, \underline{\underline{L}}^2)\lambda^+ - \det \underline{\underline{L}} = 0 \ . \qquad (20)$$

This relationship is also sketched in Figure 1. It will be noted, as indicated by (15) and (20) that the slope of the constant λ^+ contours in this region are opposite in sign and $\frac{1}{2}$ the magnitude of the slope in COBA. We shall discuss the physical significance of these observations shortly.

First, however, it is useful to summarize our argument to this point. Specifically, we have seen that each flow type, from the general class $\underline{u} = (\underline{\underline{E}}+\underline{\underline{\Omega}})\cdot\underline{x}$ corresponds to a single point in the accessible region of the $(\det \underline{\underline{L}}, \mathrm{tr}\, \underline{\underline{L}}^2)$ plane. Further, only one λ^+ contour passes through any point in this plane. Thus, the strength of any given flow is uniquely specified as $\lambda^+[\nabla\underline{u}:\nabla\underline{u}^T]^{1/2}$ and the criterion (7) can thus be applied to determine if the specified flow is weak or strong. For any given value of $[\nabla\underline{u}:\nabla\underline{u}^T]^{1/2}$, there is a single contour $\lambda^+ = \alpha[\nabla\underline{u}:\nabla\underline{u}^T]^{-1/2} = \text{const.}$ which divides the domain of possible flows into strong flows and weak flows. All flows that lie "above" the critical λ^+ contour in the $(\det \underline{\underline{L}}, \mathrm{tr}\, \underline{\underline{L}}^2)$ plane are

strong, and the microstructural length scale R will experience exponential growth. This growth will be monotonic in time for flows which lie to the right of the discriminant OC, and oscillatory for flows which lie to the left. All flows which fall "below" the critical λ^+ contour are weak.

Several other consequences of Figure 1 should be noted. First, for a given value of $\mathrm{tr}\,\underline{\underline{L}}^2$, the strongest possible flow occurs on the right boundary of the accessible domain ($G > 0$). Given the strain rate $\underline{\underline{E}}$, $\mathrm{tr}\,\underline{\underline{L}}^2$ depends only on the magnitude of the vorticity, while $\det \underline{\underline{L}}$ depends also on its orientation relative to the principal axes of strain rate. Thus, it may be seen that the strongest flow, for a specified magnitude of the vorticity, occurs when $\underline{\underline{E}}$ has the form of a uniaxial extension and the vorticity vector is aligned parallel to the principal axis of extension. The weakest flow, for a given ω^2, is described by the point on the discriminant OC where the vorticity vector is perpendicular to the compression axis.

Second, along the bounding curve A → B, the magnitude of the vorticity is increased and the flow becomes weaker as reflected by decreasing values of λ^+, until finally, at B, we have a completely rotational flow for which $\lambda^+ = 0$. Third, in the region between BOC and BC, the rate of strain tensor has the form of a biaxial extension and the strongest flow of this class again occurs at the boundary BC, where the vorticity is aligned parallel to the principal axis of compression. However, λ^+ for this case is only equal to $\frac{1}{2}$ its value at the same value of $\mathrm{tr}\,\underline{\underline{L}}^2$ for the case of uniaxial extension. This suggests that (for $G > 0$) the maximum value of λ^+ in the accessible domain, and therefore the strongest flow, occurs at the point A, which is a uniaxial extension with zero vorticity. This may indeed be demonstrated

numerically by showing that the λ^+ contour through A intersects the accessible domain only at A.

Finally, a remark is needed concerning two-dimensional flows which lie along the $\det \underline{\underline{L}} = 0$ axis. These are special in that the $\lambda^+ = 0$ contour also lies along the segment OB and consists of those flows for which the magnitude of the vorticity exceeds the magnitude of the effective strain $G\underline{\underline{E}}$. When $G = 1$, simple shear flow lies at the point O and when $G < 1$, simple shear is always weak, since it falls between O and B along the contour $\lambda^+ = 0$. The unrepresentative feature of two-dimensional flows which fall on the $\lambda^+ = 0$ contour is that they are weak for any arbitrarily small value of the restoring parameter α.

IV. A Strong Flow Criterion for Microstructures Characterized by an Irreducible Second Order Tensor

We turn now to the development of a criterion for strong flow for systems in which the microstructure can be characterized by a second order symmetric tensor $\underline{\underline{A}}$. As we have noted previously, the requirement of symmetry derives from the observation that the first departures from isotropy (of the shape of the microelements or of the statistical distribution of orientations, say) are quadratically small (Hinch and Leal, 1975). The analysis of the preceding section determines the conditions where $(\mathrm{tr}\,\underline{\underline{A}})^{\frac{1}{2}}$ becomes unbounded, for the special case in which $\underline{\underline{A}} = \underline{R}\underline{R}$ and $\underline{\underline{A}}$ is governed by equation (1). Here, we consider the case in which the physics of the microstructure requires $\mathrm{tr}\,\underline{\underline{A}} = 0$ (as, say, by volume conservation noted earlier), and the linearized version of the governing equation for $\dot{\underline{\underline{A}}}$ is equation (3).

The development of a criterion for strong flow for microstructures characterized by a second order tensor follows the general principles used in the preceding section, i.e. we determine the eigenvalues of the linear equation (4). In view of the constraint that tr $\underline{\underline{A}} = 0$, only five of the six eigenvalues for (4) are independent; indeed, (4) is represented more usefully for our purposes by writing five linearly independent component equations for A_{ij} in terms of a vector, say $\underset{\sim}{A}^*$, which then allows representation of (2) as $\underset{\sim}{A}^* = \underline{\underline{D}}\underset{\sim}{A}^*$ where $\underline{\underline{D}}$ is a 5x5 matrix. The matrix $\underline{\underline{D}}$ can be written in terms of the $\underline{\underline{L}} = (G\underline{\underline{E}} + \underline{\underline{\Omega}})/[\nabla\underline{u}:\nabla\underline{u}^T]^{\frac{1}{2}}$ and thus the condition for existence of a strong flow, i.e unbounded growth of the microstructural length scales, is

$$\lambda^+ \equiv \max \mathrm{Re}(\lambda_i) \; > |\alpha|[\nabla\underline{u}:(\nabla\underline{u})^T]^{-\frac{1}{2}}$$

where $\lambda_i (i = 1, .., 5)$ are the eigenvalues of the matrix $\underline{\underline{D}}$.

The characteristic equation for D is

$$\lambda^5 + \frac{1}{6}\left[4\mathrm{tr}(\underline{\underline{L}}^T\underline{\underline{L}}) - 11\mathrm{tr}\underline{\underline{L}}^2\right]\lambda^3 + \left[2\mathrm{tr}(\underline{\underline{L}}^{T^2}\underline{\underline{L}}) - 5\det\underline{\underline{L}}\right]\lambda^2$$
$$+ \frac{1}{6}\left[-2\mathrm{tr}\underline{\underline{L}}^2\mathrm{tr}(\underline{\underline{L}}^T\underline{\underline{L}}) + (\mathrm{tr}\underline{\underline{L}}^2)^2 - 6\mathrm{tr}(\underline{\underline{L}}^T\underline{\underline{L}})^2 + 6\left(\mathrm{tr}(\underline{\underline{L}}^T\underline{\underline{L}})\right)^2\right]\lambda$$
$$- \frac{2}{3}\left[\det\underline{\underline{L}}\left(2\mathrm{tr}(\underline{\underline{L}}^T\underline{\underline{L}})\right) - (\mathrm{tr}\underline{\underline{L}}^2)\right] = 0 \; . \qquad (26)$$

where the coefficients have been written in terms of the invariants of $\underline{\underline{L}}$.

The method for determination of flow strength for systems described (approximately) by (4) is now evident. The characteristic equation (26) is solved for five eigenvalues; the largest positive real part is proportional to the flow strength. Since a graphical representation of the

type used in Figure 1 is not possible in this case of a tensorial microstructure, we adopt the alternative of comparing the vector and tensor models in several specific flows in order to expose the differences between them.

Potential Flows

Consider first the potential flow, written without loss of generality as $[\underline{\underline{E}}] = \begin{pmatrix} \alpha & 0 & 0 \\ 0 & \beta & 0 \\ 0 & 0 & -(\alpha+\beta) \end{pmatrix}$; $\underline{\underline{\Omega}} = \underline{\underline{0}}$. The effects on the strong flow criterion of the additional physical features of the tensor description of the microstructure (compared to the vector description) are most obvious for this class of flow types. For uniaxial extension $\alpha = 2$, $\beta = -1$, and the eigenvalues obtained from (26) are $\lambda = yG/\sqrt{6}$ with $y = 2,-1,-1,-2,-2$, so that $\lambda^+ = 2G/\sqrt{6}$. More surprisingly, however, inspection of (26) indicates that $(\lambda - 2G/\sqrt{6})$ is a factor of the characteristic equation for any arbitrary elongational flow. Hence, $\lambda = 2G/\sqrt{6}$ is an eigenvalue (in fact, the largest) for any choice of α and β. We conclude that all elongational flows are of equal strength for microsctructures described by (4). This result is in marked contrast to the prediction for vectorial microstructures, where the strengths of elongational flows (i.e. the values of λ^+) are found to vary with the flow type from the strongest flow, uniaxial extension, to the weakest, biaxial extension (line segment CA in Figure 1).

The responses of the two models differ for elongational flows because microelement volume conservation is incorporated into the tensor model. A vectorial microelement in a purely elongational flow aligns in the principal direction of greatest strain rate, and the length scale grows at a rate which depends on the strain rate in only that direction. Thus, in a uniaxial flow, the length scale growth rate is twice as large for the vectorial model as it is in a biaxial extension. However, when the microstructure is endowed with a traceless tensorial description, the rate of extension in any given direction is related to the rates of extension and/or compression in the other principal directions through the requirement of volume conservation (as for a viscous drop) or conservation of total probability in the case of a suspension (or solution) of Brownian particles. In biaxial elongation, for example, the "tensorial" microelement is compressed along the principal axis of strain rate (say, 1), and the resultant "squashing" contributes to the extensional deformation in the 2-3 plane because of the $\mathrm{tr}\,\underline{\underline{A}} = 0$ condition. Indeed, the coupling between different modes of deformation in the traceless, tensorial model is responsible for the prediction that all elongational flows have equal strength in their ability to deform the microstructure. When a vector microelement is subjected to biaxial extension, on the other hand, it rotates into the 2-3 plane and then stretches at a rate which depends only on the rates of elongation of the flow in the 2-3 plane. Thus, in contrast to the traceless tensorial microstructural model, the strengths of different elongational flows, as predicted by the vector model, all differ depending upon the rates of

extension in the direction of stable "particle" orientation in each case.

Two-Dimensional Flows

The eigenvalues for the class of two-dimensional flows are

$$0, \pm \left[\frac{1}{2}\,\mathrm{tr}\,\underline{\underline{L}}^2\right]^{1/2}, \quad \left[\frac{4}{3}\,\mathrm{tr}(\underline{\underline{L}}^2) - \frac{2}{3}\,\mathrm{tr}(\underline{\underline{L}}^T\underline{\underline{L}})\right]^{1/2} .$$

The first three occur also for microstructures characterized by a vector, but the additional pair can assume larger values under some circumstances which indicates that the predicted value for λ^+ can differ for the two models. It has already been shown that the vector and tensor models do indeed differ for two-dimensional elongational flow. On the other hand, the two models predict identical flow strengths for pure rotation, which is always weak, as well as simple shear flow, which can be strong only if $G^2 > 1$, and for all two-dimensional flows with sufficient rotation.

Effects of Vorticity on the Flow Strength

As a further example, let us consider the class of flows defined by

$$[\underline{\underline{E}}] = \begin{pmatrix} 2 & 0 & 0 \\ 0 & -1 & 0 \\ 0 & 0 & -1 \end{pmatrix} , \qquad [\underline{\underline{\Omega}}] = \begin{pmatrix} 0 & a & 0 \\ -a & 0 & b \\ 0 & -b & 0 \end{pmatrix}$$

This particular class of flows is of interest because both the magnitude of the vorticity relative to the pure straining part of the velocity gradient and the orientation of the vorticity relative to the principal straining axes can be adjusted independently through the parameters a and b. The pure straining part of the motion has the form of uniaxial extension with largest principal rate of strain axis in the 1-direction.

The vorticity vector is aligned parallel to this axis for $a = 0$, $b \neq 0$ and is perpendicular to it for $a \neq 0$, $b = 0$. We can determine the effect of the orientation of vorticity by putting $a = \sin\theta$, $b = \cos\theta$ (so that $\omega^2 = a^2 + b^2 = 1$) and finding $\lambda^+(\theta)$, where θ is the angle between the vorticity vector and the extension axis. This calculation has been performed for the case $G = 1$ for both the vector and tensor models, and the results are shown in Figure 3. The real parts of the entire set of eigenvalues are shown for completeness, but the strength of the flow is proportional to the largest of these.

Figure 3 shows that the flow is strongest for both models when the vorticity vector is parallel to the principal direction of extension and is weakest when the vorticity vector is perpendicular to the direction. When the orientation of the vorticity vector is nearly parallel to the extension axis, the microstructure rotates mainly around the extension axis, i.e. in the 2-3 plane. Thus, the straining motion experienced by the microelements is nearly a constant uniaxial elongation. However, when the vorticity vector is oriented perpendicular to the extension axis, the rotation of the microstructure occurs in a plane containing the extension axis. Then the microelements are subject to alternate periods of extension and compression as they rotate. As a consequence, the "average" rate of strain and hence the flow strength are decreased. The vector model exhibits less sensitivity to the orientation of the vorticity than the tensor model. This is due to the fact that a vectorial microelement spends a greater proportion of time aligned in the direction of principal rate of strain compared to the tensorial microelement. On the other hand,

the tensor microelement is deformed by compression as well as extension via the conservation of volume feature present in the tensor model. As a consequence, the flow strength is determined by different eigenvalues for small and large values of θ. The eigenvalue which predicts the flow strength for large values of θ is complex, indicating that growth of the microelement length scales occurs in an oscillatory fashion. The cross-over of the eigenvalues for the tensor model occurs whenever $\omega^2 > 0.1$ for the given form of $\underline{\underline{E}}$ and $\underline{\underline{\Omega}}$. The effect of making the magnitude of the vorticity larger compared to the magnitude of $\underline{\underline{E}}$, i.e. $\omega^2 = a^2 + b^2 > 1$ is to decrease the flow strength, especially for large values of θ. If ω^2 is made sufficiently large, the vector model, too, will predict a complex eigenvalue with largest real part, much like the tensorial result in Figure 3. The point of intersection of the two eigenvalues shown in Figure 3 tends toward lower values of θ as ω^2 is increased.

We consider finally the case in which the magnitude of the vorticity is permitted to vary. In that case, $[\nabla\underline{u}:\nabla\underline{u}^T]^{\frac{1}{2}}$ is not fixed and so comparisons must be made between values of $\lambda^+[\nabla\underline{u}:\nabla\underline{u}^T]^{\frac{1}{2}}$. We again consider

$\underline{\underline{E}} = \begin{pmatrix} \alpha & & \\ & \beta & \\ & & -(\alpha+\beta) \end{pmatrix}$ and $\underline{\underline{\Omega}} = \begin{pmatrix} 0 & a & 0 \\ -a & 0 & b \\ 0 & -b & 0 \end{pmatrix}$. The qualitative factors may be shown by asymptotic analysis of the flow in the limits $\omega^2 = a^2 + b^2 << 1$ and $>> 1$.

(a) $a = \varepsilon$, $b = 0$, $\alpha > 0$, $\beta < 0$, $|\alpha| > |\beta|$ with $\varepsilon << \|\underline{\underline{E}}\|$:

In this case, the magnitude of vorticity is $O(\varepsilon)$ with the vorticity vector aligned in the 3-direction. The flow strength for the vector model is readily obtained as the largest of the following eigenvalues:

$$\lambda_1[\nabla\underline{u}:(\nabla\underline{u})^T]^{\frac{1}{2}} = \alpha + \varepsilon^2\left(\frac{1}{\beta - \alpha}\right) + O(\varepsilon^3)$$

$$\lambda_2[\nabla\underline{u}:(\nabla\underline{u})^T]^{\frac{1}{2}} = \beta - \varepsilon^2\left(\frac{1}{\beta - \alpha}\right) + O(\varepsilon^3)$$

$$\lambda_3[\nabla\underline{u}:(\nabla\underline{u})^T]^{\frac{1}{2}} = -(\alpha + \beta) + O(\varepsilon^3)$$

If the straining part of the motion has the form of a uniaxial extension, $\alpha = 2$, $\beta = -1$, then $\lambda^+[\nabla\underline{u}:(\nabla\underline{u})^T]^{\frac{1}{2}} = 2 - \frac{1}{3}\varepsilon^2 + O(\varepsilon^3)$. The tensor model yields a similar result under the same conditions: $\lambda^+[\nabla\underline{u}:(\nabla\underline{u})^T]^{\frac{1}{2}} = 2 - \frac{28}{3}\varepsilon^2 + O(\varepsilon^3)$. The addition of vorticity clearly inhibits the flow strength in both cases (as expected) but this effect is much more pronounced in the case of a tensorial microstructure.

(b) $a = 0$, $b = \varepsilon$, $\alpha > 0$, $\beta > 0$, $|\alpha| > |\beta|$ with $\varepsilon << \|\underline{\underline{E}}\|$. This choice of parameters gives a small degree of vorticity with the vorticity vector aligned parallel to the largest principal axis of extension of $\underline{\underline{E}}$. In this case, both the vector and tensor models predict that the flow strength is unchanged by the addition of vorticity. The decrease in the value of λ^+ owing to the addition of vorticity is exactly balanced by the increase in magnitude of the (total) velocity gradient $[\nabla\underline{u}:(\nabla\underline{u}^T]^{\frac{1}{2}}$.

(c) $a = \omega$, $b = 0$ with $|\vec{\omega}| >> \|\underline{\underline{E}}\|$. We now consider the opposite limit, that is, when the magnitude of the vorticity is much greater than the straining part of the motion. First, consider the case in which the vorticity vector is aligned in the 3-direction. The asymptotic result for the vector model is

$$\lambda_1[\nabla\underline{u}:(\nabla\underline{u})^T]^{\frac{1}{2}} = -(\alpha + \beta)$$

$$\lambda_2[\nabla\underline{u}:(\nabla\underline{u})^T]^{\frac{1}{2}} = (\alpha + \beta)/2$$

$$\lambda_3[\nabla\underline{u}:(\nabla\underline{u})^T]^{\frac{1}{2}} = (\alpha + \beta)/2$$

When $\underline{\underline{E}}$ has the form of uniaxial elongation, $\lambda^+[\nabla\underline{u}:(\nabla\underline{u})^T]^{\frac{1}{2}} \to \frac{1}{2}$ for the vector model, while the flow strength approaches unity for the tensor model.

(d) $a = 0$, $b = \omega$, with $|\vec{\omega}| >> \|\underline{\underline{E}}\|$. As long as the vorticity vector is aligned exactly parallel to the largest principal rate of strain axis of $\underline{\underline{E}}$, the flow strength remains unchanged even when $|\vec{\omega}| >> \|\underline{\underline{E}}\|$.

Cases (a) and (b) indicate that the addition of vorticity to a flow which is nearly irrotational inhibits the strength of the flow. The effectiveness of the inhibition decreases to zero as the vorticity vector approaches the principal rate of strain axis. The fact that the tensor model is more sensitive to the addition of vorticity is similar to the results discussed above for the effect of the orientation of the vorticity on the flow strength. As the vorticity increases in magnitude, the effective strain rate is precisely the average as seen by a particle rotating rapidly in the plane perpendicular to $\vec{\omega}$.

V. Prediction of Macromolecular Extension in Turbulent Flow

Although the exact mechanism is not known by which polymer additives in extremely low concentrations reduce drag in turbulent flow, substantial evidence suggests that the phenomenon is intimately connected to the degree of flow-induced extension of the polymer molecules (Berman, 1978; Hinch, 1977; Lumley, 1969). It seems of interest then to use available models of the type discussed here to predict the degree of macromolecular extension induced by a turbulent flow. We follow the approach of Moore (1980) who calculated an average stretched length for nonlinear dumbbells in a similar "model" turbulent flow. Here we are interested in the comparison between the responses of microelements described by a vector and by a tensor. Our basic postulate is that significant macromolecular extension occurs when the flow is strong and persists for a time long compared with the molecular relaxation time $1/\alpha$. Whether or not strong flow occurs locally within a turbulent flow depends on the local forms and magnitudes of the rate of strain and vorticity tensors as well as on the orientation of the vorticity with respect to the principal rate of strain axes.

We assume that the kinematics of the turbulent flow are known *à priori* from other sources, perhaps a model or alternatively experimental data for velocity distributions. However, once the kinematics of the flow are specified, most likely in some statistical sense, then the strong flow criterion can be directly applied to determine the macromolecular extension induced by the specified flow.

For the purpose of predicting macromolecular extension, we model the local turbulent flow at a fixed point in space by a sequence of discrete homogeneous flows, each of which persists for a specified time interval. The form of the velocity gradient tensor during each interval is specified by a "known" (or assumed) statistical description of the kinematics. A simple statistical representation will be employed here for illustrative purposes. The rate of strain tensor $\underline{\underline{E}}$ is <u>assumed</u> to have the form

$$[\underline{\underline{E}}] = \begin{pmatrix} A & & \\ & -AS & \\ & & -A(1-S) \end{pmatrix}$$ where A and S are uniformly distributed random variables on the closed intervals [-2,2] and [0,1], respectively. The magnitude of the vorticity vector $|\vec{\omega}|$ is taken to be an independent random variable uniformly distributed on a closed interval $[0,\omega^*]$ where the maximum vorticity ω^* ($\omega^* > 0$) is a parameter. The orientation of the vorticity vector is a random vector uniformly distributed on the unit sphere, and is taken to be independent of the particular form and relative magnitude of the pure straining part of the motion. This particular representation of a turbulent flow is statistically isotropic, but not homogeneous. More complicated descriptions of turbulence are, of course, possible (e.g. Phan-Thien and Tanner, 1978), and these may present a physically more realistic representation of the detailed kinematics, but our simpler model is sufficient to illustrate the calculation of molecular extension induced by a flow with known (albeit oversimplified) kinematic statistics. Thus, this simple model of turbulent flow consists of a sequence of sets of values fo S, A, $\vec{\omega}$ (both orientation and magnitude),

and we determine the strength of the flow for each set. Of course, the existence of strong flow for a particular randomly chosen set of values indicates exponential growth of the microelement length scale(s) only over the time interval for which the particular set of values persists. Significant macromolecular extension in a strong flow will occur only when the flow persists for a sufficiently large period of time. We assume here that every realization of the velocity gradient $\nabla\underline{u}$, subject to the above statistical description, persists for a fixed time interval T. The velocity gradient is constant during the time interval, but the values of $\nabla\underline{u}$ for subsequent intervals are independent of all previous intervals. Furthermore, we consider only the limit where the interval timescale T is much larger than the relaxation time of the molecule $1/\alpha$. In this limit, we assume that each realization of the turbulent flow persists for a sufficiently large time to fully extend a macromolecule if the form of $\nabla\underline{u}$ for that realization produces a strong flow. A more realistic description of the flow would include some statement on the statistics of the timescale T which could possibly be correlated with the instantaneous form and magnitude of $\nabla\underline{u}$. In this case, macromolecular extensional growth rate could be estimated from the strong flow criterion applied over an assumed distribution of timescales, and a statistical measure of extension could then be predicted. Here, though, only the asymptotic limit of large T is considered.

The problem is reduced to determination of strong flow for a large number of velocity gradient realizations specified by A, S, $|\vec{\omega}|$, and the orientation of $\vec{\omega}$. The strength of the flow for a given value of $\nabla\underline{u}$

is calculated by solving the appropriate characteristic equation, (15) or (26) depending on the microstructure model used. This could be done analytically, in principle, by finding the distribution function for the coefficients of the characteristic equation, since the distribution functions of A, S, $|\vec{\omega}|$, and orientation are quite simple. Nevertheless, determination of the distribution function which depends on five randomly distributed variables (orientation requires specification of two independent angles) involves algebraic complexity unwarranted in this case. Therefore, a numerical scheme is employed. The five variables which together specify $\nabla\underline{u}$ are chosen for each realization on the stated closed intervals by a random number generator. The coefficients of the appropriate characteristic equation are calculated, and the equation is solved by a Newton-Raphson routine. The flow strength $\lambda^{+}[\nabla\underline{u} + (\nabla\underline{u})^{T}]^{\frac{1}{2}}$ is then computed easily for each realization. A histogram of the flow strengths is formed for a large number of realizations. The results of the calculation are shown in Figure 4 in terms of the cumulative distribution of flow strengths non-dimensionalized by the maximum possible flow strength (uniaxial elongation). Several values for the parameter ω^{*}/G are shown. The ordinate represents the fraction of realizations for which the flow strength exceeds the dimensionless flow strength on the abscissa. Since a flow is strong if $\lambda^{+}[\nabla\underline{u}:(\nabla\underline{u})^{T}] > |\alpha|$, Figure 4 gives equivalently the fraction of polymer molecules exhibiting exponential growth of the length scale(s) for a system with dimensionless relaxation constant $\alpha[\lambda^{+}[\nabla\underline{u}:(\nabla\underline{u})^{T}]^{\frac{1}{2}}]_{max}$, subject to the assumptions mentioned previously. The dimensionless relaxation depends implicitly on the value of the

material constant G. The curves were computed based on 2500 realizations; increasing the number to 25000 resulted in numerical differences of less than one percent.

The fraction of molecules experiencing full extension is reduced as the relaxation constant increases. This is an obvious consequence of the restoring force preventing the flow from distorting the polymer molecule. Indeed, if the relaxation constant is larger than the maximum flow strength possible under the particular statistical description chosen, no macromolecules extend due to the flow.

The inhibiting effect of vorticity is easily seen in Figure 4. For a given value of α, the fraction of molecules which are extended decreases as the vorticity increases. The curve for $\omega^*/G = 0$ represents the degree of extension experienced in statistical assortment of pure extensional flows. At the other extreme, as the intensity is increased, the curves tend toward definite limits. Although it is not shown in the figure, the numerical values for the case $\omega^*/G = 10^6$ differ from those for $\omega^*/G = 200$ by less than one percent. Asymptotic behavior for the case of large vorticity is expected based on the results from the calculations for flow strength in a homogeneous flow with large vorticity in the previous section. The fact that the flow strength, and hence the fraction of macromolecules which are extended, tends toward a nonzero limit as vorticity is increased without bound is a distinguishing characteristic of the three-dimensional nature of the flow. The flow strength in a two-dimensional flow necessarily tends toward zero as the magnitude of the

vorticity is made infinitely large. In terms of the present example, the curves for large values of ω^*/G would approach zero degree of extension if the flow were confined to two-dimensions. The reason for this difference between the two cases is the fact that in two-dimensional flows vorticity induces rotation of the plane containing the principal rate of deformation axes, i.e. the vorticity vector is perpendicular to this plane. An alternative statement is that for two-dimensional flows, the eigenvalues of $\underline{\underline{E}}$ must lie in the plane of rotation owing to $\underline{\underline{\Omega}}$. In three-dimensional flows, this is never the case, and hence, there is always a component of the principal axes of deformation which is effective in stretching the macromolecules even if the rate of rotation increases without bound.

The vector and tensor models show similar qualitative behavior though the tensor model predicts uniformly greater extension for a given value of ω^*/G. The difference appears greater at larger values of the relaxation constant except for the large vorticity cases. The asymptotic limits for large vorticity also differ for the two models as can be seen from the two curves for $\omega^*/G = 200$.

A simplified description of the statistics of the turbulent flow has been chosen to illustrate the calculation. Equipped with a more realistic specification of the turbulent flow, the extension in real flows could be predicted. We may speculate further that the structure of the turbulence requires correlations between the pure straining motion and vorticity which have been taken as independent variables here. Additionally, an attempt could be made to investigate extension in structural regimes of turbulence thought to play a role in drag reduction such as the viscous sublayer.

VI. Droplet Breakup

As a second example of the application of the strong flow criterion, we consider the deformation and breakup of immiscible Newtonian drops suspended in a Newtonian fluid which undergoes a prescribed deformation at zero Reynolds number. On dimensional grounds, drop deformation is then a function only of the dimensionless shear rate $\varepsilon = \mu\gamma a/\sigma$, where γ is the strain rate, a is the undeformed drop radius, and σ is the interfacial tension between the drop and the continuous phase. Furthermore, breakup must occur when this shear rate exceeds a critical value which depends on the ratio η of the drop viscosity μ to the viscosity of the suspending fluid and the tensorial character of the applied flow.

Experimental confirmation of a critical rate of deformation is provided by Rumscheidt and Mason (1961), Karam and Bellinger (1968), Grace (1971), Torza, Cox and Mason (1972), and Lee (1972). In all of these experiments, however, drop breakup was studied in either two-dimensional simple shear flow or hyperbolic elongation. The value of the dimensionless deformation parameter at breakup, ε_{crit}, was found to depend on which of the two flows was considered, as well as ratio η. Unfortunately, however, the data from the various studies show considerable scatter and the measured values for ε_{crit} vary by as much as a factor of three in some instances.

Barthés-Biesel and Acrivos have suggested that breakup is a manifestation of nonexistence of solutions to its steady state deformation problem. We adopt the more fundamental point of view (which also seems

more appropriate when hysteresis is known to occur) that breakup occurs as a result of unbounded growth of some length scale for the drop. This suggests that we may regard breakup as a consequence of strong flow conditions.

In order to use the strong flow criterion, we must estimate the two material parameters α and G, each as a function of η. The simplest available choice is to use the coefficients derived by Frankel and Acrivos in analyzing small deformations (from sphericity) of a viscous drop. It is not clear that these are the best choice, however, since we are interested in breakup which occurs frequently for drop shapes that are significantly nonspherical. Indeed, only very high viscosity drops ($\eta >> 1$) break up when only slightly deformed and in that case α, G are reasonably approximated by its near-sphere analysis.

Now, α represents the elasticity (Hookian spring constant) of the surface tension membrane, and since the material does not strain-soften the value obtained from a small deformation analysis can be reasonably expected to apply for large deformations. In regard to G on the other hand, we noted earlier that G = 0 for a rigid sphere, and hence a small change from sphericity is liable to produce a relatively large proportionate change in G. In fact, we find that the predictions for breakup using the near-sphere value for G are poor, and in consequence, adopt a semi-empirical procedure for estimation of the efficiency factor G in which data for ε_{crit} in one homogeneous flow are used to evaluate G for a particular value of the viscosity ratio. This value of G is then assumed to be appropriate for all flows, which assumes tacitly that the

shape of the deformed drop at incipient breakup does not depend on the particular flow which induces the overall deformation process. It should be clear, though, that G and hence the drop shape at breakup remain a function of the viscosity ratio. This approximation is likely to be a crude one, but is consistent with the strong flow notion that breakup occurs by a simple "tearing apart" of the drop. Of course, this simplified view of dispersion cannot predict any of the details of the breakup process such as the development of pressure instabilities, or any phenomena that are a consequence of a time dependent velocity gradient. In order to illustrate the procedure, we evaluate the parameter G from data for ε_{crit} in hyperbolic elongation and then use the same value in the vector and tensor models to predict ε_{crit} for simple shear flow where a comparison with other available data is possible.

The coefficient α can be obtained from the small deformation analysis of Frankel and Acrivos (1970)

$$\alpha = \frac{-40(\eta + 1)}{(2\eta + 3)(19\eta + 16)} \frac{\gamma}{\varepsilon}$$

The strong flow criterion is then written as

$$\lambda^{+}[\nabla \underline{u} : (\nabla \underline{u})^{T}]^{\frac{1}{2}} > \frac{40(\eta + 1)}{(2\eta + 3)(19\eta + 16)} \frac{\gamma}{\varepsilon} \qquad (27)$$

where λ^{+} is the largest real part of the eigenvalues calculated from equation (15) or (26). Hyperbolic elongation can be defined as $\nabla \underline{u} = \gamma \begin{bmatrix} 1 & 0 \\ 0 & -1 \end{bmatrix}$. The values for $\lambda^{+}[\nabla \underline{u} : (\nabla \underline{u})^{T}]^{\frac{1}{2}}$ for this flow are $G\gamma$ and $\sqrt{4/3}\, G\gamma$ for the vector model and tensor model, respectively. Thus, at

incipient breakup, the following expressions for G can be deduced from (27) — note, at incipient breakup, that the inequality becomes an equality and

$$G = \frac{40(\eta + 1)}{(2\eta + 3)(19\eta + 16)} \frac{1}{\varepsilon_{crit}} \quad \text{(vector)}$$

$$G = \frac{\sqrt{3/4}\ 40(\eta + 1)}{(2\eta + 3)(19\eta + 16)} \frac{1}{\varepsilon_{crit}} \quad \text{(tensor)} \tag{28}$$

Thus, given data for ε_{crit} in hyperbolic flow, G can be evaluated for each model as a function of the viscosity ratio η . The data for ε_{crit} for hyperbolic elongation from Lee (1972) will be used since it is the most extensive in the range of values for η where breakup occurs in both shear and hyperbolic flows. The values of ε_{crit} and the calculated value of G are given in Table 1 for several values of η.

The calculated values of G are now used to predict ε_{crit} for simple shear flow specified by $\nabla \underline{v} = \gamma \begin{bmatrix} 0 & 1 \\ 0 & 0 \end{bmatrix}$. The values of the flow strength for simple shear flow are $\frac{1}{2}(G^2 - 1)^{\frac{1}{2}}\gamma$ for the vector model and $\frac{1}{2}(G^2 - 1)^{\frac{1}{2}}\gamma$ for $1 \leq G \leq 3$ and $1/\sqrt{3}\ (G^2 - 3)^{\frac{1}{2}}\gamma$ for $G > 3$ for the tensor model. The corresponding expressions from the strong flow criterion for ε_{crit} in simple shear are then

$$\varepsilon_{crit} = \frac{80(\eta + 1)}{(2\eta + 3)(19\eta + 16)} (G^2 - 1)^{\frac{1}{2}}, \quad G > 1$$

$$= \infty \qquad\qquad , \quad G < 1$$

for the vector model, and

$$\varepsilon_{crit} = \frac{80(\eta + 1)}{(2\eta + 3)(19\eta + 16)} (G^2 - 1)^{-\frac{1}{2}} \qquad 3 > G > 1$$

$$= \frac{40\sqrt{3}\ (\eta + 1)}{(2\eta + 3)(19\eta + 16)} (G^2 - 3)^{-\frac{1}{2}} \qquad G > 3$$

$$= \infty \qquad G < 1$$

These predicted values for ε_{crit} in simple shear flow are shown in Figure 5. We shall discuss these results below in more detail. It is noteworthy, however, that the qualitative shape of the relationship between ε_{crit} and η is not only similar to that observed experimentally for simple shear flow, but is also much different from that for hyperbolic extension which was the source of our expressions for G. Let us now consider these results in more detail.

The semi-empirical approach gives a prediction for ε_{crit} as a function of η that is in qualitative agreement with the experimental data for simple shear flow as we have just noted. Breakup in this particular flow occurs only for values of the viscosity ratio η in the range $\sim 10^{-2} < \eta < 4$. The strong flow criterion predicts accurately the upper limit on η where breakup is still possible. The models also give good agreement with the minimum value of ε_{crit} (≈ 0.4) although the model predictions of this minimum occur at values which differ somewhat from the experimental result, $\eta \simeq 1$. Quantitative agreement with the data must be regarded as fortuitous to a certain extent, since the data for breakup in simple shear vary considerably between studies. Also,

uncertainty in the data for breakup in hyperbolic flow will be reflected in the results shown in Figure 5 since these data were used to evaluate the model parameter G. However, the data of Lee (1972) and Grace (1971) for hyperbolic elongation, the only available data for this flow, show relatively good agreement compared to the scatter among available results for simple shear flow.

The most important conclusion from the present results is that the models seem capable of correlating ε_{crit} for drop breakup in different flow types. The value for ε_{crit} in hyperbolic flow is approximately 0.2 and is relatively independent of η between 1 and 100. But when these data are used to evaluate G as a function of η and then predict ε_{crit} for simple shear flow, the model successfully indicates where breakup is no longer possible. Although this result by no means validates all the assumptions of our appraoch, it supports the basic premise that the effects of flow type on dynamic phenomena such as drop breakup can be correlated with a measure of the flow strength.

Conclusions

The common feature of the class of systems of interest is that the microstructures are capable of large distortions if the flow is sufficiently strong. It has been shown that a useful criterion for strong flow depends upon the type of model which is used to describe the microstructure. The nature of this choice depends apparently on whether or not some property of the microstructure is conserved during deformation. Hence, for volume or probability density conserving systems, one might

advocate use of a traceless tensor model; for "compressible" microstructures, a vector model seems appropriate.

Even when this decision is made, however, it appears that different choices for the description of the microstructure can themselves generate different results for the strong flow criterion, insofar as they appear to have different values for the strain efficiency parameter G. This paradox is resolved, in principle, by retention of the nonlinear higher order terms of the constitutive model. From the point of view of model building, however, if G is determined from experimental data then a choice of the description of the microstructure is effectively made. It is hoped that this choice is the relevant one with respect to the particular strong flow phenomenon under study, e.g. droplet breakup, but this can only be tested by further comparison with experimental data.

The strong flow criteria examined here are simple with known physics and explicit constitutive assumptions. They satisfy the essential requirement of easy application to arbitrary three-dimensional flows and seem to produce qualitatively correct results, at least for the drop breakup problem. However, the full benefit of this simple approach can be realized only with the aid of detailed numerical models that describe the kinematics of a complicated flow system. Equipped with a suitable description (even a complicated one) of the kinematics in a mixing device or agitator, for example, the strong flow criterion could be used to predict emulsion properties such as minimum droplet size. Examples of additional applications include prediction of melt fracture, breakup of particle aggregates and calculation of macromolecular extension in laminar flows with complicated boundaries.

References

Barthés-Biesel, D. 1972 Ph. D. Thesis, Stanford University.

Barthés-Biesel, D. and Acrivos, A. 1973a The rheology of suspensions and its relation to phenomenological theories for non-Newtonian fluids. Int. J. Multiphase Flow, 1, 1.

Barthés-Biesel, D. and Acrivos, A. 1973b Deformation and burst of a liquid droplet freely suspended in a linear shear field. J. Fluid Mech., 61, 1.

Berman, N. S. 1978 Drag reduction by polymers. Ann. Rev. Fluid Mech. 10, 47.

Bird, R. B., Hassager, O., Armstrong, R. C., and Curtiss, C. F. Dynamics of Polymeric Liquids, Vol. 2, Kinetic Theory. John Wiley and Sons, New York, 1977.

Bretherton, F. P. 1962 The motion of rigid particles in a shear flow at low Reynolds number. J. Fluid Mech., 14, 284.

Cerf, R. 1957 La macromolécule en chaîne dans un champ hydrodynamique théorie générale. Propertiés dynamo-optiques. J. Polymer Sci., 23, 125.

Frankel, N. A. and Acrivos, A. 1970 The constitutive equation for a dilute emulsion. J. Fluid Mech., 44, 65.

Fuller, G. G. 1980 Ph. D. Thesis, California Institute of Technology.

Goddard, J. D. and Miller, C. 1967 Non-linear effects in the rheology of dilute suspensions. J. Fluid Mech., 28, 657.

Gordon, R. J. and Schowalter, W. R. 1972 Anisotropic fluid theory: a different approach to the dumbbell theory of dilute polymer solutions. Trans. Soc. Rheol., 16, 79.

Grace, H. P. 1971 Dispersion phenomena in high viscosity immiscible fluid systems and application of static mixers as dispersion devices in such systems. Engng. Foundation 3rd Res. Conf. on Mixing, Andover, New Hampshire.

Hand, G. L. 1962 A theory of anisotropic fluids. J. Fluid Mech., 13, 33.

Hinch, E. J. 1977 Mechanical models of dilute polymer solutions in strong flows. Physics Fluids, 20, 522.

Hinch, E. J. and Leal, L. G. 1975 Constitutive equations in suspension mechanics. Part I. General Formulation. J. Fluid Mech., 71, 481.

Hinch, E. J. and Leal, L. G. 1976 Constitutive equations in suspension mechanics. Part II. Approximate forms for a suspension of rigid particles affected by Brownian rotations. J. Fluid Mech., 76, 187.

Kao, S. V. and Mason, S. G. 1975 Dispersion of particles by shear. Nature, 253, 619.

Karam, H. J. and Bellinger, J. C. 1968 Deformation and breakup of liquid droplets in a simple shear field. Ind. Eng. Chem. Fundam., 7, 576.

Kuhn, W. and Kuhn, H. 1945 Bedeutung Beschraünkt Ferier Drehbarkeit für die Viskosität und Strömungsdoppelbrechung von Fadenmolekellösungen I. Helv. Chim. Acta.,28, 1533.

Leal, L. G. and Hinch, E. J. 1972 The rheology of a suspension of nearly spherical particles subject to Brownian rotation. J. Fluid Mech., 55, 745.

Lee, R. 1972 Ph. D. Thesis, University of Houston.

Lumley, J. 1969 Drag reduction by additives. Ann. Rev. Fluid Mech., 1, 367.

Moore, K. 1980 Ph. D. Thesis, Cambridge University.

Phan-Thien, N. and Tanner, R. I. 1978 Response of a nonlinear dumbbell with varying frictional coefficient in a pseudo-turbulent flow field. Physics Fluids, 21, 311.

Rallison, J. M. 1980 The effects of shear and vorticity on deformation of a drop. Appendix., in press.

Rumscheidt, F. D. and Mason, S. G. 1962 Particle motions in sheared suspensions. XII. Deformation and burst of fluid drops in shear hyperbolic flow. J. Colloid Sci., 16, 238.

Tanner, R. I. 1976 A test particle approach to flow classification for viscoelastic fluids. A.I.Ch.E. J., 22, 910.

Tanner, R. I. and Huilgol, R. R. 1975 On a classification scheme for flow fields. Rheol. Acta., 14, 959.

Taylor, G. I. 1932 The intrinsic viscosity of a fluid containing small drops of another fluid. Proc. Roy. Soc.,A138, 41.

Taylor, G. I. 1934 The formation of emulsions in definable fields of flow. Proc. Roy. Soc., A146, 501.

Torza, S., Cox, R. G., and Mason, S. G. 1972 Particle motions in sheared suspensions. XXVII. Transient and steady deformation and burst of liquid drops. J. Colloid Sci., 38, 395.

Table 1. Values for ε_{crit} from hyperbolic data and predicted values for parameter G for various viscosity ratios.

η	ε_{crit}	G (Vector model)	G (Tensor model)
0.1	0.21	1.1	0.9
1	0.21	2.1	1.8
10	0.30	0.3	0.3

Figure Captions

Figure 1. Domain of all possible flows and representative eigenvalue contours for G = 1. The dotted line corresponds to the left discriminant of the characteristic equation (see text).

Figure 2. Schematic diagram identifying particular flows with certain points of the accessible domain.

Figure 3. Dimensionless eigenvalues for a flow with arbitrary orientation of the vorticity vector (see text).

Figure 4. Degree of macromolecular extension as a function of dimensionless relaxation constant in a statistically specified three-dimensional turbulent flow.

Figure 5. Predicted values of the dimensionless deformation parameter for breakup as a function of viscosity ratio in simple shear flow. Also shown are data from Torza, Cox, and Mason (1972).

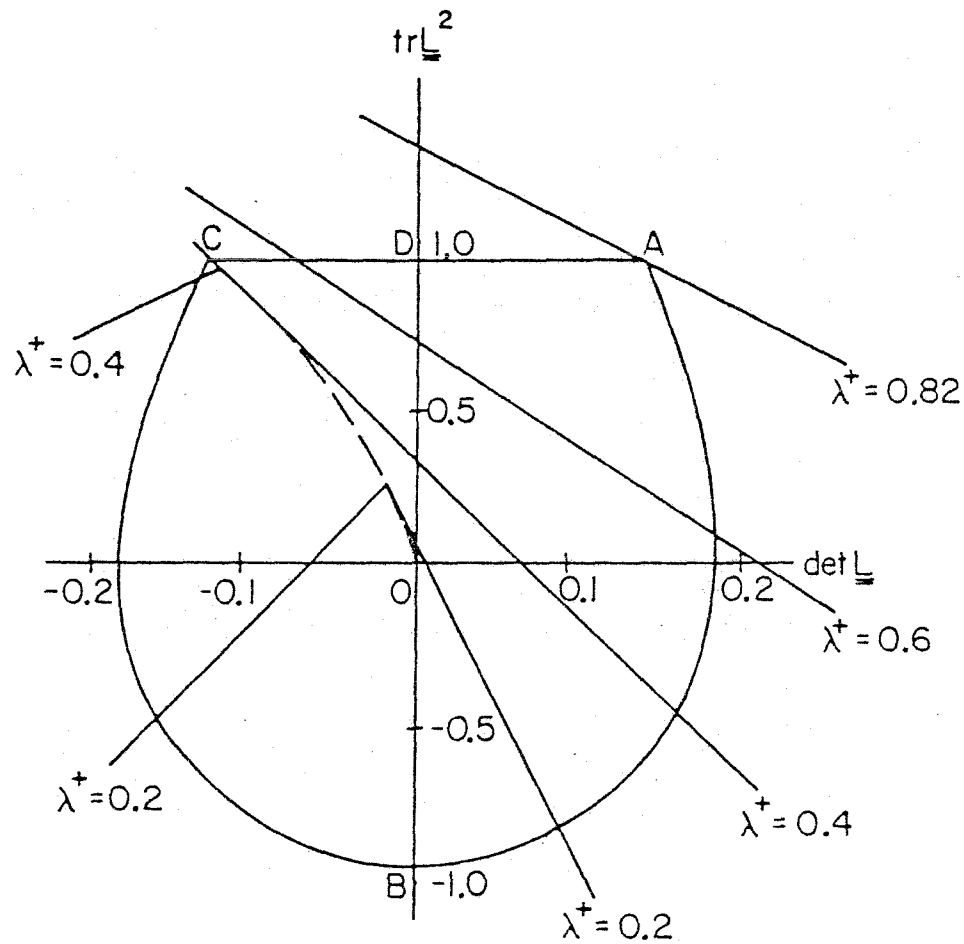

Figure 1.

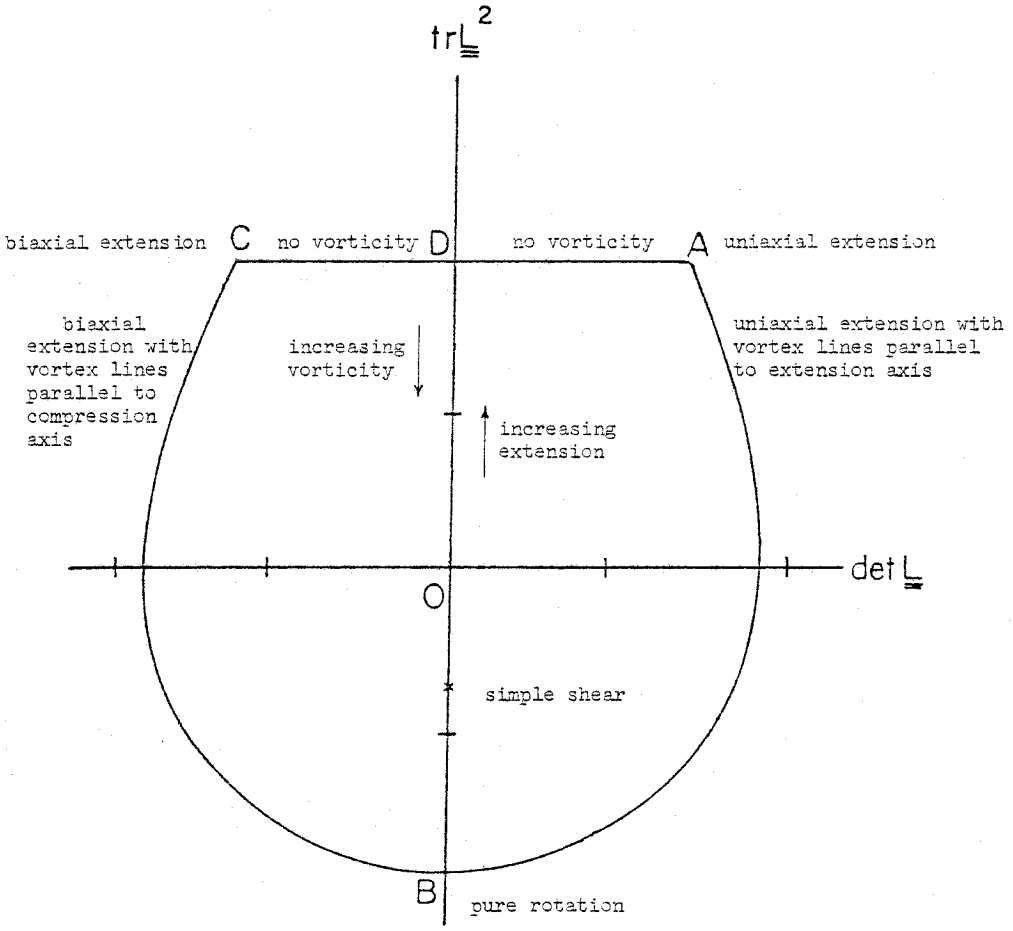
tr L 2
biaxial extension
C
no vorticity
D
no vorticity
A
uniaxial extension
biaxial extension with vortex lines parallel to compression axis
increasing vorticity
uniaxial extension with vortex lines parallel to extension axis
increasing extension
det L
O
simple shear
B
pure rotation

Figure 2.

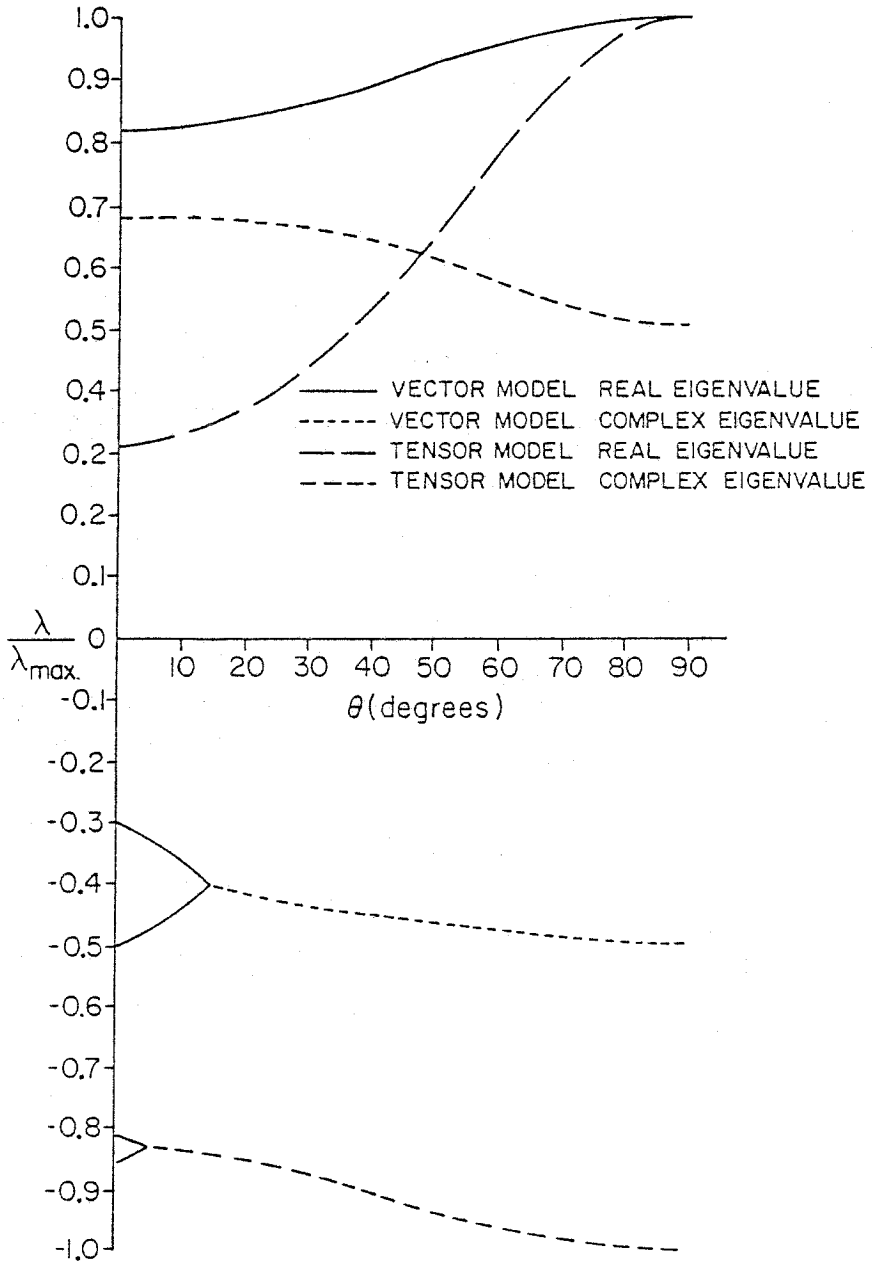
1.0
0.9
0.8
0.7
0.6
0.5
0.4
0.2
0.2
0.1
0
-0.1
-0.2
-0.3
-0.4
-0.5
-0.6
-0.7
-0.8
-0.9
-1.0
λ/λmax.
10 20 30 40 50 60 70 80 90
θ(degrees)
VECTOR MODEL REAL EIGENVALUE
VECTOR MODEL COMPLEX EIGENVALUE
TENSOR MODEL REAL EIGENVALUE
TENSOR MODEL COMPLEX EIGENVALUE

Figure 3.

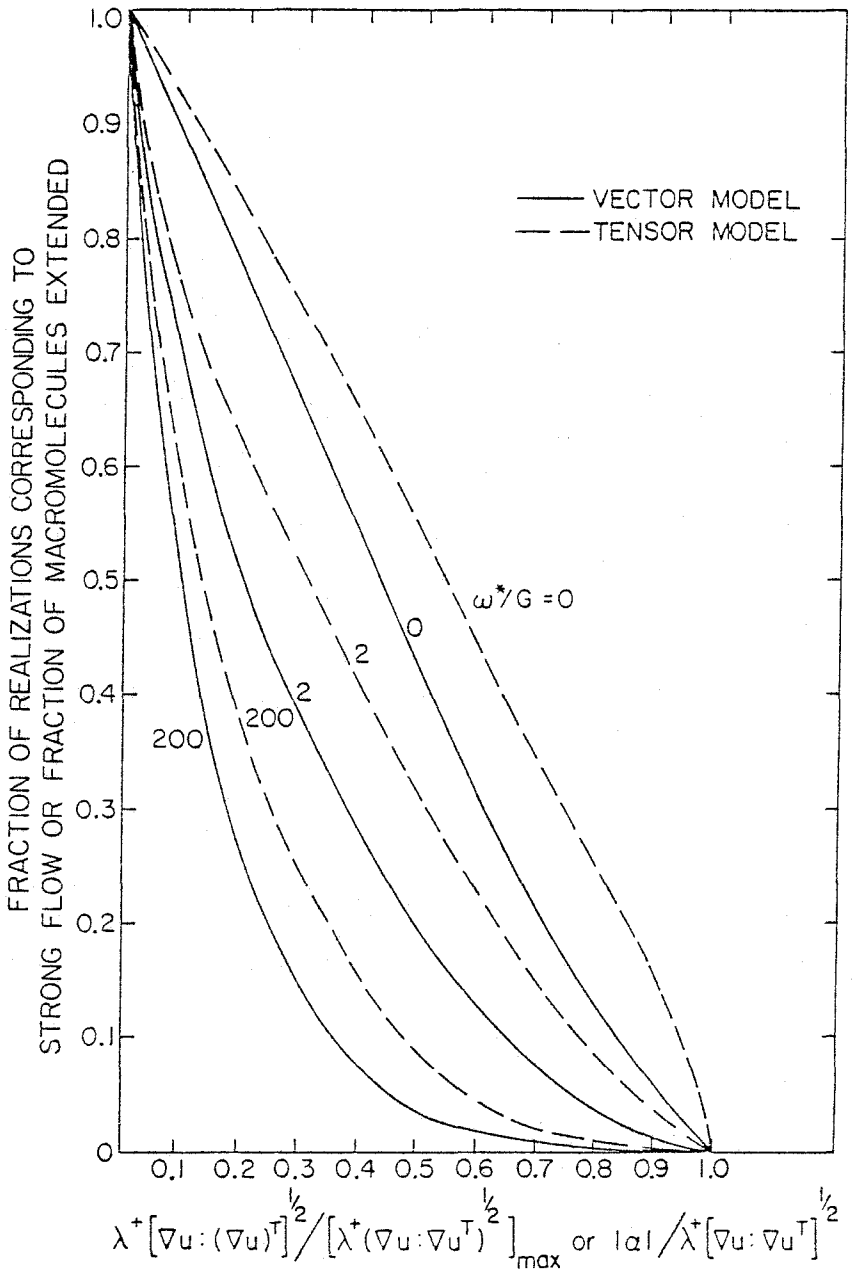
VECTOR MODEL
TENSOR MODEL
ω*/G = 0
0
2
2
200
200
FRACTION OF REALIZATIONS CORRESPONDING TO STRONG FLOW OR FRACTION OF MACROMOLECULES EXTENDED
1.0
0.9
0.8
0.7
0.6
0.5
0.4
0.3
0.2
0.1
0
0.1 0.2 0.3 0.4 0.5 0.6 0.7 0.8 0.9 1.0
$\lambda^+[\nabla u:(\nabla u)^T]^{1/2}/[\lambda^+(\nabla u:\nabla u^T)^{1/2}]_{max}$ or $|\alpha|/\lambda^+[\nabla u:\nabla u^T]^{1/2}$

Figure 4.

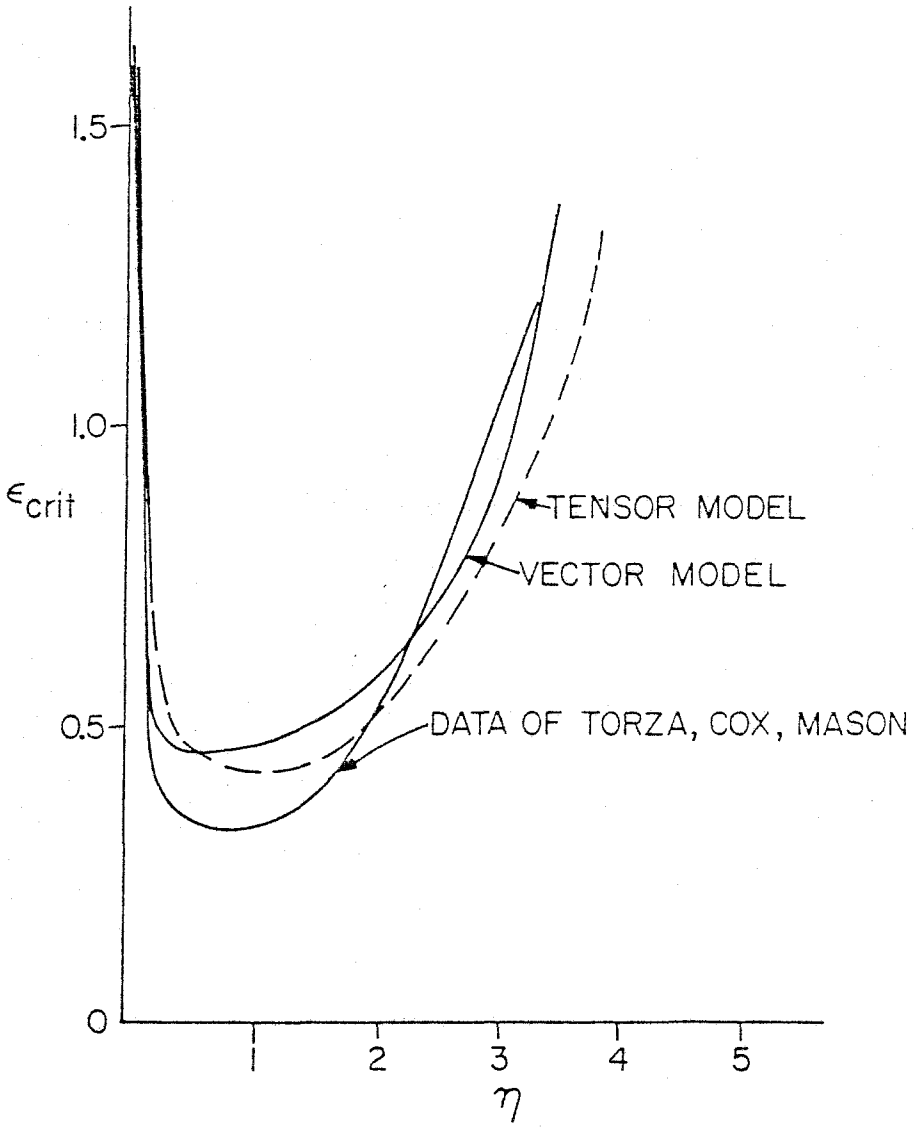
1.5
1.0
0.5
0
ϵ_{crit}
TENSOR MODEL
VECTOR MODEL
DATA OF TORZA, COX, MASON
1
2
3
4
5
η

Figure 5.

Appendix

	System: 2	3	4	5	6	2V	3V	4V	5V	6V	7V	8V	9V
	(V = 0.32 cm/s)												
0.512	0.05	0.06	0.23	0.04	0.04	0.11	0.11	0.14	0.13	0.19	0.19	0.19	0.20
	1.18	1.18	1.00	1.11	1.09	1.25	1.25	1.15	1.13	1.05	1.10	1.09	1.08
0.577	0.06	0.09	0.19	0.04	0.04	0.14	0.10	0.11	0.08	0.16	0.17	0.16	0.17
	1.08	1.08	1.00	1.09	1.13	1.36	1.26	1.13	1.23	1.07	1.09	1.11	1.11
0.660	0.08	0.07	0.15	0.04	0.05	0.10	0.10	0.10	0.09	0.13	0.13	0.14	0.14
	1.07	1.10	1.04	1.10	1.13	1.30	1.24	1.18	1.23	1.09	1.17	1.12	1.12
0.726	0.07	0.05	0.17	0.04	0.05	0.13	0.10	0.10	0.08	0.12	0.11	0.11	0.12
	1.10	1.09	1.06	1.10	1.15	1.35	1.27	1.18	1.21	1.11	1.17	1.17	1.14
0.782	0.06	0.05	0.11	0.04	0.05	0.13	0.10	0.09	0.08	0.09	0.11	0.11	0.11
	1.07	1.10	1.06	1.10	1.16	1.35	1.34	1.21	1.29	1.14	1.16	1.17	1.17
0.831	0.06	0.06	0.10	0.04	0.05	0.09	0.10	0.08	0.07	0.09	0.09	0.10	0.10
	1.08	1.12	1.06	1.10	1.16	1.38	1.37	1.23	1.28	1.17	1.22	1.20	1.20
	(V = 0.56 cm/s)												
0.512	0.09	0.09	0.20	0.06	0.07	0.17	0.17	0.17	0.15	0.21	0.21	0.21	0.21
	1.15	1.10	1.04	1.14	1.15	1.24	1.20	1.15	1.15	1.07	1.09	1.11	1.10
0.577	0.09	0.12	0.19	0.06	0.06	0.15	0.16	0.14	0.12	0.18	0.18	0.19	0.20
	1.14	1.08	1.04	1.15	1.15	1.29	1.23	1.18	1.19	1.10	1.15	1.12	1.10
0.660	0.08	0.12	0.15	0.08	0.07	0.13	0.15	0.13	0.11	0.14	0.16	0.16	0.16
	1.12	1.05	1.07	1.15	1.18	1.31	1.23	1.17	1.22	1.14	1.15	1.14	1.14
0.726	0.09	0.11	0.12	0.06	0.07	0.11	0.13	0.12	0.11	0.13	0.14	0.15	0.14
	1.11	1.10	1.08	1.15	1.21	1.37	1.23	1.21	1.25	1.15	1.17	1.18	1.17
0.782	0.08	0.09	0.12	0.07	0.07	0.12	0.12	0.11	0.09	0.12	0.12	0.13	0.12
	1.14	1.12	1.12	1.16	1.20	1.46	1.26	1.22	1.25	1.18	1.23	1.21	1.20
0.831	0.08	0.08	0.08	0.07	0.07	0.09	0.11	0.11	0.09	0.10	0.10	0.13	0.11
	1.16	1.13	1.14	1.18	1.21	1.41	1.31	1.23	1.29	1.22	1.27	1.25	1.25
	(V = 0.80 cm/s)												
0.512	0.11	0.11	0.19	0.10	0.09	0.18	0.20	0.19	0.16	0.22	0.20	0.24	0.23
	1.16	1.13	1.06	1.16	1.21	1.23	1.17	1.13	1.15	1.10	1.11	1.09	1.11
0.577	0.11	0.13	0.18	0.09	0.09	0.15	0.18	0.17	0.15	0.18	0.19	0.19	0.20
	1.16	1.09	1.08	1.15	1.21	1.30	1.21	1.17	1.20	1.08	1.14	1.12	1.10
0.660	0.13	0.12	0.16	0.10	0.08	0.14	0.16	0.14	0.13	0.16	0.17	0.17	0.18
	1.15	1.08	1.10	1.15	1.23	1.21	1.23	1.17	1.22	1.14	1.17	1.16	1.13
0.726	0.12	0.10	0.13	0.08	0.07	0.13	0.14	0.13	0.12	0.14	0.14	0.16	0.15
	1.13	1.11	1.10	1.18	1.23	1.24	1.26	1.22	1.25	1.17	1.21	1.18	1.20
0.782	0.09	0.10	0.13	0.08	0.07	0.12	0.13	0.12	0.11	0.12	0.12	0.14	0.13
	1.18	1.13	1.13	1.19	1.23	1.29	1.30	1.22	1.27	1.20	1.22	1.25	1.22
0.831	0.09	0.09	0.10	0.08	0.06	0.10	0.14	0.13	0.10	0.11	0.12	0.14	0.11
	1.18	1.18	1.16	1.23	1.27	1.35	1.33	1.27	1.31	1.21	1.28	1.33	1.27

TABLE A1. Data for h and D. For each system, drop size, and flow rate there are a pair of values. The upper is the measured value for h and the lower is the measured value of D